2015

Thermodynamic Analysis and Optimization of Supercritical Carbon Dioxide Brayton Cycles

Mahmood Mohagheghi
University of Central Florida

THERMODYNAMIC ANALYSIS AND OPTIMIZATION OF SUPERCRITICAL CARBON DIOXIDE BRAYTON CYCLES

by

MAHMOOD MOHAGHEGHI
B.Sc. Shiraz University, 2004
M.Sc. Sharif University of Technology, 2006
M.Sc. University of Central Florida, 2012

A dissertation submitted in partial fulfillment of the requirements
for the degree of Doctor of Philosophy
in the Department of Mechanical and Aerospace Engineering
in the College of Engineering and Computer Science
at the University of Central Florida
Orlando, Florida

Spring Term
2015

Major Professor: Jayanta Kapat

ABSTRACT

The power generation industry is facing new challenging issues regarding accelerating growth of electricity demand, fuel cost and environmental pollution. These challenges accompanied by concerns of energy resources becoming scarce necessitate searching for sustainable and economically competitive solutions to supply the future electricity demand. To this end, supercritical carbon dioxide (S-CO2) Brayton cycles present great promise particularly in high temperature concentrated solar power (CSP) and waste heat recovery (WHR) applications. With this regard, this dissertation is intended to perform thorough thermodynamic analyses and optimization of S-CO2 Brayton cycles for both of these applications.

A modeling tool has been developed, which enables one to predict and analyze the thermodynamic performance of the S-CO2 Brayton cycles in various configurations employing recuperation, recompression, intercooling and reheating. The modeling tool is fully flexible in terms of encompassing the entire feasible design domain and rectifying possible infeasible solutions. Moreover, it is computationally efficient in order to handle time consuming optimization problems. A robust optimization tool has also been developed by employing the principles of genetic algorithm. The developed genetic algorithm code is capable of optimizing non-linear systems with several decision variables simultaneously, and without being trapped in local optimum points.

Two optimization schemes, i.e. single-objective and multi-objective, are considered in optimizing the S-CO2 cycles for high temperature solar tower applications. In order to reduce the size and cost of solar block, the global maximum efficiency of the power block should be

realized. Therefore, the single-objective optimization scheme is considered to find the optimum design points that correspond to the global maximum efficiency of S-CO2 cycles. Four configurations of S-CO2 Brayton cycles are investigated, and the optimum design point for each configuration is determined. Ultimately, the effects of recompression, reheating, and intercooling on the thermodynamic performance of the recuperated S-CO2 Brayton cycle are analyzed. The results reveal that the main limiting factors in the optimization process are maximum cycle temperature, minimum heat rejection temperature, and pinch point temperature difference. The maximum cycle pressure is also a limiting factor in all studied cases except the simple recuperated cycle. The optimized cycle efficiency varies from 55.77% to 62.02% with consideration of reasonable component performances as we add recompression, reheat and intercooling to the simple recuperated cycle (RC). Although addition of reheating and intercooling to the recuperated recompression cycle (RRC) increases the cycle efficiency by about 3.45 percent points, the simplicity of RC and RRC configurations makes them more promising options at this early development stage of S-CO2 cycles, and are used for further studies in this dissertation.

The results of efficiency maximization show that achieving the highest efficiency does not necessarily coincide with the highest cycle specific power. In addition to the efficiency, the specific power is also an important parameter when it comes to investment and decision making since it directly affects the power generation capacity, the size of components and the cost of power blocks. Consequently, the multi-objective optimization scheme is devised to simultaneously maximize both the cycle efficiency and specific power in the simple recuperated and recuperated recompression configurations. The optimization results are presented in the form

of two optimum trade-off curves, also known as Pareto fronts, which enable decision makers to choose their desired compromise between the objectives, and to avoid naive solution points obtained from a single-objective optimization approach. Moreover, the comparison of the Pareto optimal fronts associated with the studied configurations reveals the optimum operational region of the recompression configuration where it presents superior performance over the simple recuperated cycle.

Considering the extensive potential of waste heat recovery from energy intensive industries and stand-alone gas turbines, this dissertation also investigates the optimum design point of S-CO2 Brayton cycles for a wide range of waste heat source temperatures (500 K to 1100 K). Once again, the simple recuperated and recuperated recompression configurations are selected for this application. The utilization of heat in WHR applications is fundamentally different from that in closed loop heat source applications. The temperature pinching issues are recognized in the waste recovery heat exchangers, which brings about a trade-off between the cycle efficiency and amount of recovered heat. Therefore, maximization of net power output for a given waste heat source is of paramount practical interest rather than the maximization of cycle efficiency. The results demonstrate that by changing the heat source temperature from one application to another, the variation of optimum pressure ratio is insignificant. However, the optimum CO2 to waste gas mass flow ratio and turbine inlet temperature should properly be adjusted. The RRC configuration provides minor increase in power output as compared to RC configuration. Although cycle efficiencies as high as 34.8% and 39.7% can be achieved in RC and RRC configurations respectively, the overall conversion efficiency is less than 26% in RRC and 24.5% in RC.

This work is dedicated to my family, specially my parents,

for their unconditional love, support, and encouragement.

ACKNOWLEDGMENTS

I would like to express my sincere gratitude to my advisor, Prof. Jayanta Kapat, for the learning experience, kind considerations and positive support during my PhD program. In addition, special thanks go to my dissertation committee, Prof. Alain Kassab, Dr. Muthusamy Swami and Dr. Tuhin Das for their encouragement, insightful comments and constructive questions.

I am also very grateful for the kind support and learning experience I have received from several faculty members including Late Prof. Suhada Jayasuriya, Late Prof. David W. Nicholson, Prof. Ranganathan Kumar, and Prof. Louis Chow.

Furthermore, I am thankful to the MAE department's staff for their help to prepare wonderful environment for graduate students. Specially, I must express my appreciation to Jeanine Clements, Maria McCarthy, William Scaggs and Stephanie Gavarrete for their support.

I take this opportunity to also thank my friends who have been there for me like a family when I needed them the most. My special appreciation goes to Monique Rogers for her kind support.

Finally, I would like to express my ultimate gratitude and respect towards my family, specially my parents, my uncle (Mohyeddin Sheikholeslami) and my sister (Zahra Mohagheghi) for their true love and endless support.

TABLE OF CONTENTS

LIST OF FIGURES

LIST OF TABLES

NOMENCLATURE

CCGT	Combined Cycle Gas Turbine
C, Comp.	Compressor
CSP	Concentrated Solar Power
f	Mass Flow Fraction
f_1, f_2	Normalized Objective Functions
F	Composite Objective Function
FPD	Fractional Pressure Drop
GA	Genetic Algorithm
h	Enthalpy, kJ/kg
HTR	High Temperature Recuperator
LTR	Low Temperature Recuperator
NDRIT	Non-Dimensional Recompression Inlet Temperature, K
NIST	National Institute of Standards and Technology
P	Pressure, MPa
$\dot{Q}$	Input Heat, kW
RC	Recuperated Cycle

RRC	Recuperated Recompression Cycle
RRCR	Recuperated Recompression Cycle with Reheat
RRCRI	Recuperated Recompression Cycle with Reheat and Intercooling
S-CO2	Supercritical Carbon Dioxide
T, Temp.	Temperature, K
Turb.	Turbine
w_1, w_2	Weight Coefficients
$\dot{W}$	Power, kW
WHR	Waste Heat Recovery
ΔT_{PP}	Pinch Point Temperature Difference, K
ΔT_t	Terminal Temperature Difference, K
η_{comp}	Isentropic Efficiency of Compressor
η_{turb}	Isentropic Efficiency of Turbine
η_{cycle}	Cycle Efficiency
$\eta_{Overall}$	Overall Conversion Efficiency

1. INTRODUCTION

1.1. Motivation

The future of power generation industry is mainly influenced by two factors, i.e., energy sustainability and economy. According to Prof. Richard E. Smalley (Nobel Prize Winner, 1996), energy is the humanity's first problem in the next 50 years [1]. From the sustainability point of view, four main concerns drive today's energy subject.

The first concern is the accelerating growth of energy demand. According to Energy Outlook 2012 published by British Petroleum [2], the current annual global energy demand is almost 12.4 Billion tonnes of oil equivalent (Btoe); and it is expected to grow with an average rate of 1.6%, and reach 16.5 Btoe in 2030. This trend is even more severe for global electricity demand which escalates with an average rate of 2.6% from 22.5 PWh in 2012 to 36 PWh in 2030; that is 60% increase in electricity demand over 18 years. The second concern is environmental. More than 80% of the world's energy demand and 67% of the global electricity generation are met by burning fossil fuels [3]. The combustion of fossil fuels is the main source of greenhouse gas emissions, primarily CO2, which has been believed as a major contributor to the global warming problem. According to the National Oceanic and Atmosphere administration, the concentration of CO2 in the atmosphere in May 2013 reached a daily average of 400 parts per million (ppm), the highest level for at least 800,000 years [4]. The third concern is that fossil fuel resources are finite, and they will eventually run out. In fact, fossil fuels such as oil and gas are utilized as input feed for several material and manufacturing industries, which makes them very valuable and irreplaceable commodities. Finally, the forth concern is related to energy

security and international conflicts due to the geographically uneven distribution of fossil fuel resources.

Furthermore, economic considerations have even stronger influence on the power generation industry than energy sustainability does. In the very competitive electricity market, maximizing the financial profit has always motivated the power generation industry to search for advanced technologies that can provide the highest energy conversion efficiency with the lowest possible cost. To just emphasize the significance of this matter, it suffices to mention that only one percentage point increase in the overall efficiency of national power generation would roughly result in 7.9 Billion dollars increase in net annual revenue. In addition, maximizing the power generation efficiency will considerably reduce the adverse effects of environmental pollutions. It should also be noted that any reduction in the capital or operation cost of power plants would significantly create additional increase in the net profit.

In summary, energy sustainability and economic considerations are both vital for the future of power generation industry. From the sustainability point of view, the next generation of power plants should be less dependent on fossil fuel resources. Along with energy sustainability considerations, economic incentives also encourage the power generation industry to look for less costly, yet efficient energy conversion technologies. In association with the aforementioned motivation, the supercritical carbon dioxide (S-CO2) Brayton cycles present very promising features in terms of size, efficiency, economy and their proper integration with various sustainable heat sources. Consequently, this dissertation is intended to address the thermodynamic performance of these cycles.

1.2. Background

The power generation industry relies mainly on thermal power plants as they supply over 80% of global electricity production. The working principles of thermal power plants are usually (if not always) based on a thermodynamic cycle in which thermal energy from a heat source is converted to mechanical energy. Currently, fossil fuels account for almost 85.2% of heat sources in thermal power plants worldwide [3, 5]. However, as also discussed in the previous section, it is inevitable for the power generation industry to move towards sustainable heat sources. In this regard, solar thermal energy, nuclear energy and geothermal energy are three major sustainable heat sources that are considered as the most promising options. It is noteworthy that these heat sources have a common feature in their applications; that is, the demanded thermal energy is utilized in a closed loop system. In addition to aforementioned sustainable energy sources, there is a substantial amount of energy that can be recovered from waste heat streams. There are many sources of waste thermal streams dissipated from gas turbines, energy intensive industries, and also heavy duty transportation devices. It is worth mentioning that in certain regions of the United States, the waste heat recovery (WHR) is actually considered as an equivalent form of renewable energy utilization since there are no additional environmental emissions for the extra recovered heat. For the sake of convenience, all form of energy sources described above are referred to as sustainable heat sources (SHSs) hereafter.

The steam Rankine cycle is the most common power plant technology that has practically been integrated to sustainable heat sources. However, steam power plants are complex, enormous, and expensive. Their high thermal inertia does not allow proper load following (dispatching) and fast start up. Moreover, the maximum temperature of steam Rankine cycles is

in the range of 750 to 890 K, which intrinsically makes their efficiencies stay in the range of 30% to 43% (based on HHV) from conventional to ultra-supercritical plants respectively. Although advancement in material sciences promises higher steam temperature (up to 1030 K) in the next decades, the efficiency of next generation ultra-supercritical steam power plants operating at 1030 K would be on the verge of 50%. All in all, the techno-economic characteristics of steam power plants seem to hold back this technology from being an economically appealing option for certain SHS applications such as geothermal, concentrated solar power (CSP) and Industrial waste heat recovery applications.

In contrast to the steam Rankine cycle, The Brayton cycles are generally simple, compact, and less expensive. They also offer fast start up, proper load following, and short construction time. The most well-known among the Brayton cycles is the air breathing gas turbine cycle. Air breathing gas turbines require turbine inlet temperature (TIT) of above 1750 K in order to achieve attractive efficiencies of 40% in stand-alone applications and of 60% in combined cycles. However, the practically suitable temperatures of SHSs are much below common TITs of efficient gas turbines, which leads to incompetency of the air breathing gas turbines for SHS applications.

Therefore, apposite efforts have to be made towards redesigning or inventing highly efficient yet inexpensive power cycles that employ unconventional working fluids. Addressing the aforementioned quest, over fifty pure working fluids and several multi-component organic and inorganic fluids have been proposed in the open literature [6-36] to be utilized in various configurations of power cycles. The selection of working fluid has a major impact on economic viability and social acceptance of a power plant technology. The working fluid should be

assessed based on several criteria such as environmental aspects, safety concerns, availability, and cost. Moreover, the efficiency and operating conditions of a thermodynamic power cycle significantly depend on the working fluid's thermo-physical properties such as critical pressure, critical temperature, density, specific heat, viscosity, latent heat, and fluid stability. These properties not only play important roles in thermal performance of power cycles, but also affect the size and cost of power plant components. In an extensive study, H. Chen et al. [6] evaluated 35 organic working fluids in subcritical and supercritical Rankine cycles. However, they indicate there are only a few relatively safe, inexpensive and environmentally benign nominees among organic fluids. Although certain organic Rankine cycles (ORC) may offer reasonable efficiencies, the associated organic fluids are mainly safe and beneficial for low-grade heat sources.

Considering the suitable (efficient) temperature range for SHS applications (500 to 1400 K) and also techno-economic advantages of the Brayton cycle over the steam Rankine cycle, the recuperated Brayton cycles using supercritical carbon dioxide (S-CO2) have been proposed as one of the most promising options. Carbon dioxide is environmentally benign, non-toxic, non-flammable, abundant, and inexpensive. It is a very stable compound as its thermal dissociation temperature is above 2000 K. In addition, the thermo-physical properties of carbon dioxide have been thoroughly studied; and they are easily accessible through academic and commercial data bases. Carbon dioxide has a critical pressure of 7.39 MPa, and a critical temperature of 304.2 K, which is very close to the standard ambient temperature (298.15 K). Supercritical carbon dioxide is dense, like a liquid, but it expands to fill a volume like a gas. Sudden changes in thermodynamic properties of carbon dioxide near its critical point enable the S-CO2 Brayton

cycles to present remarkable performance and high efficiency. Operating at high pressures, the cycle efficiency is inconsiderably affected by the pressure drop in heat exchangers (e.g. heaters, recuperators, and coolers). Moreover, supercritical carbon dioxide has a relatively high volumetric heat capacity; and it offers excellent heat transfer characteristics, which can be translated to small-size recuperators. The S-CO2 Brayton cycles feature high compactness, which leads to low capital cost and short construction time. Unlike the steam Rankine cycles, the S-CO2 Brayton cycles do not require clean water supplies, which is one of the most crucial issues in the power generation industry. High cycle efficiency, compactness, superior economy, and no water issues are the features which make these cycles well suited for SHS applications.

1.3. S-CO2 Brayton Cycle Concept

A simple carbon dioxide Brayton cycle is a closed loop recuperated Brayton cycle in which the working fluid is carbon dioxide. Figure 1-1 demonstrates the cycle in its simplest configuration which includes a pressurizing device (pump or compressor, depending on the inlet condition), a recuperator (also known as regenerator), a heater, and a cooler. Carbon dioxide is pressurized by the compressor (or pump), and absorbs heat through the recuperator and the heater. This route consisting of points 2, 3, and 4 is the high pressure side of the cycle. Carbon dioxide then expands in the turbine to a lower pressure level and generates power. The exhaust of the turbine still carries significant amount of thermal energy; therefore, the low pressure carbon dioxide is directed towards the low pressure side of the recuperator to exchange heat to the cold and pressurized fluid coming from the compressor. In order to close the cycle after the

recuperator, carbon dioxide needs to be cooled down in the cooler to the inlet temperature of the compressor. The route consisting of points 5, 6, and 1 is called the low pressure side of the cycle.

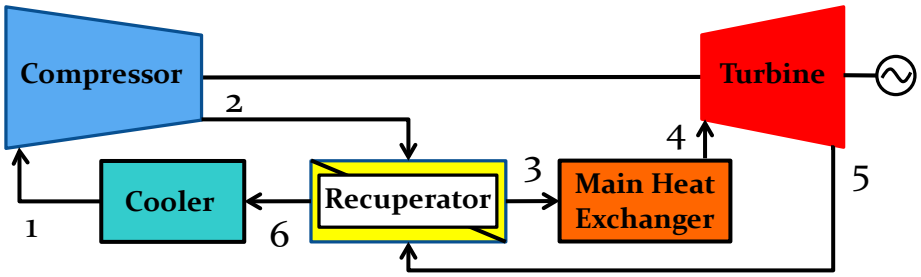

Figure 1-1: Simple carbon dioxide recuperated Brayton cycle configuration.

Ideally, there are two isentropic processes (compression and expansion), and three constant pressure heat transfer processes (cooling, recuperation, and heating). However, due to irreversibilities, the compression and expansion processes are not isentropic; and the heat transfer processes are not constant pressure either. Figure 1-2 presents an actual schematic of these processes in a T-s diagram.

Depending on the pressures of high pressure and low pressure sides of the cycle, the cycle has been called with different names. If the high pressure side of the cycle operates at pressures above the critical pressure; and the low pressure side is in subcritical pressure region, the cycle would be called transcritical CO2 cycle. On the other hand, the cycle would be called supercritical CO2 cycle if both low pressure and high pressure sides of the cycle operate above the critical pressure. These terminologies are followed by only few people. For the sake of simplicity, the majority of people use the supercritical CO2 terminology for all types of carbon dioxide Brayton cycles. In this study, it was also decided to adopt the latter terminology.

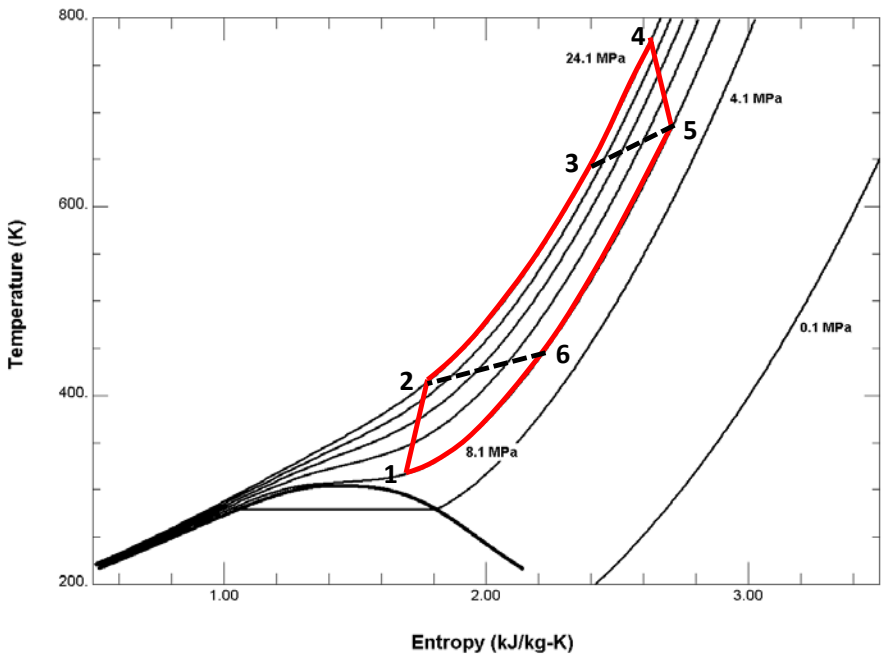

Figure 1-2: Carbon dioxide recuperated Brayton cycle T-s diagram.

In spite of similarities in T-s diagrams, the S-CO2 Brayton cycles differ from the air breathing Brayton cycles in one major aspect which is the temperature pinching in recuperators. The S-CO2 cycles usually operate at very high pressures (7 to 25 MPa); whereas, air breathing gas turbines work in pressure range of 0.1 to 3 MPa. In other words, the S-CO2 cycles operates very close to the critical point of carbon dioxide where the real gas effects are very significant. Under the real gas effect, the constant pressure specific heat (Cp) of carbon dioxide depends on both temperature and pressure. Figure 1-3 shows the h-T diagram for carbon dioxide with the constant pressure lines from 4 to 22 MPa. In this diagram, the slope at any point represents the constant pressure specific heat. The maximum slope at pressures above the critical pressure is finite and its value increases with decreasing the pressure towards the critical pressure. On the

critical pressure line, the maximum slope approaches towards quasi-infinite limit as the temperature reaches its critical value. This phenomenon is also presented in Figure 1-4 on Cp-T diagram. Note that the red line represents the pressure of 7.4 MPa which is very close to the critical pressure of carbon dioxide; and it shows severe jump at the critical temperature.

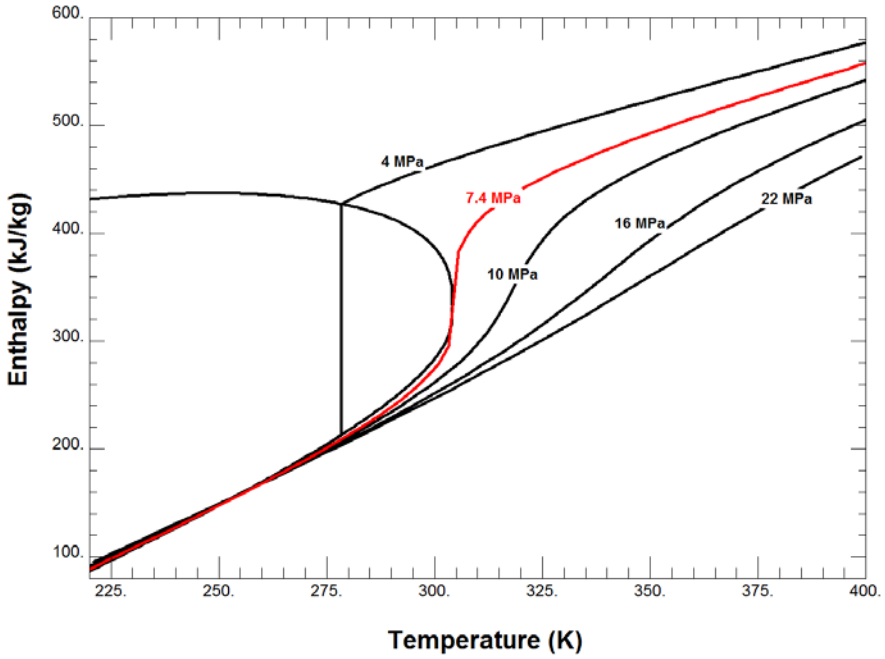

Figure 1-3: h-T diagram of carbon dioxide.

As a result in the recuperator, the high pressure stream does not have the same heat capacity as the low pressure stream does. Therefore for a constant amount of exchanged heat, the temperature variation for a high pressure stream is not the same as the one for a low pressure stream, which causes the temperature pinching problem. The temperature pinching problem limits the heat recovery potential, increases the irreversibility in recuperators, and reduces the

efficiency of cycles. The pinching problem can be best demonstrated in T-Q diagrams such as the one presented in Figure 1-5.

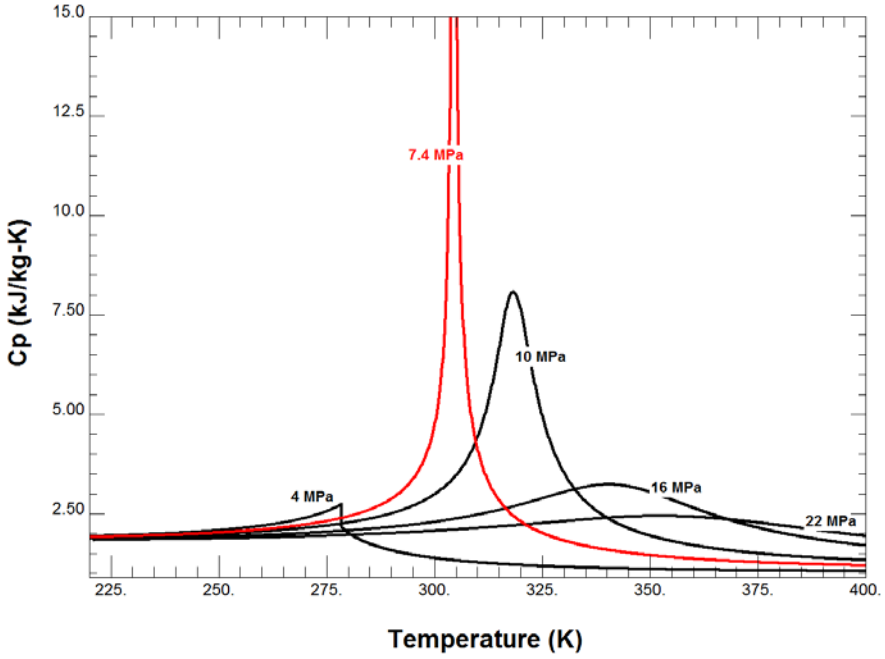

Figure 1-4: Cp-T diagram of carbon dioxide.

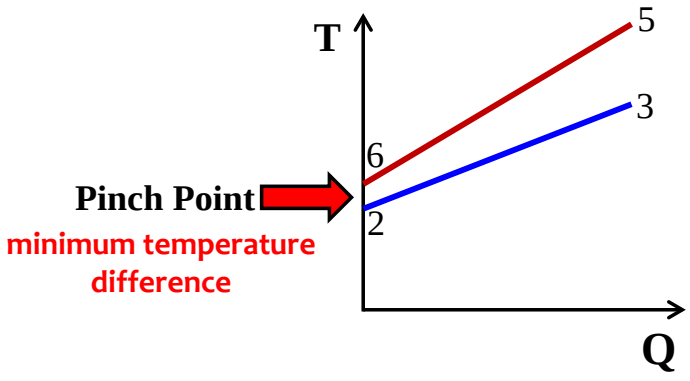

Figure 1-5: Carbon dioxide recuperated Brayton cycle T-s diagram.

To summarize, using CO2 as the working fluid brings new aspects to the analysis of the Brayton cycles. The major differences such as high pressure operation, dense working fluid, pressure-dependent and non-linear variation of thermodynamic properties, temperature pinching problem, etc. make the S-CO2 cycles function differently form the regular air breathing gas turbines.

1.4. Literature Review

1.4.1. History

The idea of using carbon dioxide as the working fluid in a power cycle was originally patented by Sulzer Bros in Germany in 1948 [37]. However, the concept was preliminary, and it had not attracted much attention until late 1960's when these cycles were rediscovered and further studied in several publications. Despite of studies all around the world including the ones in Soviet Union [38] and Switzerland [39], the major contributions were done by Feher [40-42] in the United States and Angelino [43-45] in Italy.

In the CO2 cycle proposed by Feher [41], both high pressure and low pressure sides of the cycle run above the critical pressure of CO2. However, the inlet temperature of the compression process is below the critical temperature. In other words, the compression process is in the liquid phase, which results in using a pump instead of a compressor. Therefore, Feher's cycle would be very compact and the compression-expansion work ratio is very low. He also identified the temperature pinching problem in the regeneration process; however, no solution was offered by him. The inlet temperatures to the pump and turbine were considered 293 K and 973 K respectively. He did not study the optimum pump inlet pressure as he assumed that

parameter to be constant at 2000 psia in his study. He concluded that the S-CO2 cycles present high thermal efficiency and low volume to power ratio. In the case of using a pump, the cycle is insensitive to compression efficiency. He suggested a single stage turbine and pump since the pressure ratio of his cycle was considered between 2 to 3. In a collaborative attempt, Feher and Hoffmann [42] presented a 150 kWe S-CO2 cycle design based on Feher's proposed cycle. They outlined the design procedure with more focus in major components such as pumps, turbines, and recuperators. A two shaft arrangement was suggested due to incompatible rotational speeds of turbines and compressors. After performing a parametric study, they stated that the optimum alternator shaft speed should be around 40000 rpm. They also theorized the start-up and control mechanisms. Eventually, they succeeded to present a pump efficiency of 75% and a power turbine efficiency of 85% in their design; and declared the Feher's cycle as a technically feasible power cycle.

One of the early but major contributions in this subject was performed by Angelino [43-45]. In his early study [43], he investigated only the fully condensation CO2 cycle in which the low pressure side of the cycle operates at subcritical pressure and the heat rejection occurs at temperature below the critical temperature. He concluded that the fully condensation S-CO2 cycle may offer more efficiency potential than other types of carbon dioxide cycles (e.g. supercritical and subcritical CO2 cycles). However, he discovered that heat transfer irreversibility in the regeneration process is considerably significant in the fully condensation cycle. In an attempt to reduce the heat transfer irreversibility of the regeneration process, Angelino introduced four partial condensation configurations in his second publication on S-CO2 cycles [44]. Figure 1-6 shows the partial condensation cycles he proposed.

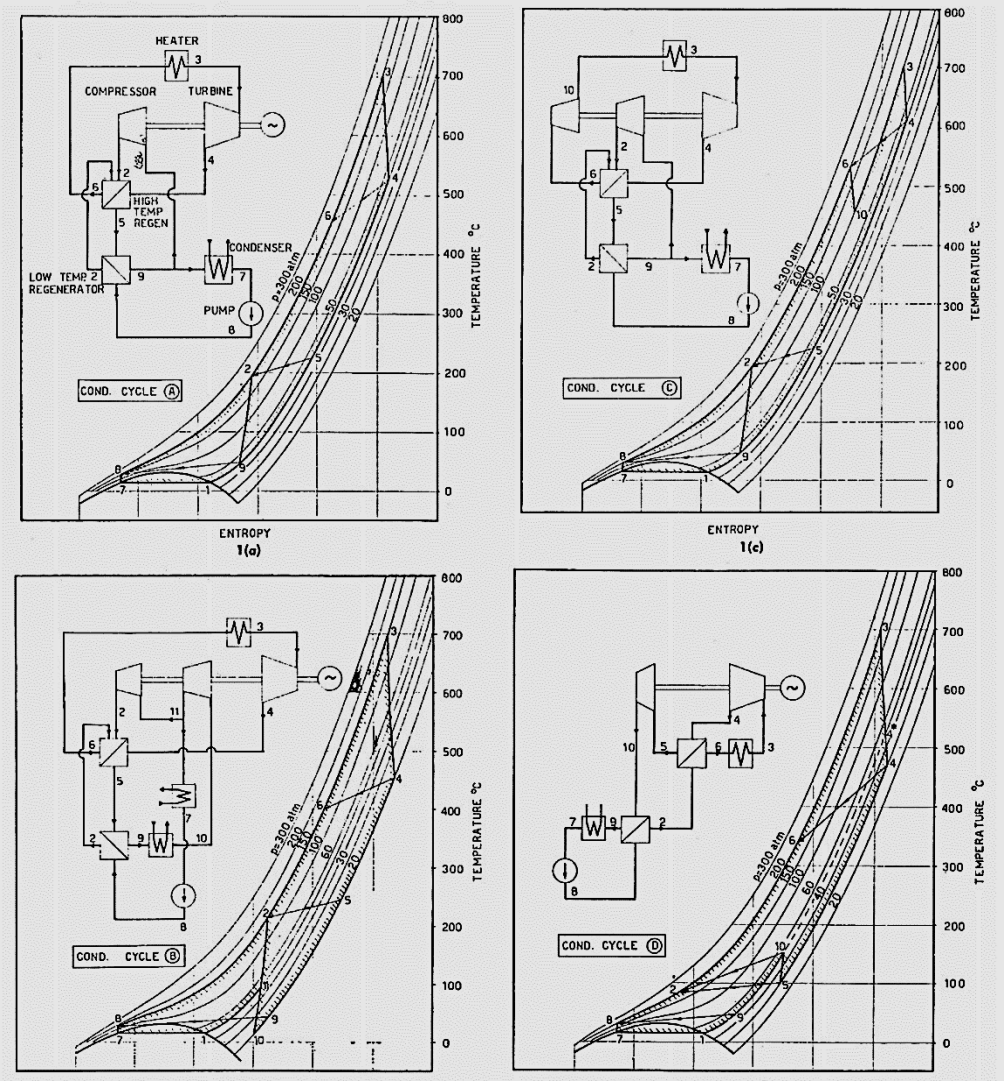

Figure 1-6: S-CO2 partial condensation configurations introduced by Angelino in [44]

The proposed configurations present different advantages. For instance, configuration A offers the highest efficiency. In configuration B, the turbine exhaust pressure is independent of the condensing pressure. Therefore, the turbine work can be increased (by higher pressure ratio) without requiring a lower heat rejection temperature. In configuration C, carbon dioxide enters the high pressure turbine immediately after the regeneration. Thus, the heat addition to the cycle occurs at lower pressure which reduces the stresses in the main heater. Finally, configuration D

was introduced in order to study and compare the effects of less compression work but more irreversibility in the regeneration to the ones in configuration A. As part of his study, he states that the extremely high density of carbon dioxide allows very small size turbomachinery designs. Compact heat exchangers can also be attained due to the high density of CO2, larger pressure drop acceptability, and higher heat transfer coefficient. Angelino concluded that at temperatures above 650 °C and with the same maximum pressure of 200 atm, the efficiency of configuration A is higher than that of reheated steam cycle. He also stated that even though the configuration A presents lower efficiency than that in the reheat steam cycle for the temperatures below 650 °C, the simplicity and compactness of S-CO2 cycle offer better economy.

Finally in his third publication [45] on S-CO2 cycles, he investigated six new configurations in addition to three of the previously studied configurations in a wider range of operating temperatures and pressures. However, he limited his studies to the cycles in which the cooling processes were in subcritical temperature region, which makes his study not pertinent for locations where dry cooling is mandatory. Figure 1-7 presents the proposed configurations in his third publication.

He found that the number of turbine stages in S-CO2 cycles is much less than that in steam turbines. Moreover, he stated that the exhaust volumetric flow rate per unit power in steam cycles is 30 to 150 times more than that in S-CO2 cycles, which results in very compact S-CO2 turbine designs. Angelino performed several parametric studies through which the effects of inlet turbine conditions (temperature and pressure), compressor inlet conditions and heater inlet temperatures on the efficiency and specific power of S-CO2 cycle were comprehensively analyzed. Ultimately, he concluded that for a cooling water temperature of 5 °C and turbine inlet

temperature of 700 °C, the most efficient configuration for the operating pressures above 200 atm is the recompression configuration; while the precompression configuration presents higher efficiency for the pressure range of 150 to 200 atm. In addition, he inferred that S-CO2 cycles can provide up to 50% more efficiency than a steam cycle operating in the same condition. He also reported that reheat S-CO2 cycles present higher efficiency than double reheat steam cycles for a cooling water temperature of below 20 °C.

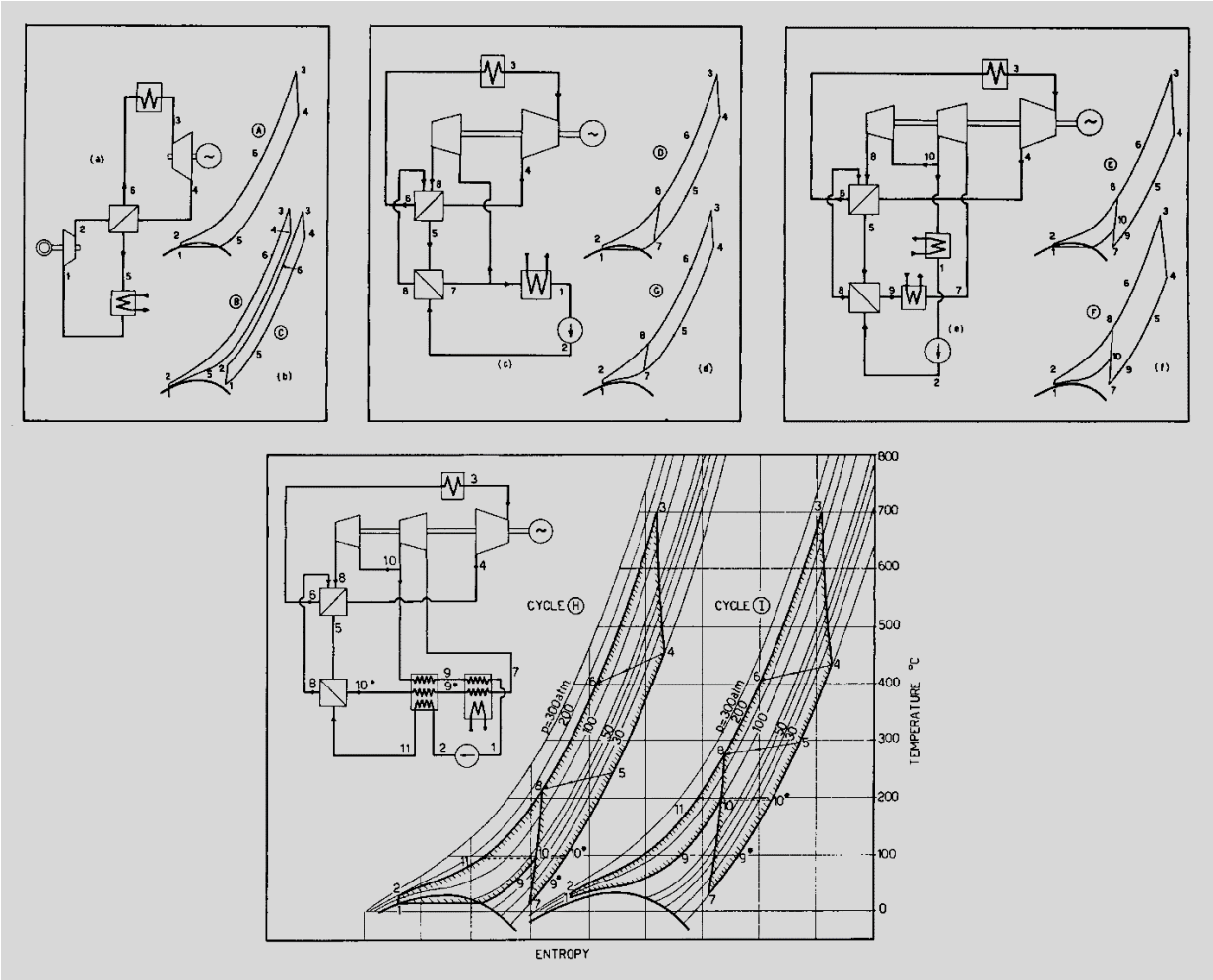

Figure 1-7: S-CO2 cycle configurations introduced by Angelino in [45]

1.4.2. Renaissance of S-CO2 Cycles

Despite all the efforts in analysis and design of S-CO2 cycles in the late 1960's and 1970's, the impulse driving the research and development of these cycles rapidly diminished in the late 1970's. It is most-likely that the decline was due to lack of knowledge and experience in design and manufacturing of turbomachineries, compact heat exchangers, seals and bearings required for the operating conditions of these cycles. Besides, the materials meeting all the thermal, mechanical and chemical requirements for the components of such cycles were either too expensive or not developed at the time. After being forgotten for almost three decades, the S-CO2 cycles began attracting more attention in the late 1990's and at the turn of this century due to substantial technological advancement. Several studies have been conducted throughout the world. However, the most comprehensive and effective efforts have been performed at MIT.

1.4.3. Studies at MIT

Following earlier studies [46, 47] at the Czech Technological University in the late 1990's, Dr. Vaclav Dostal comprehensively investigated the S-CO2 Brayton cycles in his PhD dissertation [48] which is considered as one of the most important breakthroughs in the subject. His PhD dissertation, which was in fact a collaborative research project involving several faculty members and research scholars at MIT, established an impetus for development of several other research projects at MIT and in other institutes and organizations. He employed a comprehensive code to evaluate the performance of various S-CO2 cycles consisting of compressors, turbines, recuperators and pre-coolers. The turbomachinery modeling subroutines were developed based on NASA design codes adapted for S-CO2 working fluid properties. He developed a more

detailed subroutine to model the heat exchangers. He performed primary parametric studies to locally optimize the performance of a simple S-CO2 cycle with the main focus on performance and sizing of heat exchangers. In the proposed optimization method, the length of the pre-cooler and recuperator, the split of the total heat exchanger volume between the recuperator and precooler and, the cycle pressure ratio were the only decision variables and other parameters were kept constant. After considering the addition of intercooling and reheating to the simple cycle, he stated that intercooling yields slight efficiency improvement; and it is not considered as an attractive option. Reheating offers a better potential; however, using more than one stage of reheat is economically unattractive.

After reviewing Angelino's results [44, 45], Dostal decided to investigate the recompression cycle layout through the rest of his dissertation as the most promising S-CO2 cycle layout. He compared the efficiency and capital cost of the recompression cycle with the ones in steam and helium cycles as presented in Figure 1-8. For the basic design, turbine inlet temperature was conservatively selected to be 550 °C and the compressor outlet pressure set at 20 MPa. For these operating conditions the cycle achieves 45.3 % thermal efficiency and reduces the cost of the power plant by almost 18% compared to a conventional Rankine steam cycle. The capital cost of the basic design compared to a helium Brayton cycle is about the same, but the supercritical CO2 cycle operates at significantly lower temperature. The turbine inlet temperature of an advanced design was considered 650 °C. The thermal efficiency of the advanced design is close to 50% and the supercritical CO2 cycle is almost 24% less expensive than the steam cycle and 7% less expensive than a helium Brayton cycle. It is expected in the future that high temperature materials will become available and a high performance design with

turbine inlet temperatures of 700 °C will be possible. This high performance design achieves a thermal efficiency approaching 53%, which yields additional cost savings.

He also compared the size of his S-CO2 preliminary design with the ones for helium and steam turbines designed by others. This comparison is presented in Figure 1-9. The fact that S-CO2 turbines are very compact and they require single casing are of great importance in terms of a power plant economy. Dostal also compared the efficiency of various power cycles such as helium Brayton, supercritical steam cycle and superheated steam cycle with the efficiency of S-CO2 cycle for the temperature range of 350 to 950 °C as presented in Figure 1-10. He affirmed that the supercritical CO2 cycle outperforms other cycles for the turbine inlet temperature of 550 and above.

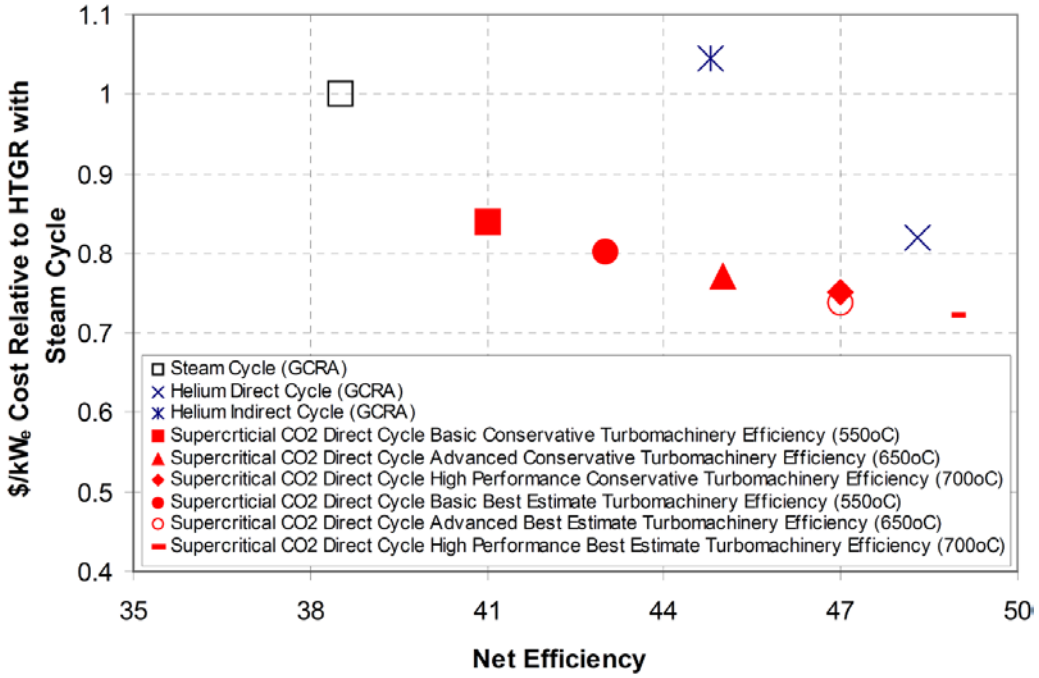

Figure 1-8: Net efficiency and relative costs for different power cycles ($/kW) [48]

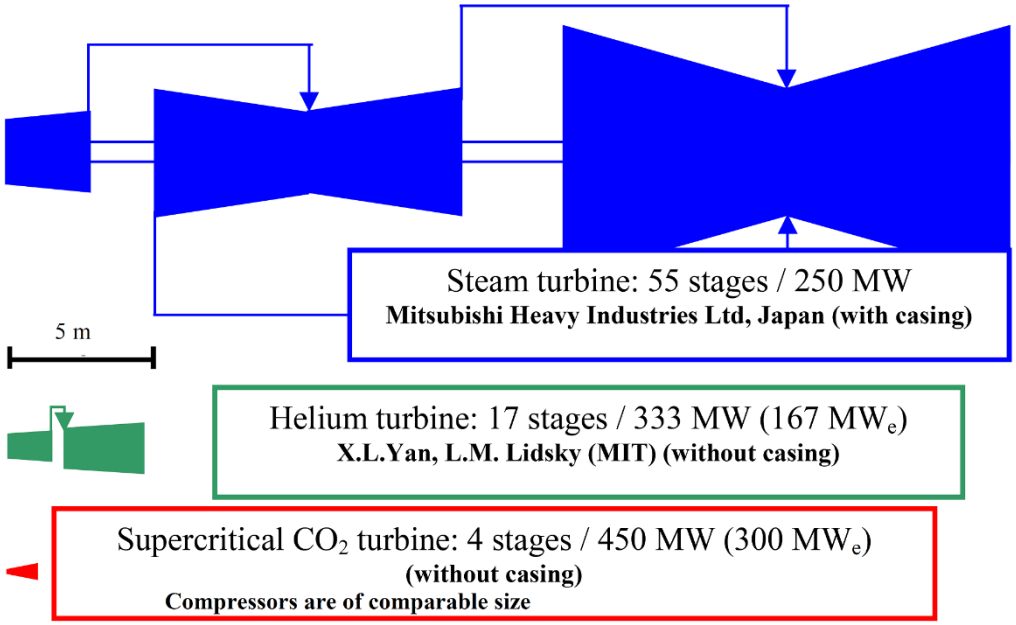

Figure 1-9: Comparison of turbine sizes [48]

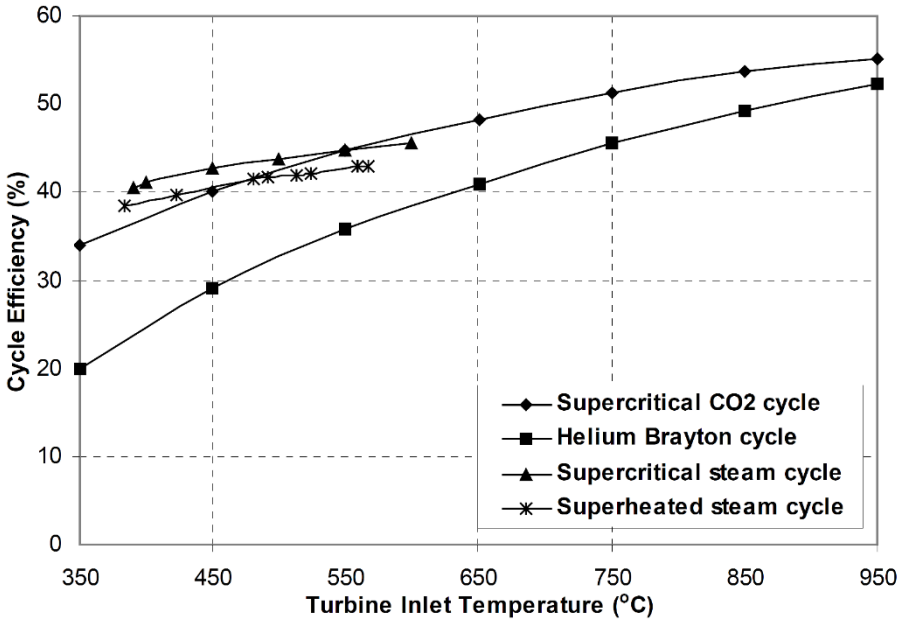

Figure 1-10: Cycle efficiency comparison of advanced power cycles [48]

1.4.4. Literature Review Closure

After the preliminary thermodynamic studies mainly by Angelino and Feher in 1960's and early 1970's, the focus of research on S-CO2 cycles was directed towards detailed design of comprising components (component-level study) such as pumps, compressors, turbines, and heat exchangers; and system-level thermodynamic studies and cycle optimization were left forgotten. In addition, the previous studies on S-CO2 cycles were merely for nuclear power applications. However, S-CO2 cycles have recently attracted considerable attention for new applications such as CSP, WHR and replacement of steam cycles in combined cycle power plants. According to the expert panelists of S-CO2 power cycle symposiums, which consist of policy makers in the U.S. Department of Energy (DOE) and leading industries in the field of power generation, the most practical and promising avenues for the utilization of S-CO2 power cycles are WHR and CSP applications. It should be noted that, the S-CO2 Brayton cycles can be utilized as the bottoming cycle in the combined cycle gas turbine (CCGT) power plants. This application, in general, can be considered as the WHR application in which the waste heat coming from the exhaust of gas turbines can be recovered and converted to power.

The recent shift towards new applications necessitates conducting a new set of system-level thermodynamic analyses of such cycles. It suffices to mention that even slight modifications in techno-economic features of a power cycle can turn a failing technology into a very appealing technology. Therefore, the thermodynamic optimization of power cycles is very crucial in the system-level studies. The previous studies on optimization of S-CO2 Brayton cycles are mostly done by parametric or gradient based methods which are limited to optimizing few decision variables; and may result in local rather than global optimum design point.

Moreover, further analysis and comparison of modifications such as recompression, reheating and intercooling at their optimum operating conditions are deemed to be essential.

Therefore, part of this dissertation is intended for system-level thermodynamic analysis and optimization of the S-CO2 Brayton cycles for high temperature CSP applications. Although maximizing the cycle efficiency in CSP applications seems to be the first priority, there are other thermodynamic performance indicators such as the specific power that needs to be considered and possibly maximized as well. Therefore, the considered optimization includes both single-objective and multi-objective optimization schemes to attain deeper understanding of the optimized performance. The optimization method is comprehensive (in contrast with parametric or gradient based optimization methods) in which the decision variables of a cycle are optimized simultaneously; and global (as opposed to local) optimum solutions are achieved.

In addition, only few studies can be found in which S-CO2 cycles have been investigated for waste heat recovery applications. And comprehensive studies, which present the optimum design variables of S-CO2 Brayton cycles for various waste heat source temperatures, have not been found. Interestingly, the WHR applications are expected to be the first among all other applications in which S-CO2 cycles will be implemented. As it will be discussed in Chapter 5, the WHR applications bring new aspects to the modeling and optimization of S-CO2 power cycles, which makes it necessary to study them independently of other applications. Consequently, this dissertation also covers the optimization of S-CO2 Brayton cycles for WHR applications.

1.5. Objectives and Scope of This Study

The primary goal of this dissertation is to optimize the conceptual design of the S-CO2 Brayton cycles for high temperature CSP and WHR applications. It should be noted that the framework of this dissertation only covers the analysis of S-CO2 power block, and it does not include the topping cycle in the WHR applications or the solar block in the CSP applications. The analysis is based on the thermodynamic performance of such cycles in design point and at steady state condition. The proposed methodology in this project is computational (mathematical modeling) and it does not involve any experimental studies. To achieve the specified goal, the following objectives have to be accomplished.

1.5.1. Objective 1

Develop a comprehensive modeling tool to reliably predict the thermodynamic performance of various configurations of the S-CO2 Brayton cycle at steady state condition. The considered configurations include a combination of recuperation, recompression, reheating and intercooling. The model should be fully flexible in terms of entirely covering the feasible design domain, and rectifying possible infeasible solutions. The flexibility of the model should also include the consideration of switching input parameters and design variables with performance variables interchangeably. Moreover, dealing with time consuming optimization problems imposes a very important factor which is the model's ability to perform the cycle calculation in a fraction of a second.

1.5.2. Objective 2

Develop an appropriate optimizer tool in order to perform both single-objective and multi-objective optimization problems. The optimizer tool should be able to integrate with the developed modeling tool, and reliably solve the optimization problems. The optimizer tools should have the capability of optimizing non-linear systems with several decision variables simultaneously, and without being trapped in local optimum points. The optimizer tools should also be easily adaptable for various objective functions as this feature would be very beneficial in analyzing the power blocks from different aspects, and also for similar projects in future.

1.5.3. Objective 3

Validate both the modeling results, and reliability and robustness of the optimization tool. The relative error of the modeling results (as compared to acquired appropriate data) should be within a reasonable range. Moreover, performance of the optimization tool is evaluated by well-known benchmark problems that are commonly used in order to rigorously test procedures specialized for multi-dimensional, non-linear optimization problems with numerous local optimums.

1.5.4. Objective 4

Perform the thermodynamic analyses and optimization, and develop a set of guidelines leading to optimum operation of the S-CO2 Brayton cycles for high temperature CSP and WHR applications. The thermodynamic analyses include both energy and exergy approaches. Combining the energy and exergy analyses provides valuable information regarding interactions

between the components and their ultimate effects on cycle performance; efficiency potential and performance improvement options; and advantages and disadvantages of considered configurations over each other.

1.6. Dissertation Organization

After the brief introduction, literature review and the project objectives that were presented in the preceding sections, Chapter 2 describes the research plan and the methodology put to use to achieve the objectives of this project. It provides concise explanations on the studied power cycle configurations, the thermodynamic modeling methodology, the optimization schemes, and the validation of the developed tools.

In Chapter 3, four configurations of S-CO2 Brayton cycles are thermodynamically optimized for maximum cycle efficiency. This optimization strategy is of high priority in all applications similar to CSP in which the closed loop heat sources are utilized. Furthermore, a thorough thermodynamic analysis based on both 1^{st} and 2^{nd} laws of thermodynamics are performed in order to understand advantages and disadvantages of the cycle configurations over each other, and also detect and quantify the sources of inefficiencies.

In Chapter 4, the importance of another design characteristic, i.e., cycle specific power is introduced. Two most promising configurations of S-CO2 Brayton cycles are selected, and a multi-objective optimization scheme are conducted to arrive at optimum trade-off solutions between cycle efficiency and specific power.

In Chapter 5, the power generation from waste heat recovery is studied. There are critical considerations regarding the WHR application, which leads to a different optimization strategy

as compared to the one in CSP applications. Ultimately, a new set of guidelines for optimum operation of S-CO2 Brayton cycles is presented.

Finally, in Chapter 6, a summary of what have been done throughout of this dissertation and main conclusions are presented. Ultimately, the contributions of this research along with suggestions for future research topics will be discussed.

2. METHODOLOGY

2.1. Introduction

The main goal of this study is to optimize the conceptual design of S-CO2 Brayton cycles for high temperature concentrated solar power (CSP) and waste heat recovery (WHR) applications. Although several aspects such as material strength, vibration, machining methods, assembling, maintenance, etc. should be considered when it comes to designing and manufacturing the components of S-CO2 Brayton cycles, the approach of this study is a system-level lumped-volume approach, in which the interactions between components are considered in order to understand how they contribute in performance indicators of the comprising system as a whole. In the system-level lumped-volume approach considered for this project, the focus is merely the thermodynamic performance of the S-CO2 Brayton cycle as a system; and it does not deal with the detailed design of components. However, the components are mathematically modeled by means of certain characteristic parameters which are accurate enough to represent the performance of components. The characteristic parameters are chosen in reasonable ranges based on current or near-future available technologies to avoid any conflict with other aspects of the design and manufacturing. As also stated in the first chapter, the scope of this study only covers the power blocks for which thorough thermodynamic analyses and optimization of S-CO2 Brayton cycles in design point and at steady state condition are performed. To this end, four objectives, which were explained in the first chapter, have to be met. This chapter addresses the designated objectives one by one through a brief description of the methodology adopted in this

study. Once again, it is worth mentioning that the proposed methodology in this project is computational (mathematical modeling) and it does not involve any experimental studies.

2.2. Modeling Tool

2.2.1. Description of Studied Configurations

Simplicity plays an important role in manufacturing and cost effectiveness of a power cycle. Although several S-CO2 power plant configurations have been proposed, only few of them are practically promising options [49]. Therefore, four most promising configurations have been selected to be investigated in this study. The considered configurations are all based on the recuperated closed-loop Brayton cycle with various modifications in order to increase thermal efficiency and/or specific power of the cycle.

The simplest studied configuration is a simple recuperated cycle (RC). Figure 2-1 depicts the RC plant layout along with its T-s diagram. In this configuration, carbon dioxide is pressurized by the compressor, and absorbs heat through the recuperator and main heater. Carbon dioxide then expands in the turbine to a lower pressure level and generates power. The exhaust of the turbine still carries significant amount of thermal energy which is recovered in the recuperator. In order to close the cycle, carbon dioxide needs to be cooled down in the cooler to the inlet temperature of the compressor. It is noteworthy that the main heater is either a heat exchanger in WHR applications or a solar receiver in CSP applications.

As also explained in the introductory chapter, the recuperation process in the RC configuration introduces significant exergy destruction (irreversibility in heat transfer) to the

cycle, which is due to temperature pinching problem. To overcome this issue, the recompression recuperation cycle (RRC) has been proposed.

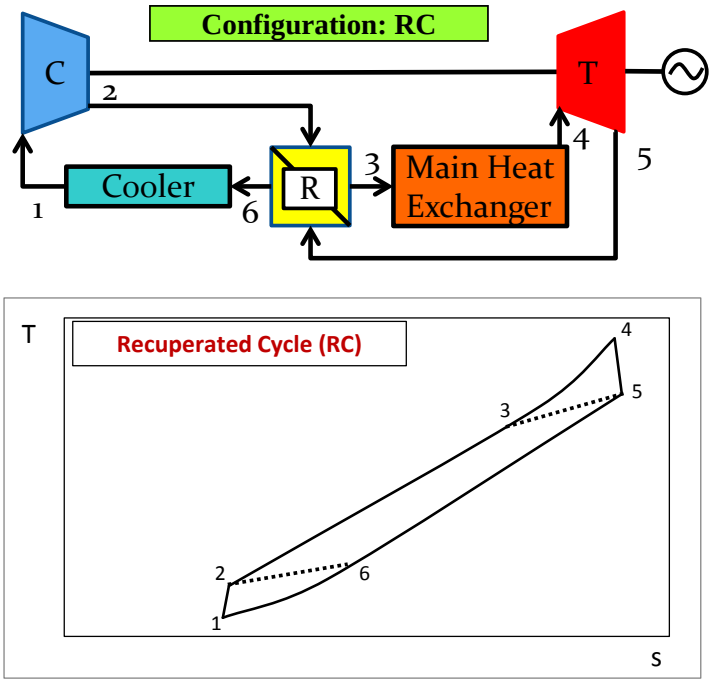

Figure 2-1: Simple recuperated cycle (RC): configuration layout (up); T-s diagram (bottom)

As illustrated in Figure 2-2, RRC configuration employs two distinct recuperators which are the high temperature recuperator (HTR) and low temperature recuperator (LTR). The low pressure flow is divided into two streams after leaving the LTR and the cooler #2 at point 9. A fraction of the flow rejects heat to the cooler #1 and enters the main compressor (C #1), while the other fraction is pressurized in the recompression compressor (C #2). Both flow fractions are mixed at point 3, and enter the high pressure side of the HTR and the main heater. After expanding in the turbine, the flow is directed towards the low pressure side of the HTR and LTR to preheat the high pressure flow.

Utilizing double recuperation in the RRC configuration reduces the total heat capacity of the flow going through the high pressure side of the LTR. This alleviates the pinching problem and reduces the exergy destruction in the recuperation process as illustrated in Figure 2-3. It is noteworthy to mention that the heat capacity value determines the slope of heat transfer lines in the T-Q diagrams.

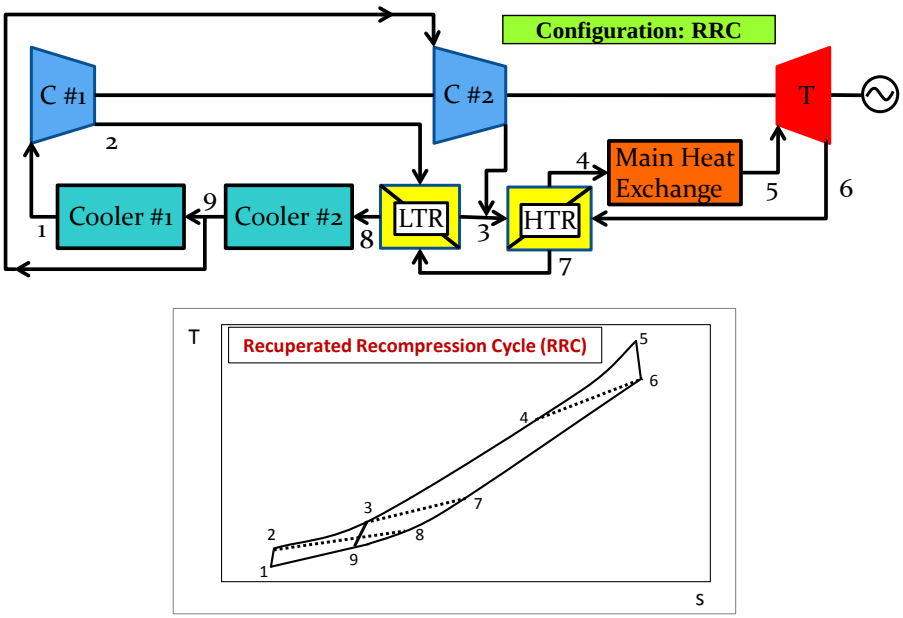

Figure 2-2: Recompression recuperated cycle (RRC): configuration layout (up); T-s diagram (bottom)

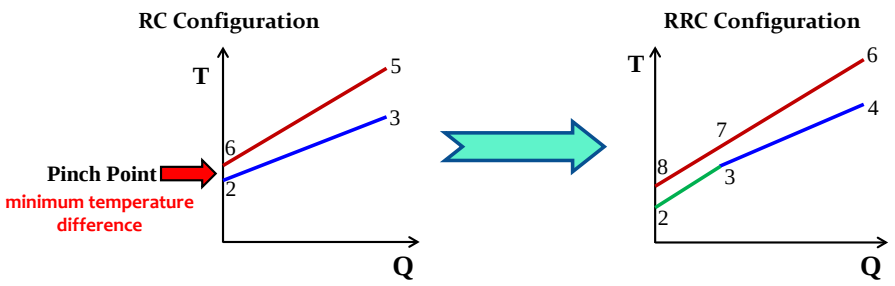

Figure 2-3: The effect of double recuperation in RRC on temperature pinching and exergy destruction

In order to study the effect of reheating on S-CO2 Brayton cycles, the recompression recuperated cycle with reheat (RRCR) has also been modeled. Figure 2-4 shows the layout of the RRCR configuration along with its T-s diagram.

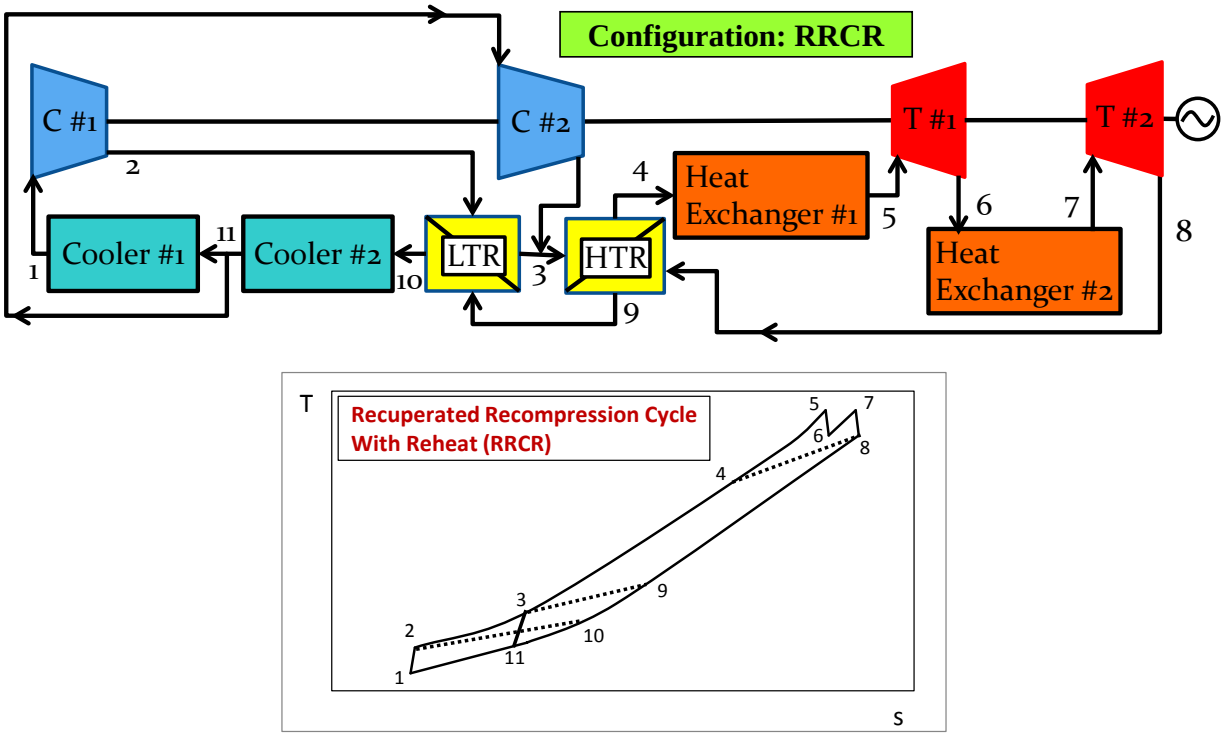

Figure 2-4: Recompression recuperated cycle with reheat (RRCR): configuration layout (up); T-s diagram (bottom)

The last considered configuration is the recompression recuperated cycle with reheat and intercooling (RRCRI). Although the combination of double recuperation with reheating and intercooling increases the complexity level, it may be justifiable as this configuration is expected to offer significant improvement in both efficiency and specific power. The layout of RRCRI configuration and its T-s diagram are presented in Figure 2-5.

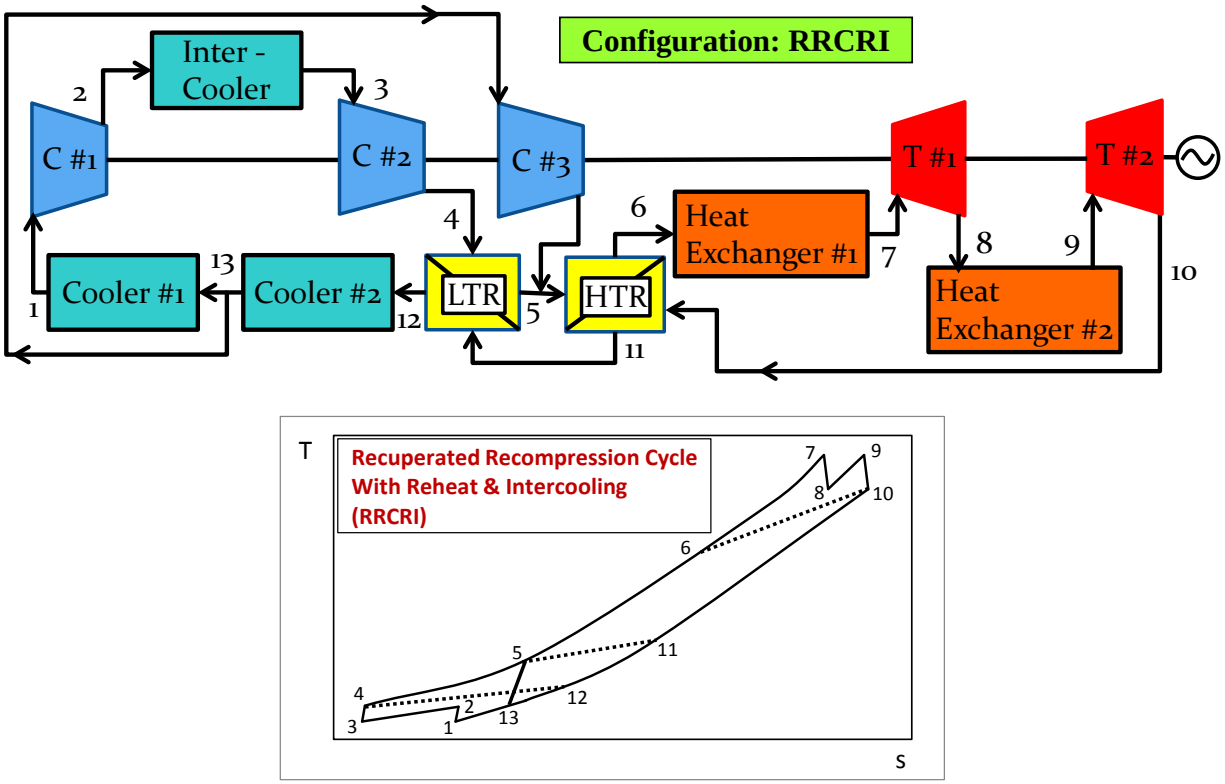

Figure 2-5: Recompression recuperated cycle with reheat and intercooling (RRCRI): configuration layout (up); T-s diagram (bottom)

A system-level modeling tool has been developed in FORTRAN programming language, which enables one to predict and analyze the thermodynamic performance of the aforementioned S-CO2 Brayton cycle configurations at steady state condition.

2.2.2. S-CO2 Properties

The first step in thermodynamic modeling of S-CO2 cycles is the calculation of the working fluid properties. In order to calculate the thermodynamic properties of carbon dioxide, a set of FORTRAN source codes were put to use as certain subroutines in the developed main modeling program. These FORTRAN source codes are presented by National Institute of

Standards and Technology (NIST) in a software package named “REFPROP” [50]. The REFPROP is a computer program which can generate several databases for fluid properties. It does not utilize any experimental data, aside from certain constant parameters such as critical and triple points of the pure fluids. The program uses the most accurate equations of states and thermodynamic relations to calculate the properties of fluids. The equations are generally valid over the entire vapor and liquid regions of the fluid, including supercritical states; the upper temperature limit is usually near the point of decomposition of the fluid, and the upper pressure (or density) limit is defined by the melting line of the substance. In the case of carbon dioxide, the employed equations are extracted from the original work published by Span and Wagner [51].

2.2.3. Assumptions

This study is based on the thermodynamic performance of S-CO2 Brayton cycles in design point and at steady state condition. The choice of heat source and application introduces certain limitations and determines the values of input parameters such as maximum allowable turbine inlet temperature (TIT) and minimum allowable compressor input temperature. In addition, the deviation between the real and ideal processes in turbines and compressors is considered by assuming constant isentropic efficiencies, which has also been suggested in system level optimization problems by many authors [49, 52-55]. The isentropic efficiencies of turbines and compressors are input parameters to the model. Moreover, as suggested by other authors including Angelino in [43] and Chacartegui et. al. in [56], the pressure drop in the heat exchangers and ducts are also taken into account by introducing fractional pressure drop (FPD)

as an additional input parameter. The FPDs can be implemented in the modeling either in a piecewise manner or immediately downstream of the compressors. The assumed values of input parameters for each application (WHR or CSP) will be presented in the corresponding chapters.

In addition to input parameters, the choice of variables is of great importance. The variables in the modeling are categorized into decision variables and dependent variables. The dependent variables are calculated through the modeling procedure by using the decision variables. The dependent variables include the cycle performance indicators such as the cycle efficiency, specific power, exergy flows, irreversibilities, cooling loads, recuperated heat, effectiveness of heat exchangers, etc. The decision variables determine the thermodynamic performance of the cycle; therefore, the optimization should be performed on them. As long as all decision variables are independent from each other, the decision variables and dependent variables can be replaced one another depending on the type of analysis and conclusion one may wish to implement. The author has tried to identify as many decision variables as possible in a way that the modeling demonstrates more flexibility and the optimization displays more meaningful and valuable results. The considered decision variables for each cycle configuration are listed in Table 2-1. Note that the parenthesized numbers in Table 2-1 correspond to the points presented in the plant layout (Figure 2-1, Figure 2-2, Figure 2-4, Figure 2-5) for each configuration.

Table 2-1: Decision variables in all configurations

Decision Variables in Configuration: RC	Decision Variables in Configuration: RRC
Compressor Inlet Temperature, T(1)	Main Compressor Inlet Temperature, T(1)
Turbine Inlet Temperature, T(4)	Turbine Inlet Temperature, T(5)
Minimum Terminal Temperature Difference, ΔT_t	Inlet Temperature of Recompression, T(9)
Compressor Inlet Pressure, P(1)	Minimum Terminal Temperature Difference, ΔT_t
Compressor Outlet Pressure, P(2)	Main Compressor Inlet Pressure, P(1)
	Main Compressor Outlet Pressure, P(2)
	Main Compressor Mass Flow Fraction
Decision Variables in Configuration: RRCR	**Decision Variables in Configuration: RRCRI**
Main Compressor Inlet Temperature, T(1)	Main Compressor Inlet Temperature, T(1)
Turbine Inlet Temperature, T(5)	Inlet Temperature of 2nd Compressor, T(3)
Reheat Temperature, T(7)	Turbine Inlet Temperature, T(7)
Inlet Temperature of Recompression, T(11)	Reheat Temperature, T(9)
Minimum Terminal Temperature Difference, ΔT_t	Inlet Temperature of Recompression, T(13)
Main Compressor Inlet Pressure, P(1)	Minimum Terminal Temperature Difference, ΔT_t
Main Compressor Outlet Pressure, P(2)	Main Compressor Inlet Pressure, P(1)
Inlet Pressure of Reheater, P(6)	Inlet Pressure of Intercooler, P(2)
Main Compressor Mass Flow Fraction	2nd Compressor Outlet Pressure, P(4)
	Inlet Pressure of Reheater, P(8)
	Main Compressor Mass Flow Fraction

2.2.4. Modeling Procedure

The overview of the system-level modeling procedure is presented in Figure 2-6. The input parameters and decision variables are known inputs to the model. The major components in a recuperated S-CO2 Brayton cycle are compressors, turbines, recuperators, and coolers. A set of equations for each component is formed by applying the energy and mass conservation laws; and depending on the component, either turbomachineries or heat exchangers, definitions such as

isentropic efficiencies and minimum terminal temperature difference (TTD) are employed to complete the sets of equations. Then completed sets of equations are solved through an iterative and sequential algorithm; and the values of unknown dependent variables such as outlet thermodynamic states of compressors, turbines, and recuperators are attained. Ultimately, the cycle's performance indicators such as cycle efficiency, specific power, and so forth are calculated.

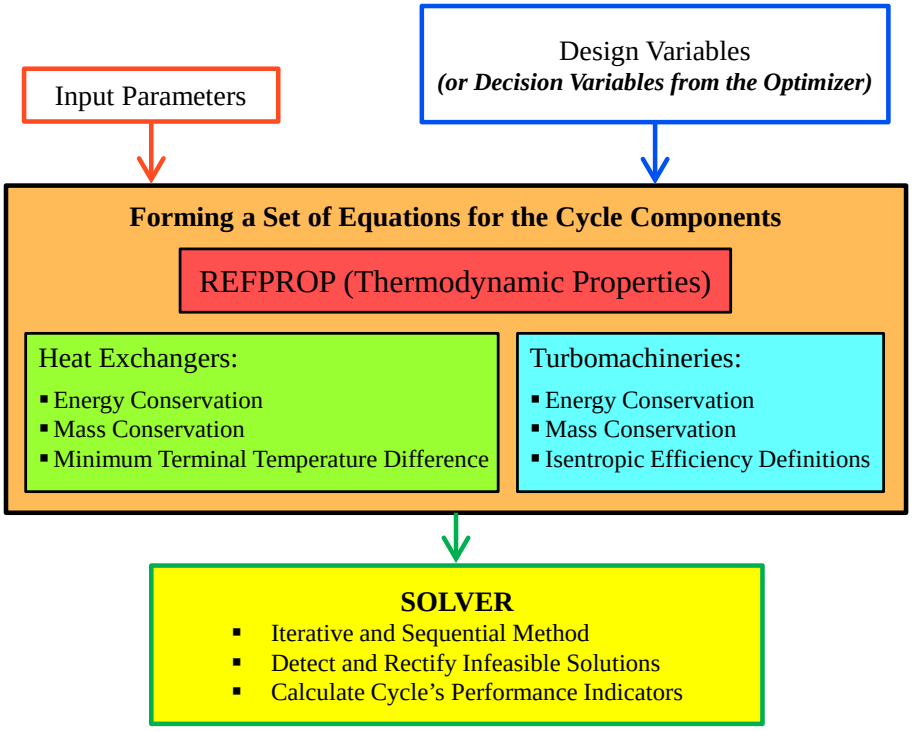

Figure 2-6: The overview of the system-level modeling

The modeling procedure starts with fixing all the thermodynamic states of the cycle. Note that a thermodynamic state is considered as a fixed (or known) state if two independent thermodynamic properties are known. This means all the required thermodynamic properties (in the region of interest) can be computed by knowing any combination of pressure with

temperature, enthalpy, or entropy via REFPROP. The input parameters and decision variables are known inputs to the model; and unknowns are the dependent variables. The inlet and outlet pressures of compressors are known (decision variables). Therefore, the pressure of all states can be calculated by using the values of fractional pressure drop. Since the inlet temperature of all compressors and turbines are also known via decision variables, the inlet states of the compressors and the turbines are concluded to be fixed (known). Considering the fact that the outlet specific entropy is equal to the inlet specific entropy in an isentropic process, the isentropic outlet of the compressors and turbines are also fixed. By using Eq. (2-1) and Eq. (2-2), the actual outlet states of the compressors and turbines are calculated using the values of the isentropic efficiencies.

$$\eta_{comp} = \frac{h_{out,is} - h_{in}}{h_{out} - h_{in}} \tag{2-1}$$

$$\eta_{turb} = \frac{h_{in} - h_{out}}{h_{in} - h_{out,is}} \tag{2-2}$$

In the RC configuration, the equation set for the recuperator is formed by applying the conservation of mass and energy. The set of equations is completed by using the definition of terminal temperature difference. However, the recuperator modeling in other configurations, which involve recompression, is different from the one in the RC configuration. Since all recompression configurations (RRC, RRCR and RRCRI) employ the same double recuperation process, the procedure for computing the unknown states associated with LTR and HTR is explained based on the RRC configuration.

In the RRC configuration, the states 2 and 3 are fixed (compressor outlet). The mass flow rate going from point 2 to 3 can be generally any value depending on the value of mass flow fraction (decision variable). Therefore, the minimum terminal temperature difference (which is the pinch point temperature difference under certain conditions) can occur at any end (that is, either at hot end between 3 and 7, or at cold end between 2 and 8) of the low temperature recuperator (LTR). As a first guess, the minimum terminal temperature difference is assumed to be at the cold end between points 2 and 8. The temperature of point 8 is calculated by Eq. (2-3), which makes point 8 as a fixed state. Equation (2-4) determines the enthalpy of point 7.

$$T_8 = T_2 + \Delta T_{PP} \tag{2-3}$$

$$h_7 = h_8 + [(f)_{2-3} \times (h_3 - h_2)] \tag{2-4}$$

In order to test the first guess on the location of the minimum terminal temperature difference, the temperature of point 7 should be compared to the temperature of point 3. If the temperature difference between points 3 and 7 is less than the minimum terminal temperature difference, our first guess was wrong; and the pinch point location is at point 3. Then, the same procedure can be employed to calculate the enthalpy of point 8 by using Eq. (2-5) and Eq. (2-6).

$$T_7 = T_3 + \Delta T_{PP} \tag{2-5}$$

$$h_8 = h_7 - [(f)_{2-3} \times (h_3 - h_2)] \tag{2-6}$$

The last unknown state (point 4) can be fixed by using Eq. (2-7).

$$h_4 = h_3 + (h_6 - h_7) \tag{2-7}$$

After solving the sets of equations, cycle's performance indicators such as cycle efficiency, specific power, exergy flows, irreversibilities, cooling loads, recuperated heat, effectiveness of heat exchangers, and so forth are calculated.

The presented procedure is a simplified description of the actual algorithm that has been coded. The model is designed to be fully flexible so that it can easily be integrated with the optimizer tool (Genetic Algorithm) in a black box approach. Since the thermodynamic model is supposed to be integrated with the GA optimizer tools, it is possible that the combination of input decision variables leads to mathematically faultless solutions, but physically infeasible regions. Therefore, it is essential to identify appropriate indicators of ill-conditioned solutions and contrive several check points and remedies into the code in order to rectify any infeasible solutions.

2.3. Optimization Tool

2.3.1. Genetic Algorithm (Optimizer Justification)

The thermodynamic performance of energy systems is generally nonlinear, discontinuous; and has several local optima. In many cases, several decision variables exist which makes the optimization space multi-dimensional. As the number of decision variables increases, the interaction between subsystems and mathematical relations become tremendously complex; and traditional gradient based optimization algorithms become more tedious and in some cases even impractical. Since genetic algorithm (GA) presents uniquely advantageous features in optimization problems, it has been selected in this study as the optimizer core in both

the single-objective and multi-objective optimization schemes. In contrast with gradient based optimization methods, GA is a powerful evolutionary optimization method and can be competently adopted to address almost any optimization problem. GA has the capability of optimizing non-linear systems with several decision variables simultaneously, and without being trapped in local optimum points. The main advantage of GA is that it does not require any analytical or numerical derivatives of the system's governing equations, which eliminates extra mathematical preparation and complexities in modeling. In other words, GA treats the system as a black box. As it is also depicted in Figure 2-7, in the black box approach, the optimizer and the model are two separate entities. The optimizer analyzes the system behavior and the only interaction between the optimizer and the simulator (computational model) is in the form of the decision variables and the corresponding values of the system's performance indicators (or the fitness function). Moreover, GA finds the global optimum solution as opposed to gradient based algorithms that may be trapped in a local optimum point as a result of unfitted initial guess.

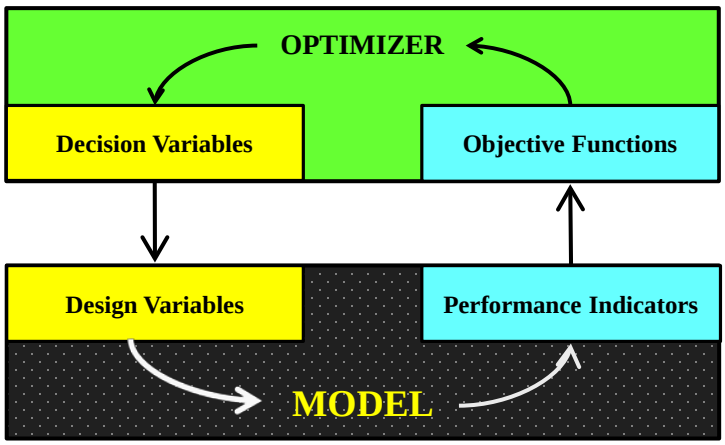

Figure 2-7: The interactions of optimizer and model in a black box approach

This optimization approach also makes it possible to perform the system-level optimization. In contrast to optimization of components individually, the system-level optimization not only considers the performance of components, but also takes into account the interactions among them. In other words, the system-level optimization yields the ultimate goal which is the optimum performance of the system as a whole, not the components individually. To that end, an in-house main program, in which genetic algorithm (GA) is the optimizer core, has been coded in FORTRAN programming language. The integration of the modeling and optimization tools is significantly facilitated by developing in-house codes for both entities in FORTRAN programming language. Employing the fast processing FORTRAN language also ensures reasonable computational run-time which is essential in optimization problems.

2.3.2. Brief Description of GA as Optimizer Core

The first task in utilizing the GA is to specify the optimization domain. The domain of optimization is specified by the variation range of all decision variables. Then, the fitness function (or objective function) is defined based on one or more cycle performance indicators to be maximized. The operation of Genetic Algorithm can be described in five steps:

1) A random population of individuals is generated. The identity of each individual is determined by a combination of values for the decision variables.

2) The fitness function (objective function) for each individual is evaluated and individuals are sorted based on this criterion.

3) The fittest individuals, or in other words, individuals with greater values of fitness function are selected as parents to the next generation. For this purpose, fundamental genetic

rules (marriage, mutation and talent preservation) are applied to this selected group and a new generation with the same number of individuals as the previous generation is generated.

4) The new generation is again evaluated based on the fitness function. It is expected that the new generation that had healthy parents is better than the previous generation.

5) This process continues till health or fitness of the best individual does not change for several generations.

For more information on GA one may refer to [57-59].

2.3.3. Multi-Objective Optimization Scheme

In this study, two system-level optimization schemes (i.e. single-objective and multi-objective) are considered for closed loop heat source (e.g. CSP) applications. The optimization is merely based on thermodynamic analysis. Therefore, the objective or fitness function is defined based on the thermodynamic performance indicators of the cycles. The main performance indicator of thermodynamic power cycles in such applications is the efficiency which is considered as the objective function to be maximized in the single-objective optimization scheme. In addition to the cycle efficiency, the cycle specific power is a comparably important parameter when it comes to investment and decision making. Thus, a multi-objective optimization is to be carried out in which cycle efficiency and specific power are competing objectives, and should be maximized simultaneously. The purpose of this optimization scheme is to determine the trade-off curve that exists between the different objectives. In this way, a range of optimum solutions (Pareto front) is presented to decision makers, which enables them to

choose the desired compromise between the objectives and avoid naive solutions obtained from single-objective optimization.

There are several approaches to solve multi-objective optimization problems using evolutionary based algorithms. In this study, a weight-based (or preference-based) multi-objective optimization scheme is chosen. This method basically forms a composite objective function (Eq. (2-10)) as the weighted sum of the objectives, where a normalized weight for an objective is proportional to the preference factor assigned to that particular objective. This approach transforms a multi-objective optimization problem to several single-objective optimization problems. The described multi-objective optimization problem can be stated in the form of Eq. (2-8) through (2-11).

$$Maximize\ f_1 = \eta_c\ (cycle\ efficiency) \tag{2-8}$$

$$Maximize\ f_2 = \phi_{sp}(specific\ power)$$

In general, the values of objective functions can vary with different orders of magnitude, which can potentially induce a biased optimization process in the favor of one objective over the other. In order to rectify this issue, the objective functions should be normalized by means of Eq. (2-9) before implementing them in Eq. (2-10).

$$f_1 = \frac{\eta_c}{\eta_{c,max}} \quad ; \quad f_2 = \frac{\Phi_{sp}}{\Phi_{sp,max}} \tag{2-9}$$

A composite objective function would be:

$$F = w_1 f_1 + w_2 f_2 \tag{2-10}$$

Based on the designers experience or higher level information at hand one can choose a preference vectors (w1 and w2) corresponding to each objective functions and then the composite function is optimized to find a single trade-off optimal solution by a single-objective optimization algorithm. Further, the above procedure is used to find multiple trade-off solutions by using an incremental preference vectors and repeating the above procedure as shown below.

$$
\begin{aligned}
F &= 1(f_1) + 0(f_2) \\
F &= 0.9(f_1) + 0.1(f_2) \\
F &= 0.8(f_1) + 0.2(f_2) \\
&\;\;\vdots \\
F &= 0(f_1) + 1(f_2)
\end{aligned}
\tag{2-11}
$$

The use of above method results in several sets of optimal solution clusters which are superposed next to each other to form the optimum trade-off curve. The trade-off curve is in fact a range of optimum solutions which is also known as Pareto front. Figure 2-8 depicts how the Pareto front dominates other feasible solutions and provides the optimum trade-off curve.

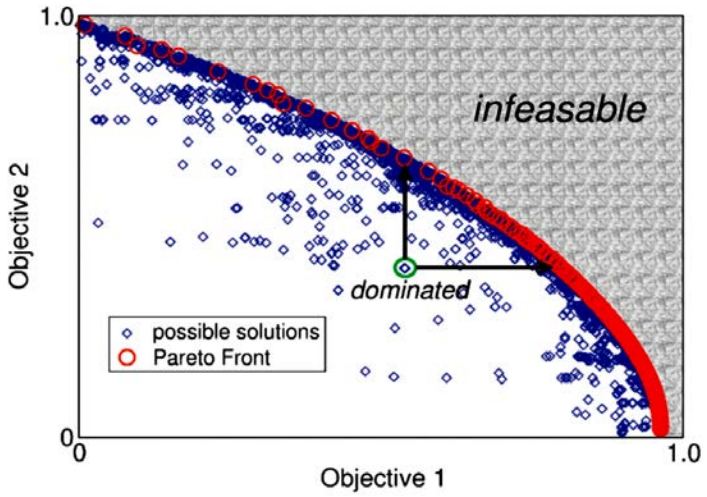

Figure 2-8: Schematic of a Pareto front in a two objective optimization problem

The results of this optimization scheme provides not only an optimum thermodynamic trade-off curve between the efficiency and the specific power, but also better techno-economic insight into the S-CO2 Brayton cycles for closed loop heat source applications such as CSP.

2.4. Tools Validation

2.4.1. Validation of Modeling Tool

Since the experimental data for the S-CO2 Brayton cycles in a laboratory scale is not either sufficient or available, and neither pilot nor commercial scales have been built yet, the validation of the modeling results is performed through result comparison with reliable published data. One of the major challenges is to find apposite publications that provide enough modeling details in terms of the algorithm, input parameters, design variables, and performance indicators. The preliminary search revealed that there were only a few publications on this subject, and not all of them present the required details for the validation purpose. The author also learned that all

available publications referred to the algorithm presented by Dostal at MIT [48] as their modeling approach. As compared to the modeling algorithm used in this study, Dostal's approach is different in input design variables; and it presents less flexibility in terms of covering the feasible design domain completely. Ultimately, the author was able to identify two publications by Dostal [60, 61] that provide enough details to rectify the issue with the difference in input design variables. These publications present several modeling results for both simple recuperated (RC) and recompression (RRC) configurations. Table 2-2 presents the results comparison of various design points for the RC configuration. The constant parameters are tabularized in the top section; and the cycle efficiency is calculated in different pressure ratios. The results comparison presents almost perfect conformity.

Table 2-2: Validation results for the RC configuration

Tmin (K)	Tmax (K)	P max (Kpa)	Turbine Efficiency (%)	Compressors Efficiency (%)
305.15	823.15	20000	90	89

Pressure Ratio	Efficiency (%) (Dostal)	Efficiency (%) (CATER)	Difference (%)
2.1	38	37.98	0.02
2.4	36.16	36.15	0.01
2.8	38.27	38.27	0
3.7	38.03	38.04	-0.01
4	37.65	37.66	-0.01

Similarly, the validation was also performed for the RRC configuration; and the results are presented in Table 2-3 and Table 2-4 for various pinch point temperature differences. These results are based on constant pressure ratio in Table 2.4, and constant TIT in Table 2-4. The validation results of the RRC configuration also demonstrate negligible differences in the cycle

efficiency except in one case with the efficiency difference of 0.16%. Detailed examination of the published data revealed that the error was due to miscalculation of CO2 properties at turbine exit in [61].

Table 2-3: Validation results for the RRC configuration (variable TIT, constant pressure ratio)

Tmin (K)	P min (Kpa)	P max (Kpa)	Turbine Efficiency (%)	Compressors Efficiency (%)
305.15	7692.3	20000	90	89

Tmax	ΔTpp	Recompressed Fraction	Efficiency (%) (MIT)	Efficiency (%) (CATER)	Difference (%)
823.15	8.49	0.400	45.3	45.307	-0.007
923.15	7.81	0.405	49.5	49.340	0.160
973.15	9.95	0.410	51.3	51.316	-0.016

Table 2-4: Validation results for the RRC configuration (constant TIT, variable pressure ratio)

Tmin (K)	Tmax (K)	P max (Kpa)	Turbine Efficiency (%)	Compressors Efficiency (%)
305.15	823.15	25000	90	89

Pressure Ratio	ΔTpp	Recompressed Fraction	Efficiency (%) (Dostal)	Efficiency (%) (CATER)	Difference (%)
2.6	8.26	0.2354	44.6	44.59	0.01
2.7	9.37	0.2824	45.1	45.07	0.03
2.8	10.45	0.3159	45.5	45.46	0.04
2.9	11.16	0.338	45.8	45.8	0
3	11.85	0.3547	46.1	46.08	0.02

2.4.2. Validation of Optimization Tool

In the realm of optimization, benchmarks are used to assess how effectively optimizer codes can perform. Therefore, two extreme benchmarks were identified to evaluate the

developed optimization code. These benchmarks are considered as stringent standards for nonlinear and multidimensional optimization problems with numerous local extrema. This class of optimization is considered as the most convoluted optimization problems.

The first identified benchmark is known as Rastrigin's function which is a combination of De Jong function and cosine terms in the form of Eq. (2-12).

$$f(x) = 10n + \sum_{i=1}^{n} [x_i^2 - 10\cos(2\pi x_i)] \tag{2-12}$$

Figure 2-9 displays this function in 2-D. It is non-convex, multimodal and additively separable. It has one global minimum and several local optima whose locations are regularly distributed in the optimization domain. Test area is usually restricted to a hyphercube in which all decision variables are allowed to vary between -5.12 and +5.12. The function value equals zero at its global minimum point where all decision variables are zero. This function is considered as a very difficult optimization problem due to its nonlinearity, large search space and large number of local minima.

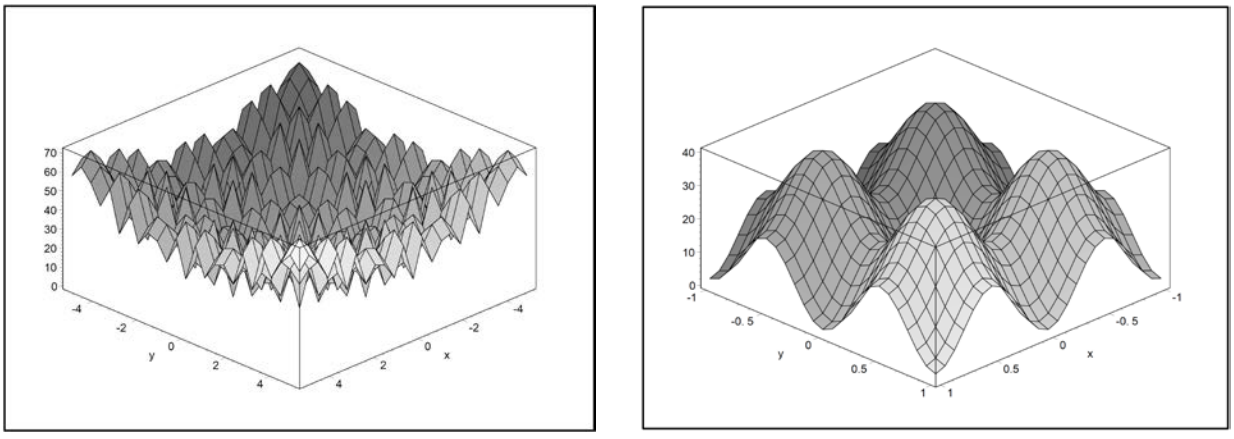

Figure 2-9: Rastrigin's function in 2-D (Left: medium scale view, Right: zoomed-in view) [62]

The second identified benchmark is known as Griewangk's function in which many widespread local minima exist. The mathematical representation of this function is in the form of Eq. (2-13).

$$f(x) = \frac{1}{4000}\sum_{i=1}^{n} x_i^2 - \prod_{i=1}^{n} \cos\left(\frac{x_i}{\sqrt{i}}\right) + 1 \tag{2-13}$$

The geometrical interpretation of this function varies with the zooming extent. In a large scale, the first overview represents a wrong impression of a convex function. However, the medium scale view displays many local extrema. Ultimately, the zoomed-in view reveals the complex arrangement of the local extrema. The optimization domain is usually defined as a hypercube in which all decision variables are allowed to vary between -600 to +600. Figure 2-10 demonstrates this function in 2-D. The function values of all local minimums in the vicinity of the global minimum are slightly higher than zero. However, the function equals zero at its global minimum where all the values of all decision variables are zero.

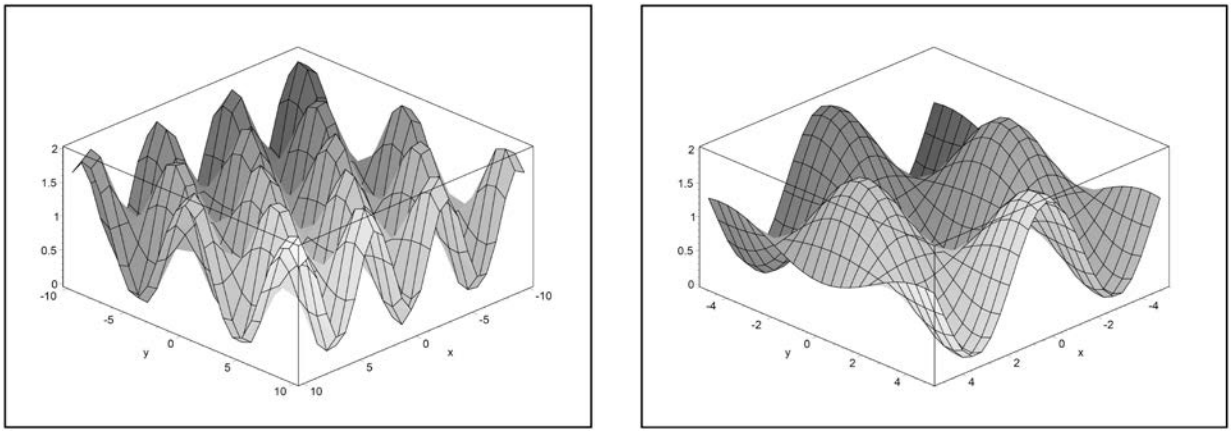

Figure 2-10: Griewangk's function in 2-D (Left: medium scale view, Right: zoomed-in view) [62]

The developed optimization tool was put to test by both Rastrigin's and Griewangk's functions. Since the maximum number of decision variables in the optimization of the S-CO2 cycle configurations is eleven (RRCRI configuration), the dimension of both functions were raised from 2-D to 11-D. It is noteworthy that these benchmarks become extremely more complicated in 11-D. The evaluation results are presented in Figure 2-11. It is evident that the optimization code was able to find the global optimum solutions in less than 20 iterations in both benchmarks. Note that the selected benchmarks are multidimensional (11-D), non-linear with several local optima in the vicinity of their global optimum points, which makes them almost impossible to be solved by traditional gradient based optimization algorithms.

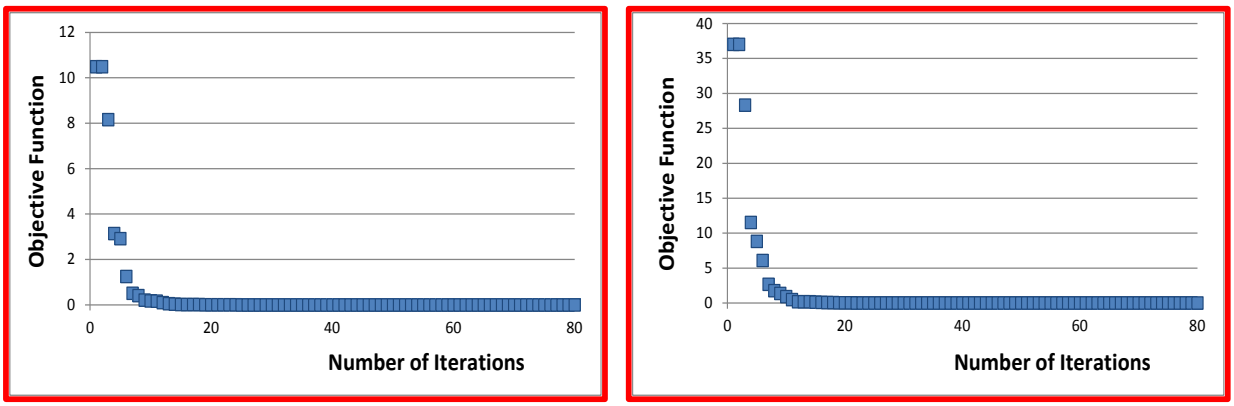

Figure 2-11: Evaluation results of the developed optimization tool by two benchmarks (Left: Rastrigin's function, Right: Griewangk's function)

3. SINGLE-OBJECTIVE OPTIMIZATION (CLOSED LOOP HEAT SOURCES)

3.1. Introduction

As discussed in the first chapter, CSP is considered as a major pathway to address the future challenges in the power generation industry. Solar thermal energy is the most abundant source of energy on the earth, and it is inherently free. The potential of electricity generation form concentrated solar thermal energy (almost 60 TW [63]) is way above the global average demand (almost 3.2 TW [2]). Moreover, there are no major air pollution and greenhouse gases associated with solar thermal electricity. Among various CSP technologies, the solar tower technology has presented the most promising features for cost competitive, large scale power generation. With this regard, this chapter is intended for thermodynamic analysis and optimization of four most promising configurations of S-CO2 Brayton cycles for solar tower applications. Nevertheless, the approach adopted in this chapter can be employed for any types of closed loop heat source applications. In other words, the choice of application mainly affects the values of two input parameters, i.e., the maximum allowable turbine inlet temperature (TIT) and the minimum allowable compressor inlet temperature (CIT).

The solar tower technology can reportedly provide a heat source with the temperature above 1400 (K) [64-66]. Therefore, the maximum allowable turbine inlet temperature (TIT) is assumed to be 1373 (K). Since the framework of this dissertation covers only the S-CO2 power block (not the solar block), the effect of solar field size and its performance are excluded from our study. Therefore, a solar heliostat field and associated tower and storage unit which can

provide constant preset thermal power at a temperature as high as desired are considered as given. Moreover, the economic feasibility of solar power projects severely depends on geographic location of the plant. The most suitable regions for solar thermal power are in desert areas where water is not easily accessible and temperature is relatively high. This implies a severe limit for the temperature of heat rejection process. Considering the fact that the U.S. DOE has persistently expressed the interest in employing dry cooling technologies for the next generation of solar thermal power plants, it is assumed that the minimum allowable temperature in the S-CO2 cycles is 320 (K). It is noteworthy that this temperature is higher than the critical temperature of CO2 (304.2 K), which means the cooling process in the cycle should take place in the temperature above the critical temperature. This condition ultimately leads to the exclusion of transcritical or condensation CO2 power cycles in solar power applications. The list of all input parameters and their values are presented in Table 3-1. These values are chosen in consistency with the common values in the literature.

Table 3-1: Input parameters

Input Parameters (Common in All Configurations)	Values (unit)
Ambient Temperature	310 (K)
Minimum Allowable Cycle Temperature	320 (K)
Maximum Allowable Cycle Temperature	1373 (K)
Available Solar Thermal Power (MW)	200 (MW)
Isentropic Efficiency of Turbines	0.9
Isentropic Efficiency of Compressors	0.89

The presented results are based on steady state condition of the power cycles at design point; and dynamic behavior and off-design performance of the cycles are not in the scope of this

study. The optimization method is comprehensive (in contrast with parametric or gradient based optimization methods) in which all the decision variables of a cycle are optimized simultaneously. The thermodynamic performances of the studied configurations are compared via energy and exergy analyses; and uncommon trends between the configurations will be elaborated.

3.2. Objective Function

In this study, optimization is merely based on the thermodynamic standpoint. Therefore, the objective or fitness function is defined as the maximum thermal efficiency of the cycle. It should be noted that the heat source in this chapter (solar tower) is in the form of closed loop heat flux source, in which the heat utilization is not constrained by temperature variation. Therefore, the heat input can be imposed into the cycle modeling as a constant parameter. In other words, the amount of heat rate captured by the cycle is equal to the generated heat rate in the source. Since a constant (200 MW) solar thermal power is assumed as the heat input to the cycle, the maximum cycle efficiency concurrently occurs when the generated power is also maximized.

3.3. Optimization Domain

In the optimization process, the decision variables are allowed to vary between predetermined upper and lower bounds; thus, the bounds should be specified in the GA code. Table 3-2 shows the upper and lower bounds of variation for the decision variables.

Table 3-2: Lower and upper bounds of decision variables

Configuration	No.	Decision Variables (unit)	Lower Bound	Upper Bound
Recuperated Recompression Cycel with Reheat & Intercooling (RRCRI) / Recuperated Recompression Cycel with Reheat (RRCR) / Recuperated Recompression Cycel (RRC) / Recuperated Cycle (RC)	1	Cycle Minimum Temperature (K) (Main Compressor Inlet)	320	420
	2	Cycle Maximum Temperature (K) (High Pressure Turbine Inlet)	723	1373
	3	Cycle Minimum Pressure (MPa) (Main Compressor Inlet)	1.5	10
	4	Cycle Maximum Pressure (MPa)	12	24
	5	Minimum Terminal Temperature Difference, ΔT_t (K)	20	50
	6	Recompression Inlet Temperature (K)	Main Compressor Inlet Temperature	LTR Exit Temperature (Low Pressure Side)
	7	Main Compressor Mass Flow Fraction	0	1
	8	Reheat (low pressure) Turbine Inlet Temperature (K)	High Pressure Turbine Exit Temperature	1373
	9	Reheater Inlet Pressure (MPa)	Low Pressure Turbine Outlet Pressure	High Pressure Turbine Inlet Pressure
	10	Second Compressor Inlet Temperature (K) (Cycle with Intercooling)	320	Main Compressor Exit Temperature
	11	Intercooler Inlet Pressure (MPa)	Main Compressor Inlet Pressure	Second (after intercooling) Compressor Exit Pressure

As it is shown in Table 3-2, certain decision variables do not have constant bounds. In other words, their lower and/or upper bounds depend on the value of some other decision variables. For instance, the pressure at which the reheating takes place in RRCR and RRCRI configurations should be bounded between the value of inlet pressure and outlet pressure of the turbine, while these pressures are varying in different cases. The intercooling pressure should also be between the lowest and highest pressure of the cycle. And the inlet temperature of the recompression compressor should always be kept below the outlet of low temperature recuperator. Therefore, the bounds of such decision variables are automatically calculated in our GA code to make sure all the decision variables are assigned with feasible values. In the case where the value of a decision variable violates some fundamental constraint of the model, which

places the solution in the unfeasible region, the associated individual is considered dead and will be excluded from the GA population.

3.4. Results and Discussion

In order to have a better understanding, the T-s diagrams associated with each configuration are shown in Figure 3-1. These T-s diagrams are drawn based on the optimization results.

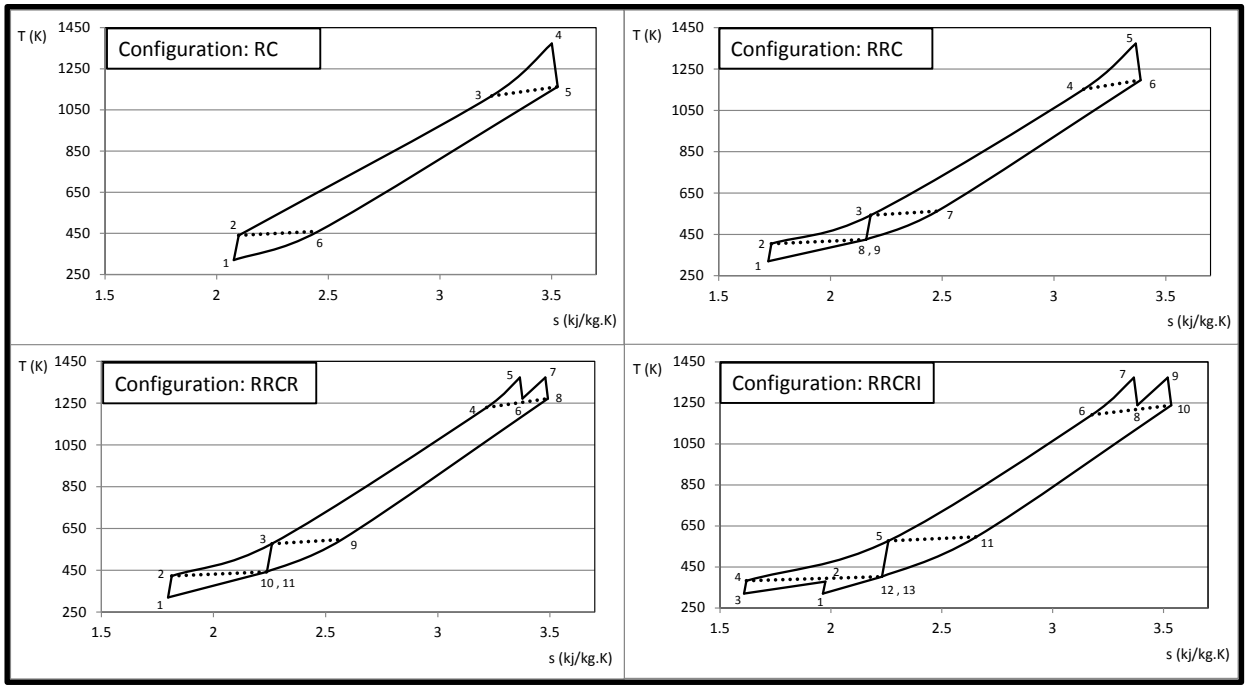

Figure 3-1: T-s diagrams of studied configurations in optimum condition

As it is displayed in Figure 3-1, the inlet temperature of recompression approaches to its maximum possible value, which results in exclusion of “cooler #1” in non-optimum condition presented in Figure 2-2, Figure 2-4 and Figure 2-5. This optimization trend is due to minimizing the heat rejection and maximizing the heat recovery in recuperators.

The optimized design variables for each configuration are also presented in Table 3-3. It should be noted that a constant solar receiver heat rate of 200 MW is assumed as an input parameter to the model; the difference between the mass flow rates in the configurations stems from the fact that the inlet temperatures to the solar receiver (including the main heater and the reheater) vary between the configurations. This issue will consequently affect the design and the efficiency of solar receiver, which is not in the scope of this study.

Table 3-3: Optimum design point

Optimum Cycle Design Point				
Design Parameters (unit)	**RC**	**RRC**	**RRCR**	**RRCRI**
1st. (main) Compressor Inlet Temperature (K)	320	320	320	320
2nd. Compressor Inlet Temperature (K)				320
Solar Receiver 1 (main heater) Inlet Temperature(K)	1118	1152	1230	1192
Turbine Inlet Temperature (K)	1373	1373	1373	1373
Solar Receiver 2 (reheater) Inlet Temperature(K)			1272	1238
Reheat Temperature (K)			1373	1373
Inlet Temperature of Recompression (K)		425	443	402
Pinch Point Temperature Difference (K)	20	20	20	20
1st. (main) Compressor Inlet Pressure (MPa)	3.27	8.17	7.23	4.81
1st. (main) Compressor Outlet Pressure (MPa)	12.00	24.00	24.00	9.32
2nd. Compressor Outlet Pressure (MPa)				24.00
Inlet Pressure of Reheater (MPa)			13.26	10.84
Main Compressor Mass Flow Fraction		0.760	0.792	0.712
Total Mass Flow Rate (kg/s)	603.0	685.9	620.7	481.9
Cycle Specific Power (kJ/kg)	184.96	170.78	192.06	257.40
Cycle Net Power (MW)	111.53	117.14	119.21	124.04
Cooling Load (Heat Rejection) (MW)	88.47	82.86	80.79	75.96
Solar Heat Source (MW)	200	200	200	200
Cycle Efficiency (%)	55.77	58.57	59.61	62.02

It is evident that there is a same trend with respect to certain design parameters followed by all configurations. The compressors inlet temperatures and pinch point temperature differences reach 320 (K) and 20 (K) respectively, which are their minimum allowable (lower

bound) values in the optimization. Moreover, the turbine inlet temperatures and reheat temperatures reach 1373 (K) which is the maximum allowable (upper bound) value in the optimization. These common trends are all in the direction of minimizing the exergy destruction in heat exchangers and compressors, minimizing the compressors intake power, and maximizing the exergy of CO2 flowing into the turbines. That the values of these design parameters approach their lower or upper bounds also indicates how critically important they are.

Interestingly, the inlet pressures to the compressors are not necessarily near the critical pressure of carbon dioxide. The maximum cycle pressure reaches its maximum allowable (upper bound) value for the configurations of RRC, RRCR, and RRCRI; however, the maximum cycle pressure in the RC configuration does not follow the same course. This result stems from the fact that CO2 thermodynamic properties such as specific enthalpy and entropy are functions of both temperature and pressure. The nonlinear dependency of the thermodynamic properties on the pressure can totally alter the optimum design pressure from what is expected. The efficiency of a recuperated S-CO2 cycle is not only a function of pressure ratio, but also a function of compressor inlet pressure. In fact, both inlet and outlet pressure of compressors significantly affect the amount of recuperated heat, turbines and compressors specific powers, cycle mass flow rate, etc. Consequently in RC configuration, working in the low pressure region has a positive effect on recuperation, which dominates the negative effect of low density CO2 entering the compressor. Since there are at least two compressors in other configurations (RRC, RRCR, RRCRI), the negative effect of low density CO2 entering the compressors is more dominant, In order to keep the total compression work minimum, the optimization leads the cycle to higher pressure region.

The maximum cycle efficiency of 62.02% is gained by RRCRI configuration. It is interesting to note that the minimum cooling load among all configurations also belongs to RRCRI cycle. Superior cycle specific power (257.40 kJ/kg), which results in less total mass flow rate, explains such a high efficiency and low cooling load in RRCRI configuration.

In addition to the compressor inlet pressure, the pressure ratio across the compressor is of great importance. Table 3-4 presents the optimum pressure ratios of compressors and turbines for each configuration. Due to the existence of two compressors in the RRC configuration, which imposes higher required compression power, the optimum compressor pressure ratio in the RRC cycle is less than that in RC configuration. Introducing reheating and inter-cooling into a cycle allows working with higher pressure ratio, which eventually increases both the cycle specific power and efficiency. Since the maximum allowable pressure has been reached in RRCR and RRCRI configurations, higher pressure ratio results in lower compressor inlet pressure.

Table 3-4: Optimum pressure rations

Optimum Pressure Ratios				
Component	**RC**	**RRC**	**RRCR**	**RRCRI**
High Pressure Turbine Pressure Ratio			1.77	2.17
Low Pressure Turbine Pressure Ratio			1.78	2.19
Turbine Pressure Ratio (Total Expansion)	3.52	2.82	3.16	4.76
High Pressure Compressor Pressure Ratio				2.59
Low Pressure Compressor Pressure Ratio				1.94
Compressor Pressure Ratio (Total Compression)	3.67	2.94	3.32	5.02

In the case of reheating, it can be concluded that the total work output of turbines is maximized when almost equal pressure ratios are maintained across high pressure and low pressure turbines. However, due to strong dependency of S-CO2 thermal properties on the

pressure in low temperature region, this course of action is not valid for inter-cooled compressors.

The optimum recuperation characteristics are presented in Table 3-5. Since the heat capacities of cold and hot streams are varying and different from each other, the definition of effectiveness is based on the ratio of actual heat transfer rate to the maximum possible heat transfer rate. This definition makes the value of effectiveness, particularly in high temperature recuperators, slightly higher than what is expected from the definition of temperature difference ratio.

Table 3-5: Optimum recuperation characteristics

Recuperator Characteristics				
Design Parameters	**RC**	**RRC**	**RRCR**	**RRCRI**
ΔT (@ Hot End of HTR) (K)	45	45	43	46
ΔT (@ Hot End of LTR) (K)		20	20	20
ΔT (@ Cold End of LTR) (K)	20	20	20	20
Total Mass Flow Rate (kg/s)	603	686	621	482
Mass Flow Fraction of Main Compressor		0.76	0.79	0.71
Total Heat Transfer (MW)	498.6	636.7	621.9	477.7
Total Exergy Destruction (MW)	11.5	13.0	11.0	10.3
Effectiveness (High Temp. Recup.)	0.98	0.97	0.97	0.97
Effectiveness (Low Temp. Recup.)		0.87	0.88	0.91
Total Temperature Rise (K)	678	747	807	810

Although the temperatures and pressures of hot and cold streams determine the effectiveness value, this quantity is predominantly influenced by the pinch point temperature difference. Considering the fact that the amount of heat transfer rates and mass flow rates are varying between the configurations; as the optimum pinch point temperature differences in all configurations are 20 (K), the author believe the recuperator with less total exergy destruction

and higher temperature rise presents a better performance. In order to reduce the exergy destruction in a heat exchanger, the temperature difference between the hot and cold streams should be kept as close as possible as it is clearly demonstrated in Figure 3-2.

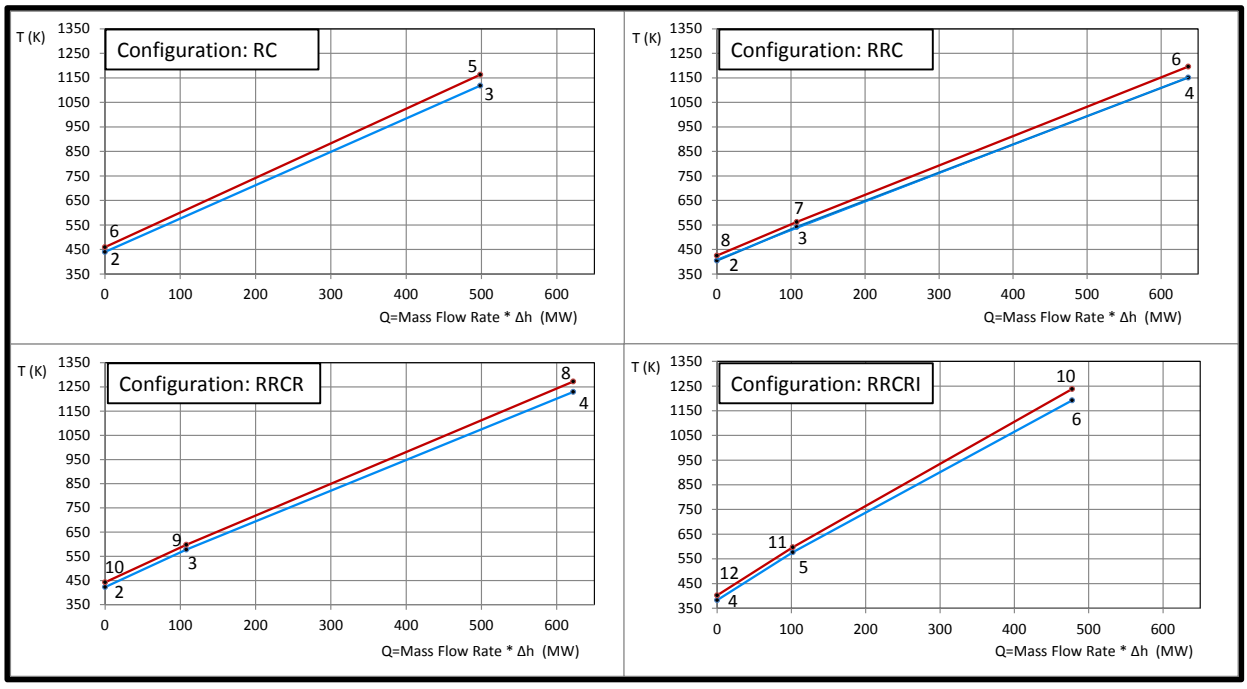

Figure 3-2: T-Q diagrams of recuperators in the studied configurations in optimum condition

The T-Q diagrams in Figure 3-2 are drawn based on the optimization results. The deviation between the hot and cold streams is due to the dependency of specific heat capacity on pressure, which results in existence of pinch point in the recuperators. Splitting the mass flow rate in the configurations with recompression enables the recuperators to demonstrate much better heat recovery. The mass flow fraction of main compressor is optimized in a way that results in almost constant temperature difference of 20 (K) along the length of the low temperature recuperator; minimizing the exergy destruction in this component.

The breakdown of energy balances for the components of each configuration is presented in Table 3-6. The comparison of the cycle specific power for the RC and RRC configurations clarifies the fact that higher cycle efficiency does not necessarily coincide with higher cycle specific power. In general, energy analysis cannot represent an effective touchstone for energy systems since it presumes the rejected heat to the environment as the only source of losses. Nevertheless, it provides supporting information for understanding the aforementioned arguments.

Table 3-6: Energy analysis at optimum condition

Energy Analysis		RC	RRC	RRCR	RRCRI
Cycle Specific Power (kJ/kg)		184.96	170.78	192.06	257.40
Component	1st. (main) Compressor	87.59	50.17	62.76	37.95
	2nd. Compressor				36.77
	Recompression		97.56	117.99	150.20
	1st. (main) Turbine	272.55	232.33	133.79	177.68
	2nd. Turbine			132.51	176.16
Cycle Net Power (MW)		111.53	117.14	119.21	124.04
Component	1st. (main) Compressor	52.82	26.15	30.86	13.02
	2nd. Compressor				12.62
	Recompression		16.07	15.21	20.83
	1st. (main) Turbine	164.35	159.35	83.04	85.62
	2nd. Turbine			82.24	84.89
Total Recuperated Heat (MW)		498.55	636.72	621.89	477.65
	High Temp. Recup.	498.55	529.02	513.84	375.72
	Low Temp. Recup.		107.70	108.04	101.93
Total Rejected Heat (MW)		88.47	82.86	80.79	75.96
	Pre-Cooler Load	88.47	82.86	80.79	32.78
	Inter-Cooler Load				43.18
Total Mass Flow Rate (kg/s)		603.01	685.88	620.67	481.89
Thermal Efficiency (%)		55.77	58.57	59.61	62.02

In contrast with energy analysis, exergy analysis not only identifies the actual deficiencies, but also quantifies them in a very meaningful manner [67]. The results of exergy analysis of each configuration are presented in Table 3-7.

Table 3-7: Exergy analysis at optimum condition

Exergy Analysis				
Exergy Destruction Inside the Cycle	**RC**	**RRC**	**RRCR**	**RRCRI**
1st. Compressor (main) (MW)	4.13	2.21	2.50	1.18
2nd. Compressor (MW)				1.13
Recompression Comp. (MW)		1.02	0.91	1.25
Compression (total) (MW)	4.13	3.23	3.41	3.55
1st. Turbine (main) (MW)	4.92	4.63	2.26	2.40
2nd. Turbine (MW)			2.24	2.38
Expansion (total) (MW)	4.92	4.63	4.50	4.77
High Temp. Recup. (MW)	11.55	9.14	7.55	6.02
Low Temp. Recup. (MW)		3.82	3.47	4.26
Recuperation (total) (MW)	11.55	12.96	11.02	10.28
Cycle (total) (MW)	20.59	20.81	18.92	18.60
Exergy (Input / Output / Loss)	**RC**	**RRC**	**RRCR**	**RRCRI**
Solar Source (input) (MW)	149.71	150.35	151.95	151.43
Net Work (output) (MW)	111.53	117.14	119.21	124.04
Heat Rejection (loss) (MW)	17.59	12.40	13.82	8.79
2nd. Law Efficiency (%)	74.50	77.91	78.45	81.91

In each configuration, there are several points of exergy destruction associated with the comprising components, an exergy loss in the heat rejection process, an exergy input from the solar source, and an exergy output in the form of net power. Note that the amount of exergy input is a nonlinear function of the temperature and the pressure at which solar heat is absorbed by S-CO2. As it is also shown in Table 3-7, the variation of mass flow rate between the configurations does not directly lead to significant variation of exergy inputs among the configurations.

Nevertheless, in order to provide easy comparison between the four configurations, the results of exergy analysis are also presented in the normalized (percentage) format in Figure 3-3.

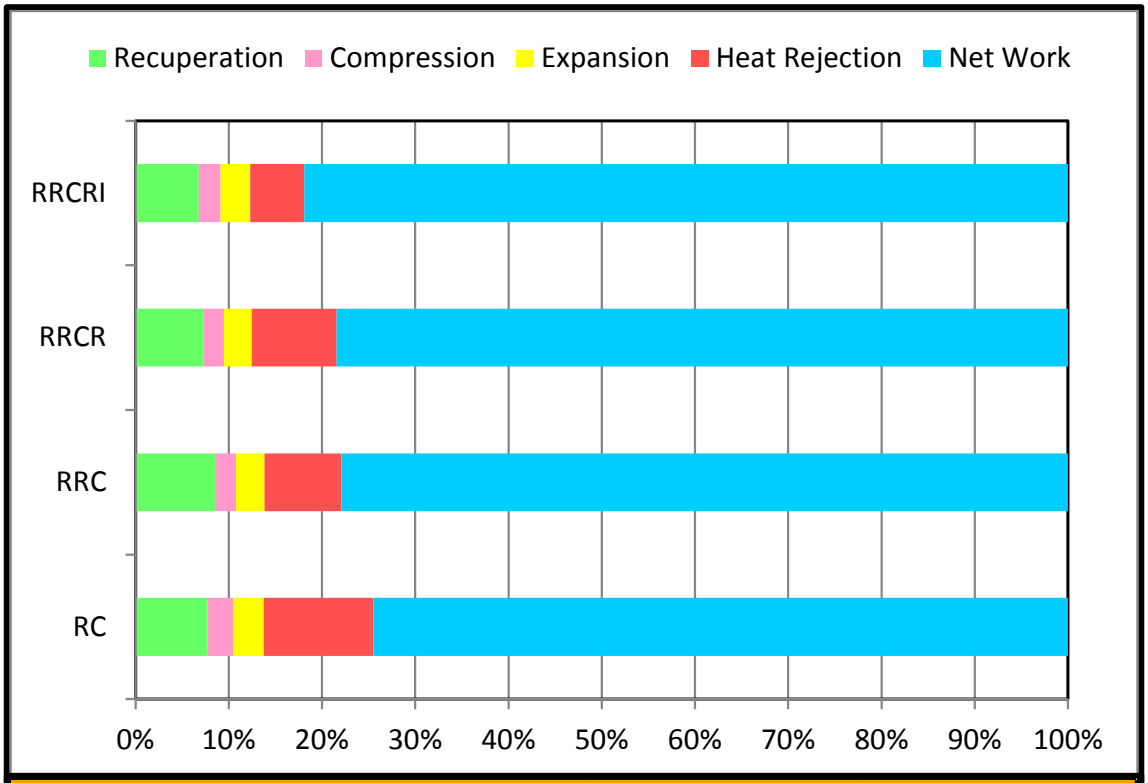

Percentage of Exergy Input / Output / Loss / Destruction				
Configuration	**RC**	**RRC**	**RRCR**	**RRCRI**
Recuperation (Destruction)	7.71	8.62	7.25	6.79
Compression (Destruction)	2.76	2.15	2.24	2.35
Expansion (Destruction)	3.28	3.08	2.96	3.15
Heat Rejection (Loss)	11.75	8.24	9.10	5.81
Net Work (Output)	74.50	77.91	78.45	81.91
Solar Source (Input)	100.00	100.00	100.00	100.00

Figure 3-3: Percentage of exergy input / output / loss / destruction for each configuration

The minimum amount of exergy destruction belongs to compression process in all configurations. The second smallest exergy destruction is that associated with the expansion processes. It should be noted that the values of isentropic efficiencies of compressors and

turbines, assumed to be 89% and 90% respectively, will affect the above statement on exergy destruction. The highest compression and expansion exergy destruction among all the configurations belongs to the RC configuration due to its large mass flow rate and high cycle pressure ratio. The amounts of exergy destruction in recuperation and exergy loss in heat rejection are rather comparable in each configuration. The addition of reheating and intercooling to the recompression cycle clearly has a positive effect on reducing the exergy destruction in recuperation. Intercooling and recompression have significant positive effects on reducing the exergy loss associated with heat rejection. Finally, reheating has a rather negative effect on the exergetic performance of heat rejection process.

The author wishes to call attention to the fact that the presented results are based on the provided assumptions; and are only valid on the optimization region confined by the lower and upper bounds of decision variables. These bounds were chosen based on the limitations imposed by material properties, manufacturing technologies, and other technical issues. Certain decision variables have reached their lower or upper bounds through the optimization process, which indicates that better performances can potentially be achieved by exceeding these bounds. For instance, a parametric study regarding the effect of pinch point temperature difference on the cycle efficiency was performed. Figure 3-4 demonstrates how higher efficiencies can be achieved by reducing the lower bound of pinch point temperature difference in the optimization.

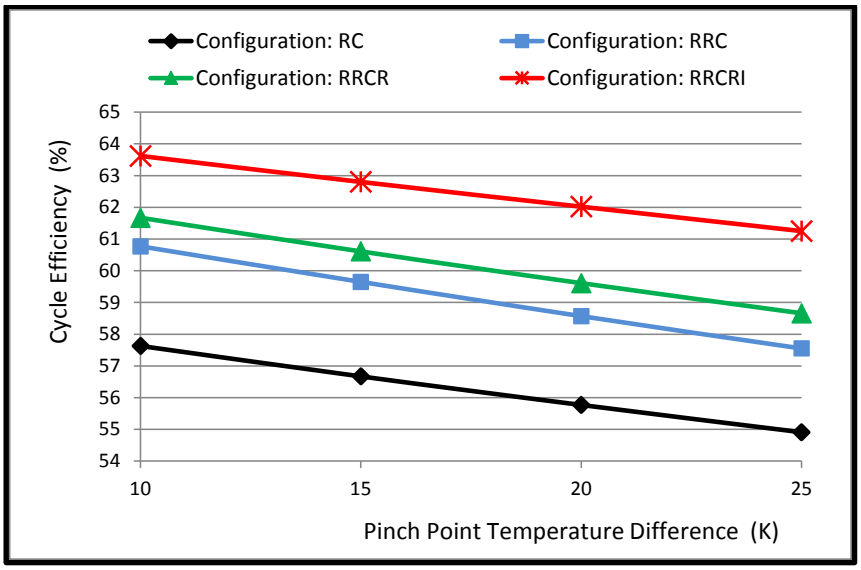

Figure 3-4: Parametric study on cycle efficiency vs. pinch point temperature difference

3.5. Conclusion

In this chapter, four most promising configurations of S-CO2 Brayton cycles have been studied. The effects of recompression, reheating, and intercooling on the thermodynamic performance of a recuperated S-CO2 Brayton cycle have been analyzed; and the optimum design point for each configuration were presented. The optimization was carried out by utilizing the genetic algorithm which is a robust method for multidimensional, nonlinear system optimization.

The optimum value of maximum cycle temperature is confined by its upper bound; and minimum heat rejection temperature and pinch point temperature difference reach to their lower bounds. Depending on the type of configuration, the optimum inlet pressure of the main compressor was found not to be necessarily near the critical pressure. Moreover, the optimum cycle pressure ratio varies between the configurations. The optimum reheat pressure is in a way that almost equal pressure ratios are maintained across high pressure and low pressure turbines.

However, this trend is not valid for intercooling pressure. The optimum mass flow fraction in the configurations with recompression minimizes the exergy destruction in the low temperature recuperator by maintaining the constant heat transfer temperature difference of 20 (K) along the length of this component. Among four major sources of deficiency, the results of exergy analysis reveal that the exergy destruction in recuperation and exergy loss in heat rejection are more significant compared to the ones in compression and expansion. They also show that the recompression has a positive effect on reducing the exergy loss in heat rejection; and reheating improves the cycle performance by reducing the exergy destruction in recuperation. The addition of intercooling to the cycle with recompression and reheating significantly reduces the exergy loss in heat rejection, and also improves the performance of recuperation.

Higher cycle efficiencies can be achieved by adding more complexity to the simple recuperated cycle, which brings about more capital cost. Although the RC configuration demonstrates lower efficiency than other configurations, it can still be an interesting option due to its simplicity and more importantly due to its substantially low working pressure.

4. MULTI-OBJECTIVE OPTIMIZATION (CLOSED LOOP HEAT SOURCES)

4.1. Introduction

As also discussed in the previous chapters, it has been observed that the surge of interest and need for sustainable power generation using solar energy has encouraged researchers to focus on Concentrated Solar Power (CSP) and specifically solar tower systems which can be deployed as large, centralized power plants to take advantage of the economies of scale. The solar tower technology presents great potential for efficient, reliable and cost-competitive electricity generation taking advantage of inherently free and abundant solar thermal energy. However, a brief look over the solar tower technology reveals the fact that reducing the electricity cost is an essential step towards competitive solar power generation. In order to achieve this goal, extensive studies have been directed towards simplification and cost reduction of concentrated solar energy harvesting systems or "solar blocks" that include heliostats, towers, receivers, storage systems, etc. Nevertheless, the efficiency and costs associated with "power blocks", which include the components responsible for thermal-to-mechanical energy conversion, also have significant contributions in the final levelized cost of electricity (LCOE). In a typical solar tower power plant, the cost of a power block accounts for almost 32 percent of the total investment cost as depicted in Figure 4-1 [68]. Therefore, any attempt towards decreasing the cost of power blocks would directly reduce the electricity generation cost. Moreover, the efficiency of power blocks indirectly affects the electricity generation cost; that is, for a fixed power plant capacity, higher efficiency of the power block implies a smaller and less

expensive solar block. Therefore, introducing a more efficient but less expensive power block has a dual positive effect, and significantly advances the solar power industry towards commercialization. Accordingly, the S-CO2 Brayton cycles have been reported as one of the most promising avenues for concentrated solar power generation due to their several rewarding features such as high cycle efficiency, superior economy, compactness and simplicity.

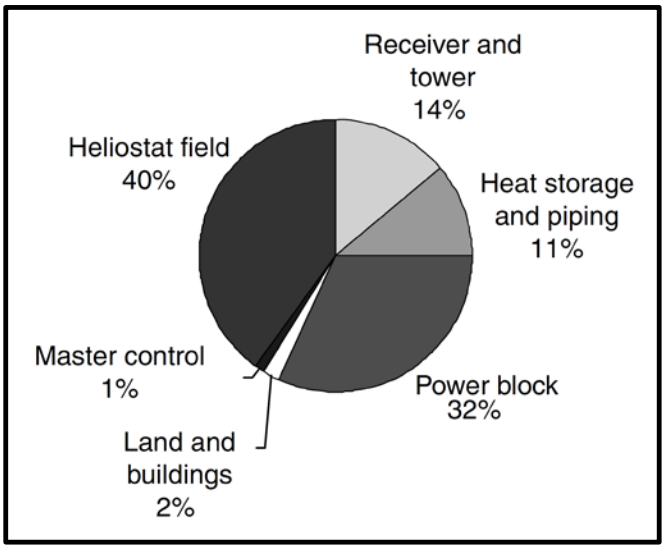

Figure 4-1: Investment costs breakdown for a typical solar tower power plant. As it can be observed, the heliostat field and the power block are the most impacting subsystems on plant investment [68]

In an effort to minimize the size and cost of solar block, Chapter 3 was intended to find the global maximum efficiency of S-CO2 cycles, in which all decision variables were optimized simultaneously. However, the results of efficiency maximization showed that achieving the highest efficiency does not necessarily coincide with the highest cycle specific power. In addition to the efficiency, the specific power is also an important parameter when it comes to investment and decision making since it directly affects the power generation capacity and the size of components.

In this chapter, the thermodynamic multi-objective optimization of the two simplest configurations of the S-CO2 Brayton cycles (i.e., the simple recuperated and recompression cycles) is presented. As listed in Table 4-1, the input parameters and their values in this chapter are the same as the ones in Chapter 2.

Table 4-1: Input parameters

Input Parameters (Common in All Configurations)	Values (unit)
Ambient Temperature	310 (K)
Minimum Allowable Cycle Temperature	320 (K)
Maximum Allowable Cycle Temperature	1373 (K)
Available Solar Thermal Power (MW)	200 (MW)
Isentropic Efficiency of Turbines	0.9
Isentropic Efficiency of Compressors	0.89

The two objective functions of cycle efficiency (η_c) and cycle specific power (Φ_{sp}) selected in this study are semi-conflicting to each other and need to be maximized simultaneously. The objective of maximum cycle efficiency is a supportive index for a smaller and less expensive solar block, and a lower fuel cost in the case of a hybrid scheme. On the other hand, the objective of maximum cycle specific power represents a smaller power block, and a lower capital cost associated with recuperators and coolers. Eventually, the employed multi-objective optimization approach leads to a trade-off curve between the objective functions. In this way, a range of optimum solutions is presented to decision makers, which enables them to choose the desired compromise between the objectives and avoid naive solutions obtained from a single-objective optimization approach.

4.2. Objective Function

As it was explained in the second chapter of this dissertation, a weight-based (or preference-based) multi-objective optimization scheme is chosen in this study. This method evaluates the weighted average of the objectives in the form of Eq. (4-1).

$$F = w_1 f_1 + w_2 f_2 \tag{4-1}$$

In general, the values of objective functions can vary with different orders of magnitude, which can potentially induce a biased optimization process in the favor of one objective over the other. In order to rectify this issue, the objective functions should be normalized by means of Eq. (4-2) before implementing them in Eq. (4-1).

$$f_1 = \frac{\eta_c}{\eta_{c,max}} \quad ; \quad f_2 = \frac{\Phi_{sp}}{\Phi_{sp,max}} \tag{4-2}$$

Further in its simplest form, the optimum solutions to 11 sets of objective functions (Eq. (4-3)) are superimposed to form the complete multi-objective optimization problem.

$$\begin{aligned} F &= 1(f_1) + 0(f_2) \\ F &= 0.9(f_1) + 0.1(f_2) \\ F &= 0.8(f_1) + 0.2(f_2) \\ &\cdot \quad \cdot \quad \cdot \\ &\cdot \quad \cdot \quad \cdot \\ &\cdot \quad \cdot \quad \cdot \\ F &= 0(f_1) + 1(f_2) \end{aligned} \tag{4-3}$$

4.3. Optimization Domain

The optimization domain is defined by assigning boundaries to the decision variables. Table 4-2 shows the lower and upper bounds of decision variables in the multi-objective optimization scheme. The first five variables are common in both configurations. In the RRC configuration, two additional decision variables, i.e. recompression inlet temperature and main compressor mass flow fraction, are introduced. Although the lower and upper bounds of recompression inlet temperature depend on the value of other decision variables, the considered decision variables are all mathematically independent of each other. It should be noted that if recompression inlet temperature reaches its lower bound and/or main compressor mass flow fraction reaches its upper bound, the RRC configuration would be transformed to the RC configuration.

Table 4-2: Lower and upper bounds of decision variables

Configuration		No.	Decision Variables (unit)	Lower Bound	Upper Bound
Recuperated Recompression Cycel (RRC)	Recuperated Cycle (RC)	1	Cycle Minimum Temperature (K) (Main Compressor Inlet)	320	420
		2	Cycle Maximum Temperature (K)	723	1373
		3	Cycle Minimum Pressure (MPa) (Main Compressor Inlet)	1.5	10
		4	Cycle Maximum Pressure (MPa)	12	24
		5	Minimum Terminal Temperature Difference, ΔT_t (K)	10	40
		6	Recompression Inlet Temperature (K)	Main Compressor Inlet Temperature	LTR Exit Temperature (Low Pressure Side)
		7	Main Compressor Mass Flow Fraction	0	1

4.4. Results and Discussion

In the case of the simple recuperated cycle, two objective functions (η_c, ϕ_{sp}) and five decision variables [T(1), T(4), ΔTPP, P(1), P(2)] are considered for optimization. The goal of the weight-based multi-objective optimization scheme applied in this study is to maximize the semi-conflicting objective functions by optimizing the corresponding decision variables. The proposed methodology leads to 11 single-objective optimization problems (Eq. (4-3)) which are then solved and combined to form 11 trade-off design solutions for the simple recuperated cycle. Without any further information, no design solution from the set of trade-off design solutions can be said to be better than any other in the set.

Figure 4-2(a) shows all the objective functions values (efficiency and specific power) which are calculated based on randomly distributed design or decision variables selected from within ranges specified in Table 4-2, at the initial step (called generation 0) of the optimization process. These solution points are all feasible design points in the RC configuration, and they are all inferior to the optimum design points of this configuration. Note that a designer may make an uninformed decision by choosing any of these inferior design points. In other words, it is nearly impossible for any designer/decision maker to choose the optimum solution or a set of best solutions without performing the optimization. The application of a genetic algorithm as a search tool makes it possible to search the design space for the most optimal solutions, where composite objective function defined by Eq. (4-1) is maximized. Figure 4-2:(b) shows the objective functions values in the RC configuration (η_c, ϕ_{sp}) after 10 iterations (generation 10) of the optimization process. The comparison of Figure 4-2:(a) and Figure 4-2:(b) demonstrates how the

design points go through an evolution towards maximizing both the cycle efficiency and specific power.

Figure 4-3 shows the trade-off between the objectives in the form of a Pareto optimal front which is generated after combining all the 11 runs. Each of the 11 single-objective optimization runs ranks one solution as the optimum solution and the rest of the solutions in that run were considered sub optimal and dominated by the optimum solution. The 11 optimum solutions from the preference-based / weight-based optimization form the Pareto optimal front for the RC configuration as depicted in Figure 4-4. It is noteworthy that more uniform distribution of the optimum solutions can be achieved by reducing the intervals between the incremental weight coefficients in Eq. (4-3). The corresponding values of the objective functions and design variables associated with the 11 optimum solutions in the RC configuration are listed in Table 4-3. The person responsible for the thermodynamic cycle design now will have multiple designs with varying efficiency and specific power in hand. For example, if a designer has to concentrate more in obtaining high cycle efficiency, he/she can concentrate in the region of Pareto optimal cluster 1 to select feasible design solutions with minimal effort. On the other hand, if one would like to have more specific power at the expense of cycle efficiency, then he/she can work with Pareto optimal cluster 3. Cluster 2 provides the Pareto optimal solutions which are moderately optimized for both objective functions. To make the life of cycle designers even simpler, one can have the Pareto front as shown in Figure 4-4, where the 11 Pareto optimum solutions are chosen based on their ranks. Now a designer can choose design point 1 (with high cycle efficiency), design point 5 (with moderate cycle efficiency and specific power)

or design point 11 (with high specific power) and their corresponding decision variables values (Table 4-3) to construct a thermodynamic cycle of his/her preference.

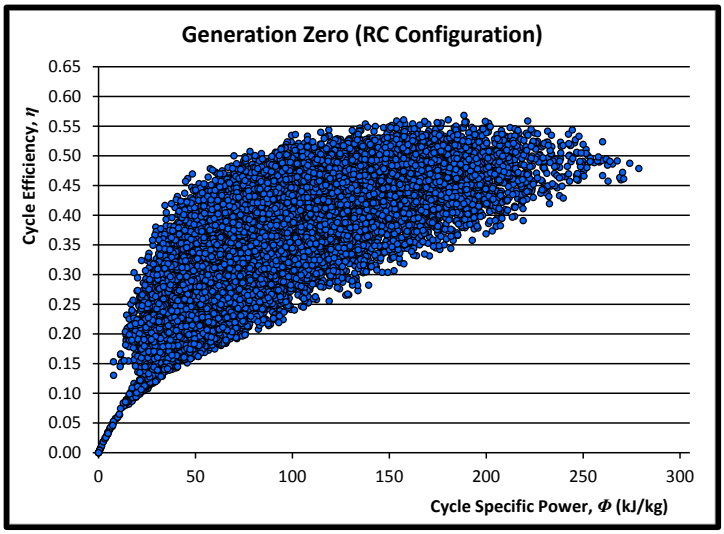

(a)

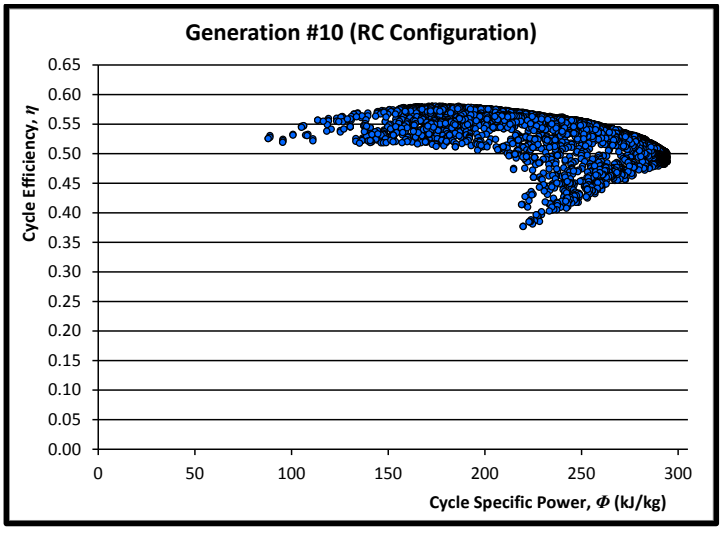

(b)

Figure 4-2: Evolution of optimization process from generation zero (a) to generation 10 (b) in the RC configuration

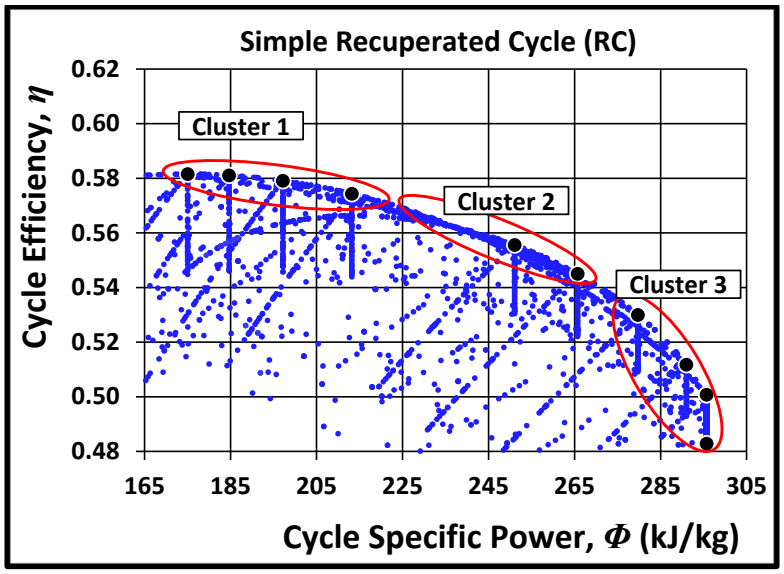

Figure 4-3: Formation of the Pareto front in the RC Configuration

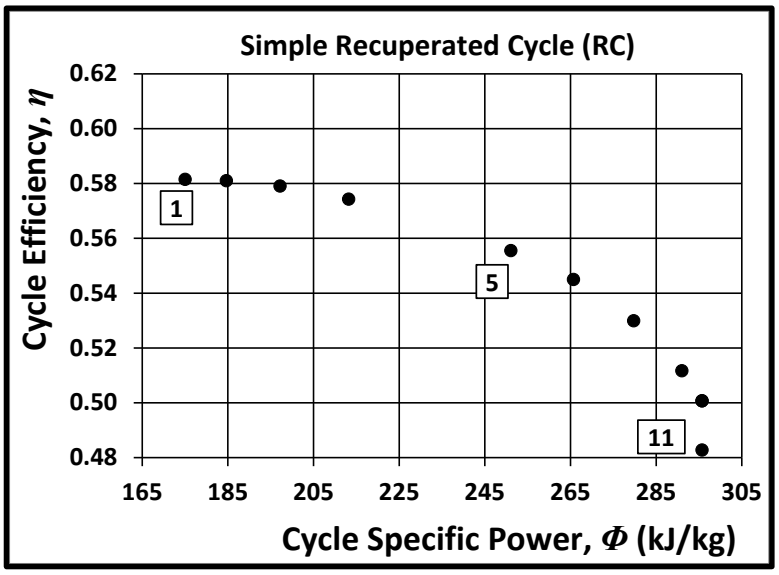

Figure 4-4: Non-dominated optimum solutions obtained form 11 single-objective optimization of the composite objective function in the RC configuration

Table 4-3: Optimum design points (RC configuration)

Optimal Case No.	η_c (%)	Φ_{sp} (kJ/kg)	Decision Variables				
			T_1 (K)	T_4 (K)	ΔT_{pp} (K)	P_1 (MPa)	P_2 (MPa)
1	58.15	175.03	320	1373	10	3.73	12
2	58.11	184.65	320	1373	10	3.41	12
3	57.91	197.17	320	1373	10	3.01	12
4	57.43	213.20	320	1373	10	2.54	12
5	55.55	251.05	320	1373	10	3.84	24
6	54.50	265.70	320	1373	10	3.05	24
7	53.00	279.73	320	1373	10	2.33	24
8	51.17	290.99	320	1373	10	1.75	24
9	50.07	295.69	320	1373	10	1.5	24
10	50.07	295.69	320	1373	10	1.5	24
11	48 ~ 50	295.69	320	1373	10 ~ 30	1.5	24

For the recompression recuperated cycle, the same two objective functions (η_c, ϕ_{sp}), but seven decision variables [T(1), T(5), T(9), ΔTPP, P(1), P(2), f], are considered for optimization. After the optimization and selection of the optimum solutions based on ranking, one can generate the Pareto optimal front shown in Figure 4-5 and Figure 4-6. Further analysis based on the Pareto optimal front and Pareto optimal clusters for the RRC configuration can be conducted in a manner similar to what was performed for the RC configuration in the previous section.

Table 4-4 lists the optimum values of decision variables and their corresponding objective functions for all the 11 optimized cases of the RRC configuration. As mentioned earlier, a designer can choose any of these 11 designs based on higher level information. The higher level information may come from various points of view such as considered applications, manufacturing issues, material limits, financial considerations, etc. in which the preference level of the objectives with respect to each other can be determined.

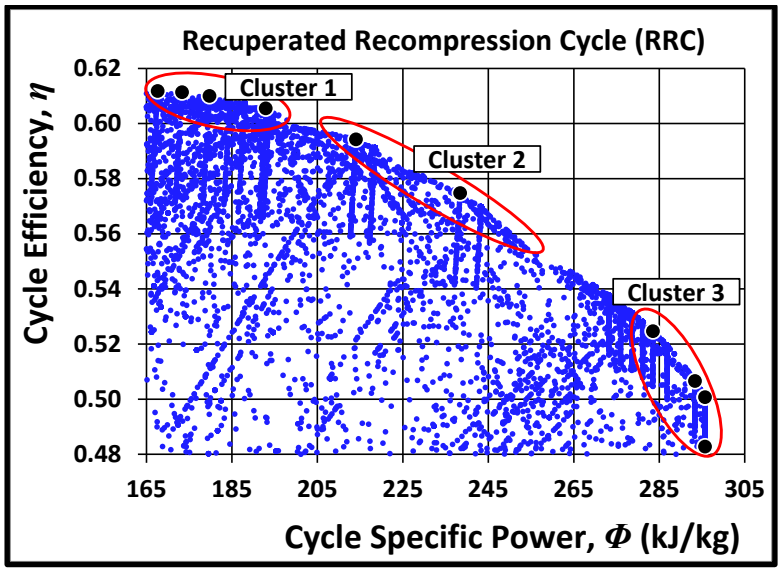

Figure 4-5: Formation of the Pareto front in the RRC Configuration

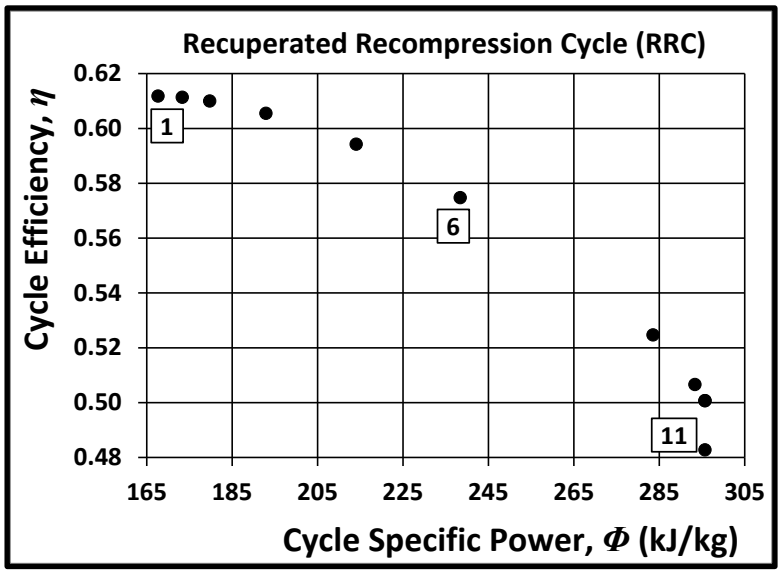

Figure 4-6: Non-dominated optimum solutions obtained form 11 single-objective optimization of the composite objective function in the RRC configuration

Table 4-4: Optimum design points (RRC configuration)

Optimal Case No.	η_c (%)	Φ_{sp} (kJ/kg)	Decision Variables						
			T_1 (K)	T_5 (K)	$T_8 = T_9$ (K)	ΔT_{pp} (K)	P_1 (MPa)	P_2 (MPa)	f
1	61.18	167.63	320	1373	401.7	10	8.84	24	0.731
2	61.14	173.33	320	1373	411.9	10	8.33	24	0.750
3	61.00	179.75	320	1373	422.2	10	7.8	24	0.769
4	60.55	192.90	320	1373	441.2	10	6.79	24	0.800
5	59.43	214.02	320	1373	470.6	10	5.33	24	0.840
6	57.48	238.39	320	1373	507.5	10	3.83	24	0.878
7	52.47	283.51	320	1373	N.A.	10	2.14	24	1
8	50.66	293.33	320	1373	N.A.	10	1.63	24	1
9	50.07	295.69	320	1373	N.A.	10	1.5	24	1
10	50.07	295.69	320	1373	N.A.	10	1.5	24	1
11	48 ~ 50	295.69	320	1373	N.A.	10 ~ 30	1.5	24	1

Considering the results provided in Table 4-3 and Table 4-4, it is evident that there is the same trend with respect to certain design variables followed by both configurations. In all cases, the turbine inlet temperatures reach 1373 (K) which is the maximum allowable (upper bound) value in the optimization. Moreover, the main compressor inlet temperatures and pinch point temperature differences reach 320 (K) and 10 (K) respectively, which are their minimum allowable (lower bound) values in the optimization. However, the minimum terminal temperature difference (pinch point) in the optimal case number 11 can independently vary without changing the cycle specific power. This is due to the fact that the weight coefficient of the efficiency is equal to zero. The results indicate that the variation of the pinch point temperature difference from 10 to 30 (K) can lead to 2% efficiency reduction. It is noteworthy that the aforementioned common trends are all in the direction of minimizing the exergy destruction in the recuperators, minimizing the compressors intake power, and maximizing the

exergy of CO2 flowing into the turbines. That the values of these design variables approach their lower or upper bounds also indicates how critically important they are, and better cycle performance can potentially be achieved by exceeding these bounds.

The compressor outlet pressure reaches its maximum allowable (upper bound) value in all optimal cases of the RRC configuration; however, this is not the case in the first optimal cluster of the RC configuration. This result stems from the fact that CO2 thermodynamic properties such as specific enthalpy and specific entropy are functions of both temperature and pressure. The nonlinear dependency of the thermodynamic properties on the pressure can totally alter the optimum design pressure from what is expected. The efficiency of the S-CO2 cycles is not only a function of pressure ratio, but also a function of compressor inlet pressure. In fact, both the inlet and outlet pressures of the compressors significantly affect the amount of recuperated heat, the turbines and compressors specific power, and the cycle efficiency. Consequently, when the preference level of the efficiency is high in the RC configuration, working in the low pressure region has a positive effect on recuperation, which dominates the negative effect of low density CO2 entering the compressor. Since there are two compressors in the RRC configuration, the negative effect of low density CO2 entering the compressors is more dominant, In order to keep the total compression work minimum, the optimization leads the RRC cycle to the higher pressure region in all 11 cases.

The results in Table 4-4 also reveal that the RRC configuration is transformed to the RC configuration by increasing the preference level of the specific power; that is, the main compressor mass flow fraction is optimized to be 100% at certain point on the Pareto front. However, the large intervals between the weight coefficients did not allow detecting the point of

convergence of two configurations. Thus, the intervals between the weight coefficients were reduced and more refined Pareto fronts were generated. Figure 4-7 displays the refined Pareto fronts of both configurations. Although the RRC configuration can present high efficiency, its specific power is limited to below 255 (kJ/kg). In other words, the RC configuration offers higher efficiency than the RRC configuration when the specific power above 255 (kJ/kg) is demanded.

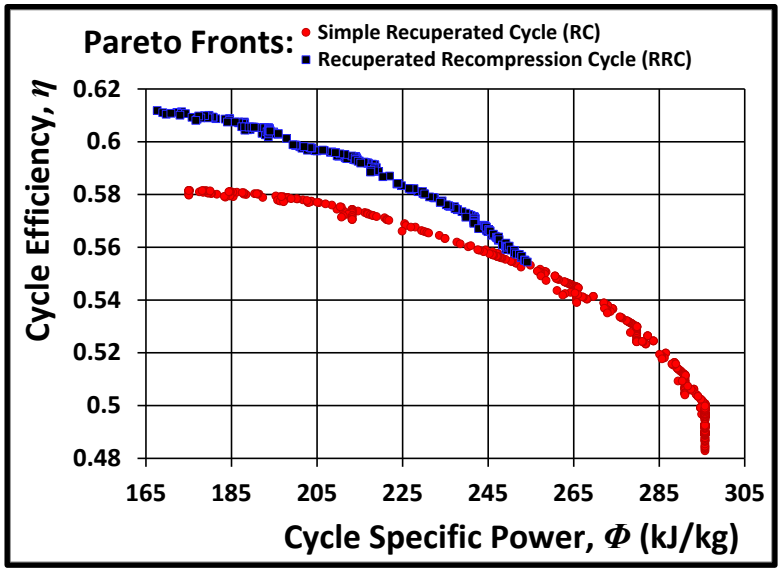

Figure 4-7: Refined Pareto fronts by reducing the intervals between the weight coefficients

The size and manufacturing of recuperators are other crucial considerations which have to be taken into account when it comes to decision making. Table 4-5 presents the effectiveness of the recuperators in the RC and RRC configurations. Since the heat capacities of the cold and hot streams are varying and different from each other, the definition of the effectiveness is based on the ratio of the actual heat transfer rate to the maximum possible heat transfer rate. This definition makes the effectiveness value, particularly in the HTR, higher than what is expected

from the definition of the effectiveness based on the temperature difference ratio. Although the temperatures, pressures and mass flow rates of the hot and cold streams determine the effectiveness value, this quantity is predominantly influenced by the pinch point temperature difference. From the technical point of view, a lower pinch point temperature difference means a higher value of the effectiveness, which can lead to larger heat exchangers. However, as also reported in [48], new heat exchanger technologies such as printed circuit heat exchangers combining with excellent heat transfer characteristics of supercritical carbon dioxide would lead to design and manufacture recuperators with very high effectiveness in reasonable sizes.

It is perceived that for some designers, the effectiveness of the recuperators reported in Table 4-5 may still seem too high for the cases where the preference level of the cycle efficiency is high. One may have two options to handle this issue. The first option is to consider a new thermodynamic cycle design with higher value of the pinch point temperature difference. In this way, the effectiveness and size of the recuperators and also the cycle efficiency will be reduced together without any gain in the specific power. On the other hand, the second option is to move towards higher specific power regions on the Pareto fronts where the effectiveness of the recuperators decreases and the specific power significantly increases with minimal reduction in the efficiency. In fact, one of the valuable advantages of generating Pareto optimal fronts for the S-CO2 power cycles in various applications can be seen in the latter strategy.

Table 4-5: Effectiveness of the recuperators in the RC and RRC Configurations

Optimal Case No.	RC Configuration	RRC Configuration	
		LTR	HTR
1	0.988	0.914	0.987
2	0.988	0.921	0.986
3	0.987	0.928	0.985
4	0.986	0.938	0.984
5	0.984	0.951	0.980
6	0.983	0.962	0.972
7	0.980	N.A.	0.979
8	0.976	N.A.	0.975
9	0.973	N.A.	0.973
10	0.973	N.A.	0.973
11	0.940	N.A.	0.940

4.5. Conclusion

The main focus of this chapter is to present a multi-objective optimization framework to optimize two configurations of the S-CO2 Brayton cycles, i.e., the simple recuperated and recompression cycles. In addition to the efficiency, the specific power is also a very important parameter when it comes to investment and decision making. It has a direct effect on the power generation capacity, the size of components and the cost of power blocks. Therefore, the two optimization objectives used in this chapter are the maximization of the efficiency and maximization of the specific power. The proposed optimization framework is built by integrating a preference-based/weight-based multi-objective optimization scheme based on a genetic algorithm with a computational thermodynamic model to calculate the performance indicators of the cycles. The results of this optimization framework show the promise of the proposed approach in the optimization of the S-CO2 cycles for various applications. The resulting Pareto

optimal fronts provide a series of optimal solutions in the form of trade-off curves between the optimization objectives, which increases the flexibility in decision making process. The comparison of the two Pareto fronts reveals the advantages of each configuration over the other. As a result, it can be suggested that the RRC configuration offers better characteristics for CSP applications. On the other hand, the RC configuration is more beneficial in applications where the size and cost of power blocks is crucial.

Although a high premium is placed on the cycle efficiency for CSP applications (higher efficiency reduces the size and cost of the solar field), targeting the highest possible cycle efficiency (optimal cluster 1 in the RRC configuration) comes with the drawbacks of low cycle specific power and high effectiveness of recuperators, which both contribute towards increasing the size and cost of heat exchangers. Therefore, as opposed to optimal cluster 1, optimal cluster 2 in the RRC configuration with more reasonable size and cost of heat exchangers can be suggested for large scale solar power generation. On the other hand, optimal cluster 1 in the RRC configuration would still be beneficial for small scale solar power plants.

Finally, it is evident that the single-objective optimization of the S-CO2 cycles for highest possible efficiency may lead to naive solutions in certain applications. In contrast, the proposed multi-objective optimization approach not only presents the optimum trade-off curve between the efficiency and the specific power, but also qualitatively provides better techno-economic insights into the analysis of the S-CO2 Brayton cycles.

5. WASTE HEAT RECOVERY APPLICATIONS

5.1. Introduction

The power generation via waste heat recovery can be an effective solution to the accelerating growth of electricity demand. The U.S. DOE estimates that 280,000 MW thermal power is discharged annually in the U.S. industries as waste heat. Electricity Potential from only industrial waste recovery is equal to 20% of U.S. Electricity Demand. Annual monetary saving is estimated to be between 70 to 150 Billion USD, with substantial reduction in greenhouse gases [69, 70]. The worldwide potential is even more considerable as these numbers represent the situation in only the United States. This chapter discusses the use of a Brayton cycle with supercritical carbon dioxide (S-CO2) as the working fluid for converting a portion of the waste heat to electric power.

Waste heat recovery can significantly help energy intensive industries which include Chemical and Petrochemical Plants, Iron, Steel and Aluminum Industries, Pulp & Paper Industry, and Cement, Glass & Nonmetallic Minerals Industries. As presented in Table 5-1 [71], over these different types of industries, there is a large variation in the temperatures at which waste heat is available. Therefore, thorough thermodynamic optimization of S-CO2 cycles is essential to arrive at the optimum design point for a specific application. However, the previous studies on S-CO2 cycles are mostly for low and medium temperature closed loop heat sources. Echogen is currently the only manufacturer which attempts to build commercial scale S-CO2 cycles for waste heat recovery applications. There have been a few studies conducted at Echogen to compare the CO2 and steam-based heat recovery systems published by Persichilli et al [72,

73], and Kacludis et al [74]. Nevertheless, comprehensive studies on WHR applications, which present the optimum design variables of S-CO2 Brayton cycles for various heat source temperatures, have not been conducted sufficiently. In this chapter, two configurations of the S-CO2 Brayton cycles i.e., the simple recuperated (RC) and recompression recuperated cycles (RRC) are thermodynamically modeled for different temperature ranges of heat recovery applications. The input parameters to the model and their values are shown in Table 5-2. After performing the optimization and comparative analysis, a number of optimum design guidelines are concluded.

Table 5-1: Waste Heat Streams Classified by Temperature [71]

Temperature Classification	Waste Heat Source	Characteristics	Commercial Waste Heat to Power Technologies
High (>1,200 °F)	• Furnaces – Steel electric arc – Steel heating – Basic oxygen – Aluminum reverberatory – Copper reverberatory – Nickel refining – Copper refining – Glass melting • Iron cupolas • Coke ovens • Fume incinerators • Hydrogen plants	• High quality heat • High heat transfer • High power-generation efficiencies • Chemical and mechanical contaminants	• Waste heat boilers and steam turbines
Medium (500 –1,200 °F)	• Prime mover exhaust streams – Gas turbine – Reciprocating engine • Heat-treating furnaces • Ovens – Drying – Baking – Curing • Cement kilns	• Medium power-generation efficiencies • Chemical and mechanical contaminants (some streams such as cement kilns)	• Waste heat boilers and steam turbines (>500 °F) • Organic Rankine cycle (<800 °F) • Kalina cycle (<1,000 °F)
Low (< 500 °F)	• Boilers • Ethylene furnaces • Steam condensate • Cooling Water – Furnace doors – Annealing furnaces – Air compressors – IC engines – Refrigeration condensers • Low-temperature ovens • Hot process liquids or solids	• Energy contained in numerous small sources • Low power-generation efficiencies • Recovery of combustion streams limited due to acid concentration if temperatures reduced below 250 °F	• Organic Rankine cycle (>300 °F gaseous streams, >175 °F liquid streams) • Kalina cycle (>200 °F)

Table 5-2: Input parameters

Input Parameters (Common in All Configurations)	Values (unit)
Ambient Temperature	300 (K)
Minimum Allowable Cycle Temperature	310 (K)
Fractional Pressure Drop (FPD)	0.02
Isentropic Efficiency of Turbines	0.9
Isentropic Efficiency of Compressors	0.89

5.2. Heat Recovery Considerations

As illustrated in Figure 5-1, one key difference between S-CO2 cycles for waste heat recovery and S-CO2 cycles for solar and nuclear applications is the thermodynamic implication of how heat is added to the cycle. For those applications in which heat is added via a closed loop system, the conservation of energy implies that the amount of added heat to the cycle is equal to the generated heat in the heat source. This type of heat sources (solar receiver or nuclear reactor) is usually in the form of heat flux source in which the heat utilization is not constrained by temperature variation (Figure 5-2). Therefore, the heat input can be imposed into the cycle modeling as a constant parameter. In contrast, for waste heat recovery applications, the heat input is applied through a heat exchange process between the working fluid (that is, carbon dioxide) and the hot waste gas. In such arrangements, the temperature of the waste gas stream decreases as the heat is transferred to the cycle's working fluid. As presented in Figure 5-3, the products of mass flow rates and constant pressure specific heats (C_P) for the waste gas and the working fluid (CO2) are not necessarily equal. Therefore, depending on the mass flow ratio of CO2 and the waste gas, there can be a pinch point at either cold end or hot end of the recovery

heat exchanger. The pinch point temperature difference is basically a very important factor that governs the amount of recovered heat and the CO2 mass flow rate in the cycle. In most common practices, the remaining thermal energy in the waste gas stream is ultimately discharged to the environment via a stack system. This implies that a portion of thermal energy in the waste gas stream is recovered in the heat exchanger and the rest is still wasted through the stack. In other words, the heat input to the cycle cannot be assumed as a constant parameter in waste heat recovery applications. On the contrary, the heat input is a nonlinear function of all decision variables in the power cycle, plus the pinch point temperature difference in the recovery heat exchanger. That is why the pinch point temperature difference in the recovery heat exchanger (main heat exchanger) is considered as a decision variable. This allows us to take into account the thermodynamic interactions of the heat recovery system and the power cycle, and ultimately find out the overall optimum design point. To this end, the following assumptions are made in the heat recovery system modeling:

(1) The waste gas is assumed to have the thermodynamic properties of air. It should be noted that because of the use of REFPROP, any arbitrary composition of the waste gas could have been considered in this calculation.

(2) The waste gas mass flow rate is fixed at 100 kg/s. Nevertheless, the results which are in the form of extensive properties can be linearly adjusted for other waste gas mass flow rates.

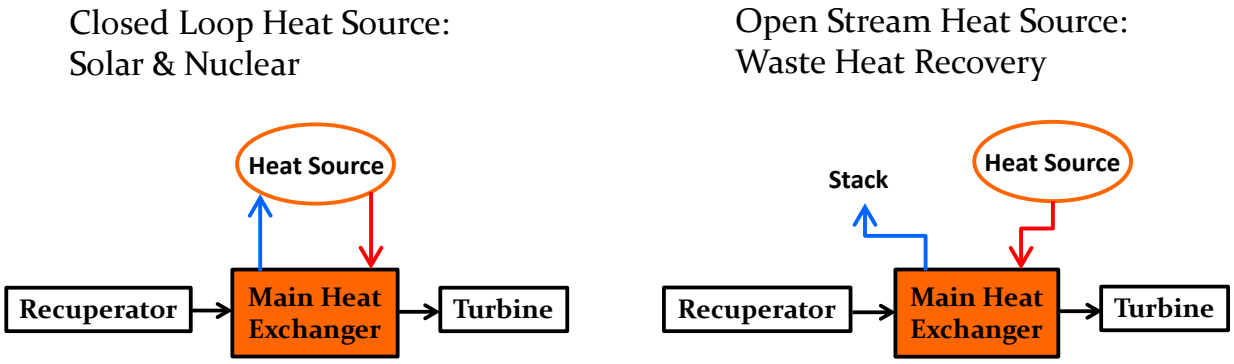

Figure 5-1: Heat Addition Process - Closed Loop vs. Open Stream

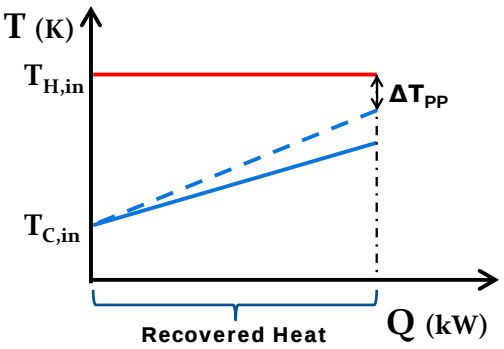

Figure 5-2: Typical T-Q diagram for heat flux source

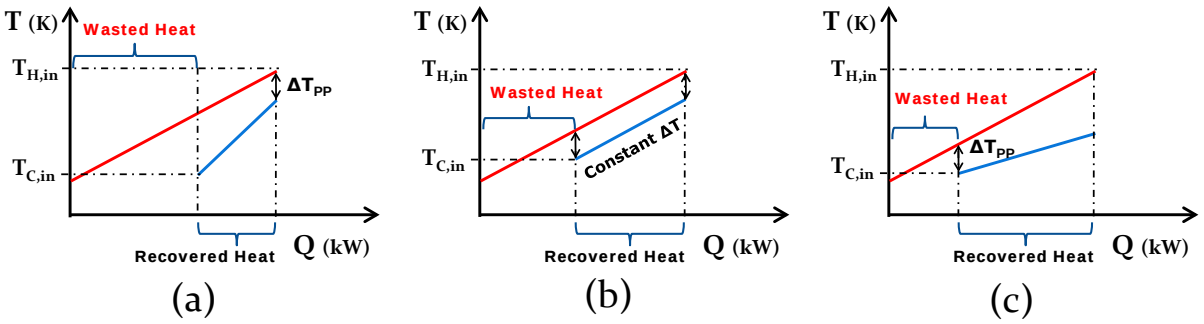

Figure 5-3: Typical T-Q diagrams in recovery heat exchangers

5.3. Optimization Domain

The domain of optimization is specified by limiting the decision variables between pre-assigned lower and upper bounds. The decision variables list and their boundaries are presented in Table 5-3. It should be noted that the pinch point temperature difference in the recovery heat exchanger is an additional decision variable as compared to the cases where a closed loop heat source is utilized.

Table 5-3: Decision variables in the RC and RRC configurations

Decision Variables in Configuration: RC	Lower Bound	Upper Bound
Compressor Inlet Temperature, T(1) (K)	310	410
Turbine Inlet Temperature, T(4) (K)	350	Variable
Terminal Temperature Difference in Recuperators, ΔTt (K)	10	40
Compressor Inlet Pressure, P(1) (MPa)	2	Variable
Compressor Outlet Pressure, P(2) (MPa)	Variable	24
Pinch Point Temperature Difference in Main Heater, ΔT_{PP} (K)	10	400
Decision Variables in Configuration: RRC	**Lower Bound**	**Upper Bound**
Main Compressor Inlet Temperature, T(1) (K)	310	410
Turbine Inlet Temperature, T(5) (K)	350	Variable
Inlet Temperature of Recompression, T(9) (K)	T(1)	T(8)
Terminal Temperature Difference in Recuperators, ΔTt (K)	10	40
Main Compressor Inlet Pressure, P(1) (MPa)	2	Variable
Main Compressor Outlet Pressure, P(2) (MPa)	Variable	24
Main Compressor Mass Flow Fraction, f	0	1
Pinch Point Temperature Difference in Main Heater, ΔT_{PP} (K)	10	400

5.4. Objective Function

In this study, optimization is merely based on thermodynamic analysis. The major focus in any power plant is to generate as much power as possible from available resources. Since the

generated power is a product of heat input and cycle efficiency (Eq. (5-1)), for a fixed heat input, this interpretation usually leads to maximization of the cycle efficiency.

$$\dot{W} = \eta \times \dot{Q} \tag{5-1}$$

As explained in section 5.2, the amount of generated heat in the heat source is equal to the heat input to the cycle for applications such as solar power. In other words, the heat input can be imposed into the cycle modeling as a constant parameter. Therefore, maximizing the cycle efficiency guarantees the maximum power generation for such applications with the closed loop heat addition.

In contrast to closed loop heat source applications, maximizing the cycle efficiency does not necessarily lead to maximum power generation in waste heat recovery applications. As illustrated in Figure 5-3, in waste heat recovery applications, the amount of recovered heat depends on minimum allowable temperature difference, mass flow ratio of the heat transfer fluids, constant pressure specific heat of CO2, and inlet temperature of the cold stream. The last three parameters depend on the cycle's design variables, which implies that there is an interaction between the recovery heat exchanger performance and the power cycle performance. Therefore, a very efficient power cycle may result in poor heat recovery, and very good heat recovery may result in low cycle efficiency. Ultimately, there is a tradeoff between the cycle efficiency and recovered heat that needs to be considered in the optimization. Therefore, the objective or fitness function in this chapter is defined as the maximum cycle power which encompasses the performance interactions between the recovery heat exchanger and the power cycle itself.

5.5. Results and Discussion

The presented results are based on 100 kg/s mass flow rate of the waste gas stream. As mentioned earlier, some results are in the form of extensive properties; thus, they can be linearly adjusted for any other values of waste gas mass flow rates. And the results based on intensive properties are valid for any waste gas mass flow rates without further adjustments. The optimization of both RC and RRC configurations was performed for several heat source temperatures from 500 to 1100 K.

Net power output for different values of the available (input) waste gas temperature is presented in Figure 5-4 for each of the two cycle configurations: RC and RRC, and for two different optimization strategies: maximizing power output and maximizing efficiency. As discussed in the previous section, for waste heat recovery applications, the maximization of net power output is of practical interest, while maximization of efficiency is shown only for comparison purposes. It is evident that maximizing the cycle efficiency does not realize the full potential of power generation in waste heat recovery applications; and therefore it is not a good strategy for the optimization. However, the difference between two optimization strategies is less significant as it goes towards lower heat source temperatures. Moreover, the results demonstrate that RRC configuration, while involving more complexity and more turbomachines, does not provide significantly higher power output even for heat source temperatures above 750 K.

Since the generated power depends on both cycle efficiency and recovered heat, Figure 5-5 can justify the results presented in Figure 5-4. The comparison between the optimization strategies shows how a very efficient cycle may perform poorly in heat recovery and eventually lead to low power generation. In contrast, maximizing the power generation will

result in the optimum balance or trade-off between the heat recovery and cycle efficiency. Figure 5-5 also explains why the power generation improvement by RRC configuration is marginal as compared to RC configuration when maximizing for power. Although the RRC configuration does provide higher efficiency, especially for higher waste gas inlet temperature, its poor performance in heat recovery will result in almost same power generation as in RC configuration.

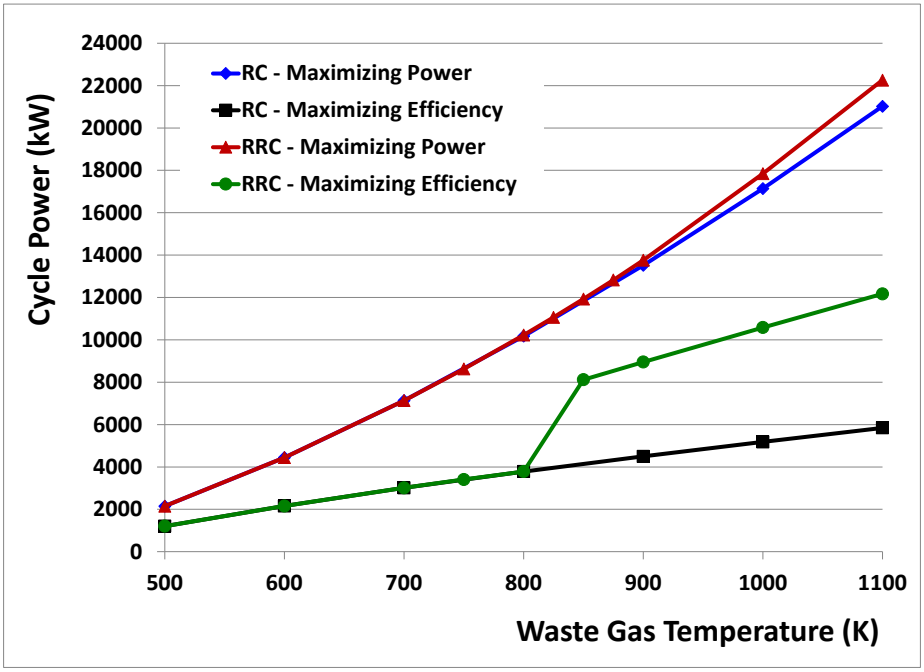

Figure 5-4: Net power output under various conditions

It should also be noted that the pinch point temperature difference in the recovery heat exchanger (main heater) plays an important role in the cycle performance. Optimization, as expected, always leads to the lowest bound of pinch point temperature difference. While maximizing efficiency, the CO2 mass flow rate gets automatically adjusted such that the temperature difference between waste gas and CO2 remains constant so as to maximize the CO2

mass flow rate for the same cycle efficiency (similar to Figure 5-3-b). However, when the optimization strategy is to maximize the power, the pinch point always occurs at the low temperature end of recovery heat exchanger (similar to Figure 5-3-c).

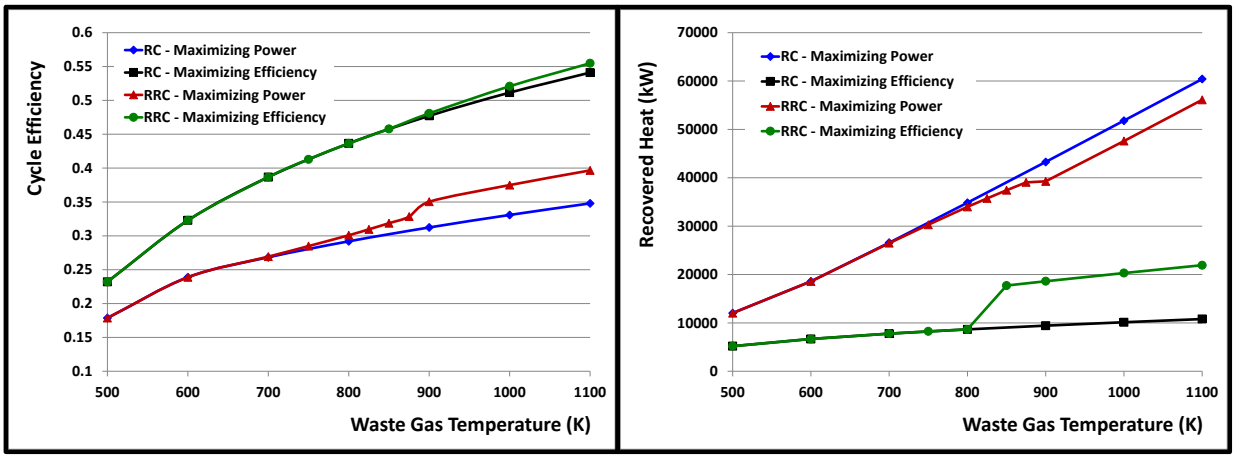

Figure 5-5: Cycle efficiency (left) and recovered heat (right) under various conditions

As maximizing net power output, rather than maximizing efficiency, is of practical interest, remaining results and discussion are presented only for the case of maximization of net power output. Table 5-4 presents the results of optimization (optimum decision variables) for RC configuration. Most decision variables reach their lower or upper bounds of optimization. The only exceptions are turbine inlet temperature and main compressor inlet pressure. As the heat source temperature goes from 500 to 1100 K, the optimum inlet pressure of the compressor changes from 8.8 MPa to 8.46 MPa, which represents an insignificant variation (2.73 to 2.84) in optimum pressure ratio. It is noteworthy that only for very low heat source temperature (500 K), the optimum turbine inlet temperature reaches its upper bound of optimization. But this is not the case as the heat source temperature increases. The optimum turbine inlet temperature does not reach its upper bound in order to benefit from large CO2 mass flow rate in the power cycle.

Table 5-4 Optimum decision variables in RC configuration based on different temperatures of waste heat source from 500 to 1100 K

Decision Variables	Waste Gas Temperature (K)						
	500	600	700	800	900	1000	1100
Main Compressor Inlet Temperature (K)	310	310	310	310	310	310	310
Terminal Temperature Difference (K)	10	10	10	10	10	10	10
Pinch Point Temperature Difference (K)	10	10	10	10	10	10	10
Turbine Inlet Temperature (K)	490	561.2	603.5	641.3	676.9	711.4	745.3
Main Compressor Outlet Pressure (MPa)	24	24	24	24	24	24	24
Main Compressor Inlet Pressure (MPa)	8.803	8.675	8.621	8.557	8.538	8.5	8.46
Cycle Pressure Ratio	2.726	2.767	2.784	2.805	2.811	2.824	2.837

Similarly, Table 5-5 presents the results of optimization (optimum decision variables) for RRC configuration, and the same trend in terms of optimum values of decision variables can be seen. Note that the optimum values of recompression inlet temperature (point 9 in Figure 2-2) are shown in a normalized representation as defined in Eq. (5-2).

$$NDRIT = \frac{T_9 - T_1}{T_8 - T_1} \tag{5-2}$$

The results indicate that for the heat source temperatures below 750 K, the optimization process changes the layout of RRC configuration; that is, the recompression cycle is transformed to simple recuperated cycle.

Flexibility of the modeling tool and comprehensiveness of optimization scheme make it possible to not only optimize the thermodynamic design parameters of cycles, but also optimize their structural layouts. The layout transformation can be done in two ways. If the value of main compressor mass flow fraction becomes one (1) in the optimization process, it means there is no mass flowing through the recompression compressor, and the cycle becomes a simple

recuperated cycle. Another way to transform the recompression cycle to the simple recuperated cycle is by approaching the recompression inlet temperature at point 9 to the main compressor inlet temperature at point 1. That is why the main compressor inlet temperature is shown here in the normalized format. And the values of zero and close to zero imply that the recompression cycle is in fact the simple recuperated cycle. As suggested by the values of decision variables (Table 5-5) and also demonstrated in Figure 5-4, it is evident that the simple recuperated cycle outperforms the recompression cycle for heat source temperatures below 750 K.

Table 5-5: Optimum decision variables in RRC configuration based on different temperatures of waste heat source from 500 to 1100 K

Decision Variables	Waste Gas Temperature (K)						
	500	600	700	800	900	1000	1100
Main Compressor Inlet Temperature (K)	310	310	310	310	310	310	310
Terminal Temperature Difference (K)	10	10	10	10	10	10	10
Pinch Point Temperature Difference (K)	10	10	10	10	10	10	10
Turbine Inlet Temperature (K)	490	561.2	602.4	633.3	657.7	693.1	727.1
Main Compressor Outlet Pressure (MPa)	24	24	24	24	24	24	24
Main Compressor Inlet Pressure (MPa)	8.803	8.675	8.633	8.675	8.956	8.848	8.773
Cycle Pressure Ratio	2.726	2.767	2.780	2.767	2.680	2.712	2.736
Main Compressor Mass Flow Fraction	1	1	0.656	0.624	0.652	0.650	0.649
Non-Dimensional Recompression Inlet Temperature - NDRIT	0	0	0.01	0.072	1	1	1

Another interesting point to note is that the pinch point for the low temperature recuperator (LTR) can be in the middle of the heat exchanger and not at either end. However, the difference between the pinch point temperature difference and the minimum terminal temperature difference is quite small, typically a few tenths of 1 K. Therefore, the minimum terminal temperature difference is used as the decision variable in this work for the purpose of

simplicity in the modeling. The author would like to point out that employing the minimum terminal temperature difference in the modeling does not cause any error in thermodynamic performance calculations as it does not violate any laws of thermodynamics.

Based on the results provided in Table 5-4 and Table 5-5, and also the above discussion, it can be concluded that by changing the heat source temperature from one application to another, there are three main design parameters that should be adjusted for optimum operation of the S-CO2 cycles. The first design parameter is the optimum pressure ratio of the cycle. But its variation for different heat source temperatures is not significant (2.73 – 2.84). However, the variations of the other two parameters, i.e., optimum CO2 to gas mass flow ratio and optimum turbine inlet temperature, are very important.

Figure 5-6 presents the mass flow rate of CO2 needed to maximize the net power output for a given amount of waste gas mass flow rate and for various waste gas temperatures. For simple RC configuration, the CO2 mass flow rate increases almost linearly with increasing waste gas temperature in order to take advantage of higher heat input, and hence higher power output, of the cycle. As mentioned before, optimization of RRC configuration leads to the RC configuration for waste gas temperature less than 750 K. For higher waste gas temperatures, the optimal CO2 mas flow rate in RRC configuration increases faster than that for RC configuration, until about waste gas temperature of 900 K, after which optimal CO2 mass flow rate starts to increase linearly with waste gas temperature. Since RRC configuration does not provide any significant increase in net power output, higher CO2 mass flow rate puts the RRC configuration at a disadvantage.

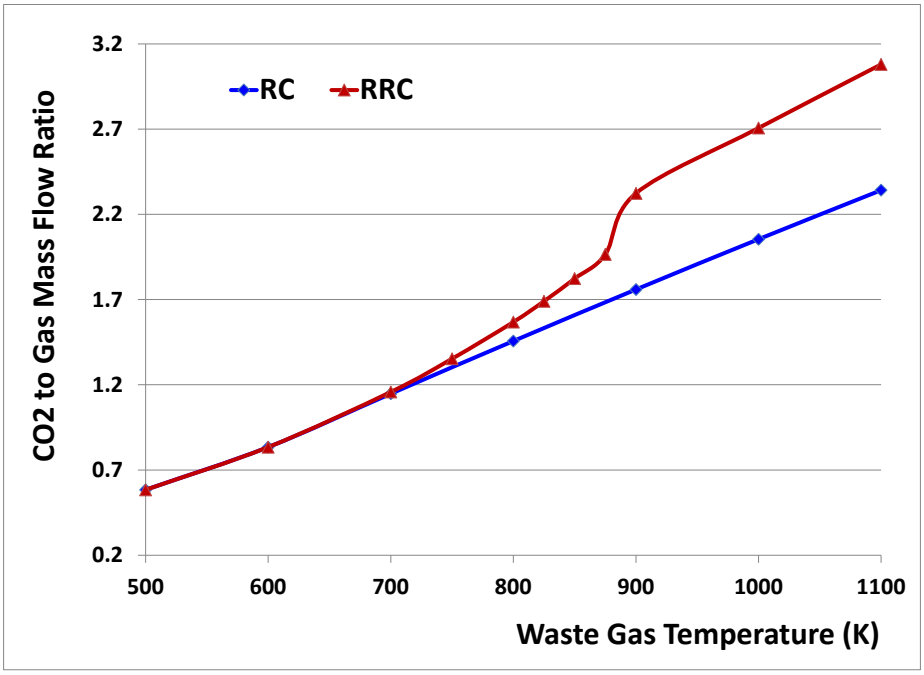

Figure 5-6: CO2 to waste gas mass flow ratio for maximization of net power output

Figure 5-7 presents the optimum turbine inlet temperatures and gas stack temperatures as functions of the waste gas temperature. The optimum turbine inlet temperature is not significantly affected by the configuration, although RRC configuration requires slightly lower turbine inlet temperature. It should be noted that the optimal turbine inlet temperature increases almost linearly with the waste gas temperature above 600 K, but at a much slower rate. For example, when waste gas temperature increases from 700 K to 1100 K, the optimum TIT increases from 603.5 K to about 745.3 K for the RC configuration. However, the low temperature end of the main heater also increases with increasing waste gas temperature, which indicates the increase in the stack temperature. However, the increase in stack temperature does not necessarily imply any reduction in the recovered heat fraction. In fact, as presented in Figure 5-8, the recovered heat fraction in the main heater increases from almost 60 % to 70 % in

the simple recuperated cycle, and up to almost 66 % in the recompression cycle. Nevertheless, there is still a good amount of heat that is not recovered by the power cycles. This is due to the nature of low pressure ratio recuperated S-CO2 cycles in which the CO2 inlet temperature to the recovery heat exchanger is relatively high. In order to integrate the effects of power cycle efficiency and heat recovery performance, overall conversion efficiency can be defined as in Eq. (5-3).

$$\eta_{Overall} = Recovered\ Heat\ Fraction \times \eta_{Cycle} \tag{5-3}$$

As depicted in Figure 5-8, although cycle efficiencies between 17.9% and 34.8% in RC configuration, and as high as 39.7% in RRC configuration can be achieved, the overall conversion efficiency is less than 24.5% and 26% in RC and RRC configurations respectively.

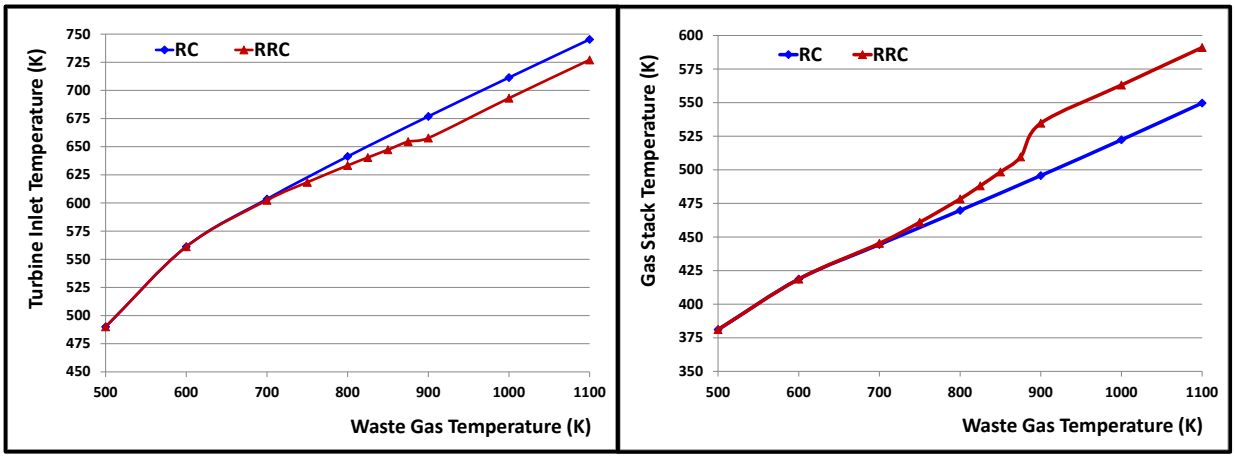

Figure 5-7: Optimum turbine inlet temperature (left) and gas stack temperature (right) for various waste gas temperatures

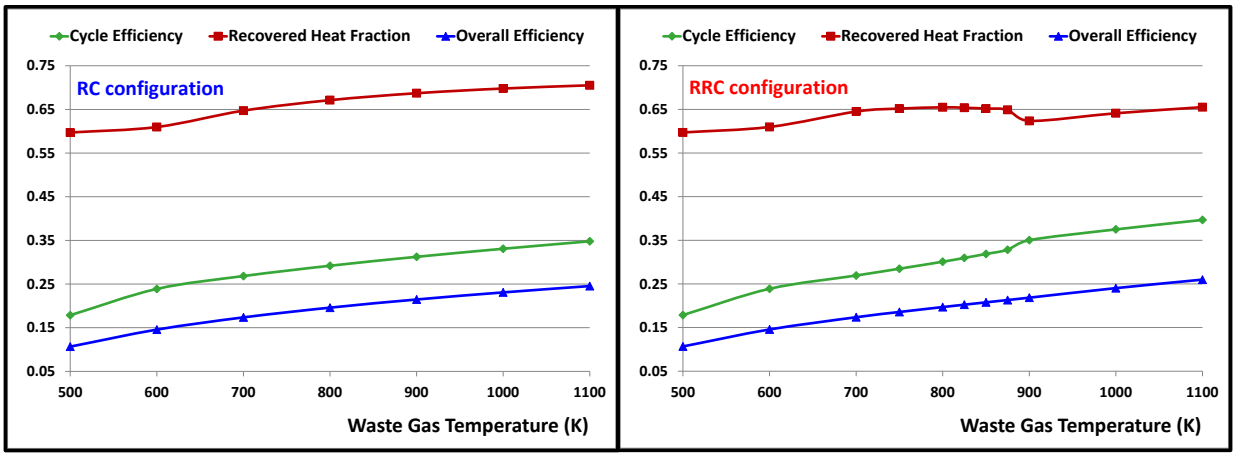

Figure 5-8: Cycle efficiency, recovered heat fraction, and overall conversion efficiency in RC (left) and RRC (right)

5.6. Conclusion

Maximization of net power output is of paramount practical interest rather than the maximization of cycle efficiency for the application of waste heat recovery. In such applications, very efficient cycle designs may suffer from low heat recovery and low power generation. That is why in addition to the cycle design parameters; the heat exchange process between the waste gas and the cycle's working fluid needs to be considered in order to arrive at the proper optimal solutions. In spite of increased complexity, the RRC configuration does not provide any appreciable benefit as compared to the RC configuration in terms of net power output. By changing the heat source temperature from one application to another, the variation of optimum pressure ratio is insignificant. However, the optimum CO2 to waste gas mass flow ratio and turbine inlet temperature should properly be adjusted. The low pressure ratios of the recuperated S-CO2 cycles limit the heat recovery potential, which leads to relatively low power generation.

6. DISSERTATION CLOSURE

6.1. Summary and Concluding Remarks

The power generation industry has always been in search of new technologies that can advance its economic features towards less expensive, but efficient electricity production. In addition, sustainability considerations have recently attracted considerable attention, which places applications such as CSP and WHR among the most promising options for the future of power generation industry. With this regard, the S-CO2 Brayton cycles have been introduced as a strong contender to replace the steam cycles in CSP, WHR and combined cycle power plants. Carbon dioxide is environmentally benign, non-toxic, non-flammable, abundant, and inexpensive. It is a very stable compound as its thermal dissociation temperature is above 2000 K. Carbon dioxide has a critical pressure of 7.39 MPa, and a critical temperature of 304.2 K, which is very close to the standard ambient temperature (298.15 K). The back work ratio in S-CO2 Brayton cycles are very low due to the high density of carbon dioxide at high pressure and near ambient temperatures, which contributes in their high efficiency even at moderate turbine inlet temperatures. Moreover, operating at high pressures, the cycle efficiency is inconsiderably affected by the pressure drop in heat exchangers (e.g. heaters, recuperators, and coolers). Supercritical carbon dioxide has a relatively high volumetric heat capacity; and it offers excellent heat transfer characteristics, which can be translated to small-size recuperators and coolers. The S-CO2 Brayton cycles feature high compactness, which leads to low capital cost and short construction time. Unlike the steam Rankine cycles, the S-CO2 Brayton cycles do not require clean water supplies, which is of high priority in the power generation industry.

Although numerous studies have been conducted to investigate the use of S-CO2 cycles for nuclear power applications, the recent change of course towards new applications such as high temperature CSP and WHR required a new set of system level thermodynamic studies. Accordingly in this study, appropriate tools for thermodynamic modeling and optimization of S-CO2 Brayton cycles have been developed in FORTRAN programming language. The modeling tool is capable of calculating the thermodynamic performance of various configurations of the S-CO2 Brayton cycles including combinations of recuperation, recompression, reheating and intercooling. The modeling tool is also fully flexible in terms of entirely covering the feasible design domain, and rectifying possible infeasible solutions. An in-house optimizer tool, which works based on genetic algorithm (GA) principles, has also been developed. Genetic algorithm provides advantageous features in optimizing non-linear systems in which several decision variables can be optimized simultaneously in order to achieve the global optimum solution. Ultimately, the thermodynamic analyses and optimization have been performed, and the results were presented in three chapters.

Chapter 3 and 4 are dedicated to comprehensive thermodynamic analyses and optimization of S-CO2 Brayton Cycles for high temperature CSP applications. Two optimization schemes, i.e. single-objective and multi-objective optimization were performed. The goal in the single-objective optimization scheme is to maximize the efficiency of various configurations of S-CO2 Brayton cycles. The conceptual idea of maximizing the cycle efficiency is directly aligned with decreasing the size and cost of the solar block (or in general any topping closed loop heat source), which is a major contributor in the levelized cost of electricity (LCOE). In addition to the cycle efficiency, the cycle specific power is a comparably important factor as it

directly influences the capacity of a power plant, the size of components, and eventually the cost of power block. Therefore, any attempt to maximize the cycle specific power would lower the size and cost of power block, which accounts for a considerable portion of final LCOE. Subsequently, the multi-objective optimization scheme was also performed.

Four configurations of S-CO2 Brayton cycle employing recuperation, recompression, intercooling and reheating were investigated for achieving their maximum efficiency. The main limiting factors in the optimization process are maximum cycle temperature, minimum heat rejection temperature, and pinch point temperature difference. The maximum cycle pressure is also a limiting factor in all studied cases except in the simple recuperated cycle. Moreover, the optimum inlet pressure of the main compressors were found not to be necessarily near the critical pressure. The optimized cycle efficiency increases as more complexities, i.e. recompression, reheat and intercooling, are added to the simple recuperated cycle. However, the simplicity of RC and RRC configurations make them more promising options. Therefore, RC and RRC configurations were chosen to be studied in the multi-objective optimization scheme. The simultaneous maximization of efficiency and specific power led to a trade-off curve (for each configuration) which is commonly called the Pareto front. The Pareto front consists of a range of optimum solutions that can be presented to decision makers enabling them to choose the desired compromise between the objectives and avoid naive solutions obtained from a single-objective optimization approach. Moreover, the comparison of the Pareto optimal fronts associated with the studied configurations reveals the optimum operational region of the recompression configuration where it presents superior performance over the simple recuperated cycle. As a result, it can be suggested that the RRC configuration offers better characteristics for CSP

applications. On the other hand, the RC configuration is more beneficial in applications where the size and cost of power blocks is crucial. Although a high premium is placed on the cycle efficiency for CSP applications, targeting the highest possible cycle efficiency comes with the drawbacks of low cycle specific power and high effectiveness of recuperators, which both contribute towards increasing the size and cost of heat exchangers. Therefore, the most efficient RRC cycle design is only suggested for small scale solar power plants, while the neighboring optimum design solutions with higher specific power and slight reduction in efficiency would be suggested for large scale solar power generation.

Finally, Chapter 5 was intended for optimization of S-CO2 Brayton cycles for a wide spectrum of heat source temperatures in WHR applications. The utilization of heat in WHR applications is fundamentally different from that in closed loop heat source applications. The heat utilization in WHR applications is in general limited by temperature pinching issue in the waste recovery heat exchanger. In other words, the heat utilization may not be 100%, and optimizing for cycle efficiency may not yield the maximum power generation. In fact, the interaction and trade-off between the heat recovery and cycle efficiency have to be considered in the optimization. The results demonstrate that by changing the heat source temperature from one application to another, the variation of optimum pressure ratio is insignificant. However, the optimum CO2 to waste gas mass flow ratio and turbine inlet temperature should properly be adjusted. The RRC configuration provides minor increase in power output as compared to RC configuration. Although cycle efficiencies as high as 34.8% and 39.7% can be achieved in RC and RRC configurations respectively, the overall conversion efficiency is less than 26% in RRC and 24.5% in RC, which is due to the limited heat recovery potential that these configurations

offer. In order to increase both the heat recovery and power generation, the author would suggest utilizing parallel compounds of non-recuperated and recuperated cycles.

The author wishes to once again point out that the presented results in this dissertation are based on the provided assumptions; and are only valid within the defined framework. The thermodynamic calculations were merely performed for core components of the S-CO2 Brayton cycles and do not include the balance of plant and other auxiliary equipment such as external cooling systems, auxiliary pumps and fans, oil and lubrication skids, and piping, bearing, seals and generator losses.

6.2. Contributions

The contributions of this project are listed as follow:

(1) Four configurations of S-CO2 Brayton cycles, i.e., RC, RRC, RRCR and RRCRI were optimized for achieving their maximum efficiency in high temperature CSP applications. The optimized cycle efficiency is found to be 55.8%, 58.6%, 59.6%, and 62.0% respectively. Furthermore, the exergy analysis was performed to identify the effect of recompression, reheat and intercooling on the cycle's performance as a system. Although addition of reheating and intercooling to the recompression cycle increases the cycle efficiency, it also introduces more complexities in design, manufacturing and operation of S-CO2 cycles. Considering the fact that S-CO2 Cycles are at the very early development stage, the simplicity in their layouts is of utmost importance in the success of their development. Therefore, the above optimal values of efficiency suggest that the RC and RRC configurations are the most promising options for the first generation of S-CO2 Brayton cycles.

(2) The global optimization approach made it possible to find the global maximum efficiency of RC configuration in high temperature CSP applications. In contrast with what is often reported in the literature, the simple recuperated cycle (RC) presents its highest efficiency when operating in low pressure regions. Considering the fact that the most challenging issues in design and manufacturing of S-CO2 cycles are related to limitations in materials, seals and bearing technologies, the low pressure operation of RC configuration is advantageous. However, this favorable feature can be at the cost of low cycle specific power.

(3) The concept of multi-objective optimization was introduced into the analysis of S-CO2 power cycles for the first time. In this project, it was realized that the maximum cycle efficiency may not be a sufficient criterion in designing the S-CO2 Brayton cycles for closed loop heat source applications. In fact, the cycle specific power can be equally important as it directly affects the size and capital cost of heat exchangers and turbomachineries. The comparison of Pareto fronts obtained from the multi-objective optimization scheme (as depicted in Figure 6-1) revealed that the RC configuration outperforms the RRC configuration when high level of preference for specific power is required.

(4) The optimization of S-CO2 Brayton cycles for waste heat recovery applications was also performed. As shown in Figure 6-2, maximization of cycle efficiency may lead to lower values of net cycle power output. In other words, maximizing the cycle efficiency does not realize the full potential of power generation, and therefore it is of no value in waste heat recovery applications. In fact, the direct maximization of generated power should be chosen as the objective function of optimization. The presented results are comprehensive, which means they can be used for any values of waste gas mass flow rates and for a wide spectrum of heat

source temperatures. Moreover, the results shed light on the fact that the RC configuration is a better choice as compared to the RRC configuration in waste heat recovery applications.

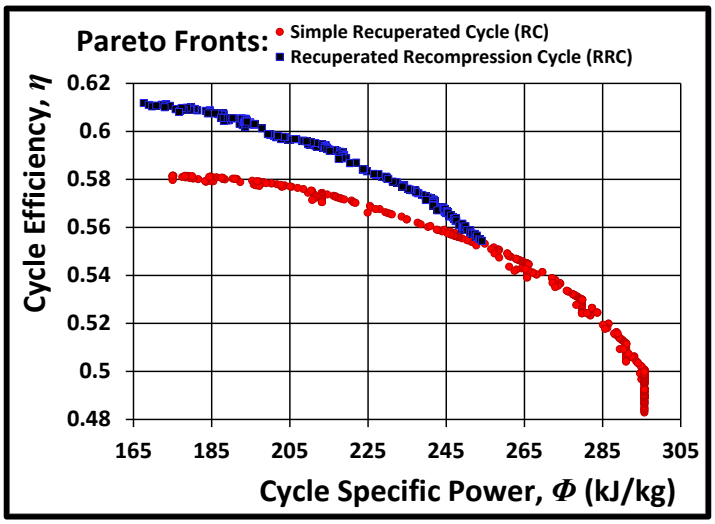

Figure 6-1: Comparison of Pareto fronts associated with RC and RRC configurations

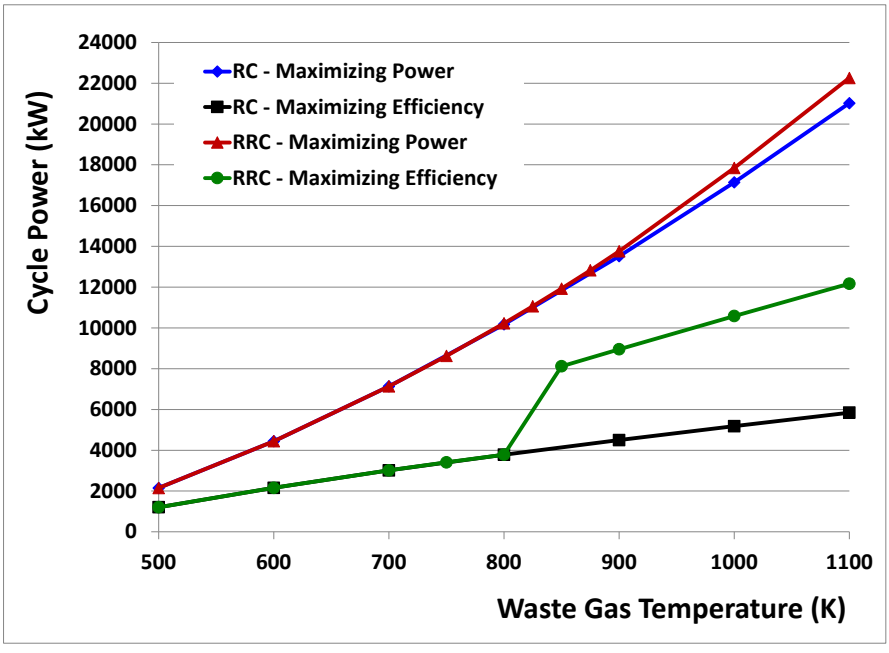

Figure 6-2: Net power output for two optimization strategies

(5) Based on the results obtained for WHR applications, it is suggested that a modified RC (mRC) configuration, where a non-recuperated and a recuperated cycle are combined in a parallel fashion, may provide more optimal recovery of waste heat. This requires future study.

(6) Finally, the flexibility in modeling and also comprehensive optimization approach made it possible to define a unique configuration for the first time. The author decided to name it "comprehensive configuration." The comprehensive configuration is a configuration that can be automatically transformed to several different specific configurations during the optimization process. In other words, by optimizing the comprehensive configuration, one may achieve the optimum solution of several configurations altogether. The comprehensive configuration is in fact the RRCRI configuration. The flexibility in modeling and also comprehensive optimization approach made the RRCRI configuration transformable to various specific configurations. Note that main compressor mass flow fraction, pressures at points 1, 2, 7 and 8 and temperatures at points 1, 6, 7 and 13 are all among the decision variables in the RRCRI configuration. During the optimization process, if certain values are assigned to these decision variables (as depicted in Figure 6-3), the comprehensive configuration can be transformed to the RC, RRC or RRCR configuration. In addition, the comprehensive configuration can be transformed to other alternative configurations such as the ones studied in [49, 60] as shown in Figure 6-4. The comprehensive configuration is a very beneficial concept when it comes to optimization of the S-CO2 Brayton cycles for different applications. As the operating temperature and pressure vary by the application, the optimum cycle layout may also vary among the aforementioned configurations. Therefore, the optimization of comprehensive configuration not only leads to the optimum temperatures and pressures, but also reveals the optimum cycle layout.

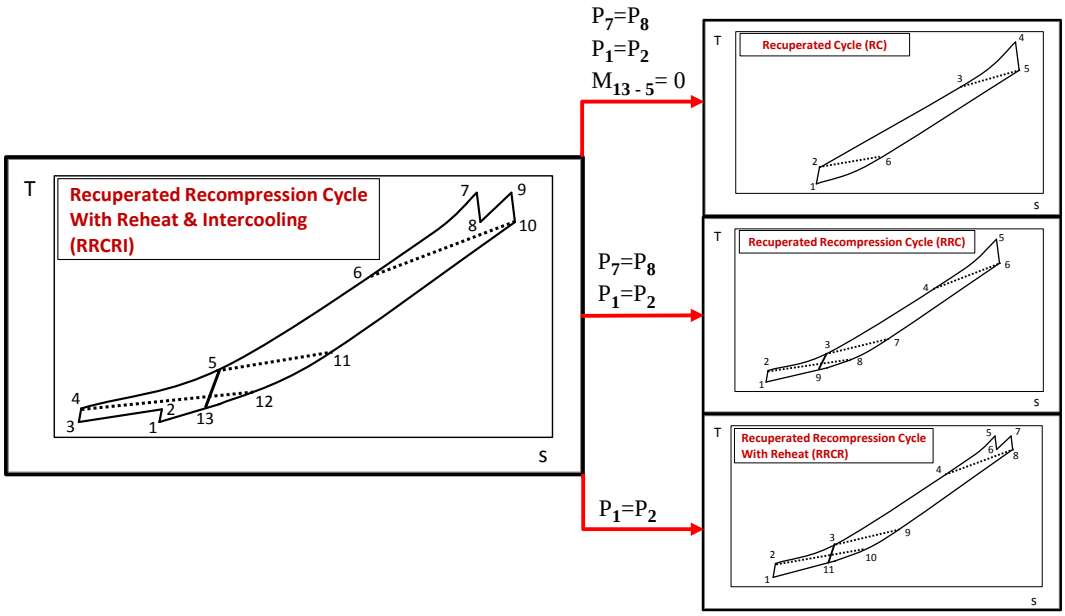

Figure 6-3: Transformation of comprehensive configuration (RRCRI) to RC, RRC, and RRCR layouts

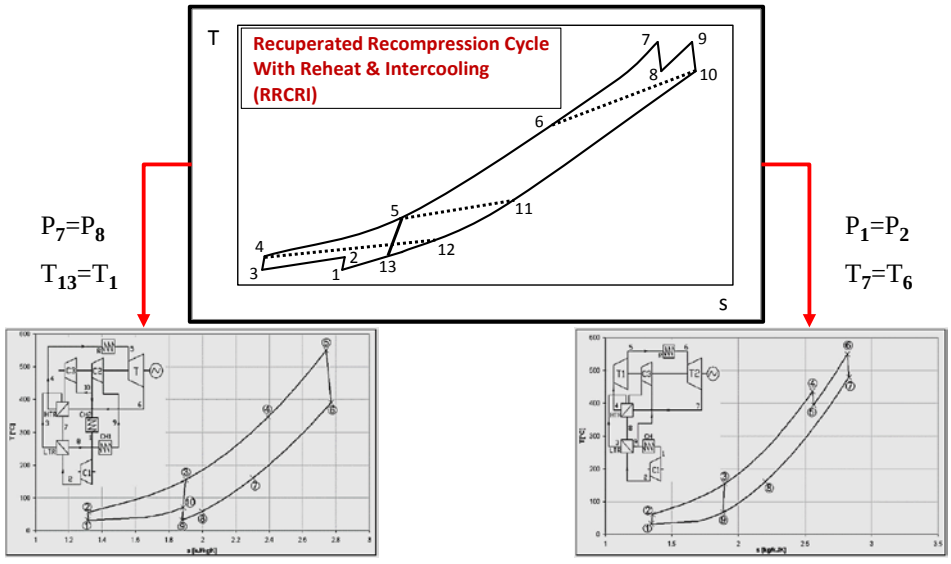

Partial Cooling Cycle

Split-Expansion Cycle

Figure 6-4: Transformation of comprehensive configuration (RRCRI) to partial cooling (left) and split-expansion (right) layouts

6.3. Recommendations for Future Research

The outcomes of this study revealed the promising potential of S-CO2 Brayton cycles for various heat source applications. They have also proved the importance of system-level thermodynamic optimization of such power cycles. The presented optimization guidelines are the starting point for several component level designs. The developed modeling and optimization tools enable the required infrastructure for a set of long term and purposeful studies which can be summarized as:

(1) Development of computationally efficient modeling tools for components such as compressors, turbines and heat exchangers that can lead to investigation of S-CO2 cycles for their dynamic performance and optimum control design.

(2) Detailed design and optimization of various turbine and compressor types, e.g. axial and radial, by utilizing streamline curvature and CFD approaches. In order to boost the computational speed in both system level simulations and component design optimization, creating several 2-D property look up tables are strongly suggested.

(3) As the heat exchangers are the largest and most expensive components in S-CO2 Brayton cycles, detailed structural analysis and thermal design of various types of heat exchangers are also essential. Several heat transfer characteristics of carbon dioxide in the supercritical region are not well studied yet. Therefore, experimental studies should be contrived to validate the available heat transfer and pressure drop correlations.

(4) The material advancement is crucial to the success of S-CO2 power cycles. The high pressure and temperature operation of S-CO2 cycles necessitates stringent material testing that covers thermal stress, creep, fatigue, solubility, decomposition and corrosion analyses.

(5) Since S-CO2 Brayton cycles operate in high rotational speeds and at very high pressure environment, the design or selection of seals and bearings is very challenging and needs to be addressed in a separate study.

(6) As also pointed out in Chapter 5, new parallel compounds of recuperated and non-recuperated S-CO2 cycles should be proposed and optimized for the WHR application, particularly for high temperature heat sources.

LIST OF REFERENCES

[1] R. E. Smalley, Top Ten Problems of Humanity for Next 50 Years, Energy & NanoTechnology Conference, Rice University, May 3, 2003.

[2] BP Energy Outlook 2030, London, 2013

[3] Key world energy statistics, International Energy Agency, 2014.

[4] National oceanic and atmosphere administration. [Online]. Available at: http://www.esrl.noaa.gov/gmd/ccgg/trends/.

[5] Electricity production in the world: general forecasts, Fifteenth inventory, 2013 edition.

[6] H. Chen, D. Y. Goswami, E. K. Stefanakos, A review of thermodynamic cycles and working fluids for the conversion of low-grade heat, Renewable and Sustainable Energy Reviews, 2010, 14: 3059-3067.

[7] Madhawa Hettiarachchi HD, Golubovic M, Worek WM, Ikegami Y. Optimum design criteria for an organic Rankine cycle using low-temperature geothermal heat sources. Energy 2007; 32:1698–706.

[8] Quoilin S. Experimental study and modeling of a low temperature Rankine cycle for small scale cogeneration. Thesis, University of Liege; 2007.

[9] Mago PJ, Chamra LM, Srinivasan K, Somayaji C. An examination of regenerative organic Rankine cycles using dry fluids. Applied Thermal Engineering 2008; 28:998–1007.

[10] Chacartegui R, Sa´nchez D, Mun˜oz J, Sa´nchez T. Alternative ORC bottoming cycles for combined cycle power plants. Applied Energy 2009; 86:2162–2170.

[11] Hung TC, Shai TY, Wang SK. A review of organic Rankine cycles (ORCs) for the recovery of low-grade waste heat. Energy 1997; 22:661–7.

[12] Chen Y, Lundqvist P, Johansson A, Platell P. A comparative study of the carbon dioxide transcritical power cycle compared with an organic Rankine cycle with R123 as working fluid in waste heat recovery. Applied Thermal Engineering 2006; 26:2142–7.

[13] Dai Y, Wang J, Gao L. Parametric optimization and comparative study of organic Rankine cycle (ORC) for low grade waste heat recovery. Energy Conversion and Management 2009; 50:576–82.

[14] Delgado-Torres AM, Garcı´a-Rodrı´guez L. Preliminary assessment of solar organic Rankine cycles for driving a desalination system. Desalination 2007; 216:252–75.

[15] Nowak W, Borsukiewicz-Gozdur A, Stachel A. Using the low-temperature Clausius–Rankine cycle to cool technical equipment. Applied Energy 2008; 85(7):582–8.

[16] Tchanche BF, Papadakis G, Lambrinos G, Frangoudakis A. Fluid selection for a low-temperature solar organic Rankine cycle. Applied Thermal Engineering 2009; 29:2468–76.

[17] Hung TC. Waste heat recovery of organic Rankine cycle using dry fluids. Energy Conversion and Management 2001; 42:539–53.

[18] Kane M, Larrain D, Favrat D, Allani Y. Small hybrid solar power system. Energy 2003; 28:1427–43.

[19] Fenton DL, Abernathy GH, Krivokapich GA, Otts JV. Operation and evaluation of the Willard solar thermal power irrigation system. Solar energy 1984; 32:735–51.

[20] Schuster A, Karl J, Karellas S. Simulation of an innovative stand-alone solar desalination system using an organic Rankine cycle. International Journal of Thermodynamics 2007; 10:155.

[21] Wei D, Lu X, Lu Z, Gu J. Dynamic modeling and simulation of an organic Rankine cycle (ORC) system for waste heat recovery. Applied Thermal Engineering 2008; 28:1216–24.

[22] Wei D, Lu X, Lu Z, Gu J. Performance analysis and optimization of organic Rankine cycle (ORC) for waste heat recovery. Energy Conversion and Management 2007; 48:1113–9.

[23] Obernberger I, Thonofer P, Reisenhofer E. Description and evaluation of the new 1.000kWel organic Rankine cycle process integrated in the biomass CHP plant in Lienz, Austria. Euorheat and Power 2002; 10:1–17.

[24] Nguyen VM, Doherty PS, Riffat SB. Development of a prototype low-temperature Rankine cycle electricity generation system. Applied Thermal Engineering 2001; 21:169–81.

[25] Drescher U, Bruggemann D. Fluid selection for the organic Rankine cycle (ORC) in biomass power and heat plants. Applied Thermal Engineering 2007; 27: 223–8.

[26] Maizza V, Maizza A. Working fluids in non-steady flows for waste energy recovery systems. Applied Thermal Engineering 1996; 16:579–90.

[27] Gawlik K, Hassani V. Advanced binary cycles: optimum working fluids. In: Energy Conversion Engineering Conference. IECEC-97, Proceedings of the 32nd Intersociety; 1997. p. 1809–14.

[28] Maizza V, Maizza A. Unconventional working fluids in organic Rankine-cycles for waste energy recovery systems. Applied Thermal Engineering 2001; 21:381–90.

[29] Angelino G, Colonna di P, Paliano. Multicomponent working fluids for organic Rankine cycles (ORCs). Energy 1998; 23:449–63.

[30] Bliem CJ, Mines G. Supercritical binary geothermal cycle experiments with mixed-hydrocarbon working fluids and a near-horizontal in-tube condenser. Report 1989.

[31] Wang X, Zhao L. Analysis of zeotropic mixtures used in low-temperature solar Rankine cycles for power generation. Solar Energy 2009; 83(5):605–13.

[32] Borsukiewicz-Gozdur A, Nowak W. Comparative analysis of natural and synthetic refrigerants in application to low temperature Clausius–Rankine cycle. Energy 2007;32(4):344–52.

[33] Radermacher R. Thermodynamic and heat transfer implications of working fluid mixtures in Rankine cycles. International Journal of Heat and Fluid Flow 1989;10(6):90–102.

[34] Stine WB, Harrigan RW. Solar energy fundamentals and design. Wiley; 1985.

[35] Andersen WC, Bruno TJ. Rapid screening of fluids for chemical stability in organic Rankine cycle applications. Industrial and Engineering Chemistry Research 2005;44:5560–6.

[36] Wang J.L., Zhao L., Wang X.D., A comparative study of pure and zeotropic mixtures in low-temperature solar Rankine cycle, Applied Energy 2010; 87(11):3366–3373.

[37] Sulzer Patent Verfahren zur Erzeugung von Arbeit aus Warme, Swiss Patent 269 599, 1948.

[38] Gokhstein D. P, Verkhivker G. P., Future Design of Thermal Power Stations Operating on Carbon Dioxide, Thermal Engineering, April, pp. 36-38, 1971.

[39] Strub R. A., Frieder A. J., High Pressure Indirect CO2 Closed-Cycle Design Gas Turbines, Nuclear Gas Turbines, pp 51-61, January, 1970.

[40] Feher E. G., Supercritical Thermodynamic Cycles for External and Internal Combustion Engines, Astropower, Inc. Engineering Report, May, 1962.

[41] Feher E. G., The Supercritical Thermodynamic Power Cycle, Douglas Paper No. 4348, presented to the IECEC, Miami Beach, Florida, August 13-17, 1967.

[42] Hoffman J. R., Feher G. E., 150 kwe Supercritical Closed Cycle System, ASME paper No. 70-GT-89, (1970).

[43] Angelino G., Perspectives for the Liquid Phase Compression Gas Turbine, Journal of Engineering for Power, Trans. ASME, Vol. 89, No. 2, pp. 229-237, April, 1967.

[44] Angelino G., Carbon Dioxide Condensation Cycles for Power Production, ASME Paper No. 68-GT-23, 1968.

[45] Angelino G., Real Gas Effects in Carbon Dioxide Cycles, ASME Paper No. 69-GT-103, 1969.

[46] Petr V., Kolovratnik M, A Study on Application of a Closed Cycle COB2B Gas Turbine in Power Engineering (in Czech), Czech Technical University in Prague, Department of Fluid Dynamics and Power Engineering, Division of Power Engineering, Departmental report Z-523/97, November, 1997.

[47] Petr V., Kolovratnik M, Hanzal V, On the Use Of CO2 Gas Turbine in Power Engineering (in Czech), Czech Technical University in Prague, Department of Fluid Dynamics and Power Engineering, Division of Power Engineering, Departmental report Z-530/99, January, 1999.

[48] Dostal, V., Driscoll, M.J., Hejzlar, P., 2004, A Supercritical Carbon Dioxide Cycle for Next Generation Nuclear Reactors, MIT-ANP-TR-100.

[49] Kulhanek, M., Dostal, V., 2011, Thermodynamic Analysis and Comparison of Supercritical Carbon Dioxide Cycles, Proceedings of Supercritical CO2 Power Cycle Symposium, Boulder, Colorado.

[50] Lemmon, E.W., Huber, M.L., McLinden, M.O., 2010, NIST Standard Reference Database 23: Reference Fluid Thermodynamic and Transport Properties-REFPROP, Version 9.0, National Institute of Standards and Technology, Standard Reference Data Program, Gaithersburg.

[51] Span, R., Wagner, W., 1996, A New Equation of State for Carbone Dioxide Covering Temperature to 110 K at Pressure up to 800 MPa, J. Phys. Chem. Ref. Data, 25(6), pp.1509-1596.

[52] Harvego, E.A., McKellar, M.G., 2011, Evaluation and Optimization of a Supercritical Carbon Dioxide Power Conversion Cycle for Nuclear Applications, Proceedings of the 19th International Conference on Nuclear Engineering, Makuhari, Chiba, Japan.

[53] Hanfei Tuo, 2012, Thermal-economic analysis of a transcritical Rankine power cycle with reheat enhancement for a low-grade heat source, International Journal of Energy Research.

[54] Yang Chen, Doctoral Thesis, 2011, Thermodynamic Cycles using Carbon Dioxide as Working Fluid-CO2 transcritical power cycle study, KTH, Stockholm, Sweden.

[55] Jiangfeng Wang, Zhixin Sun, Yiping Dai, Shaolin Ma, 2010, Parametric optimization design for supercritical CO2 power cycle using genetic algorithm and artificial neural network, Applied Energy, 87, pp.1317-1324.

[56] Chacartegui, R., Muñoz de Escalona, J.M., Sánchez, D., Monje, B., Sánchez, T., 2011, Alternative cycles based on carbon dioxide for central receiver solar power plants, Applied Thermal Engineering, 31, pp.872-879.

[57] Haupt, R. L., Haupt, S. L., 1998, Practical Genetic Algorithms, John Wiley and Sons, New Jersey.

[58] Goldberg, D., 1996, Genetic Algorithm in Search Optimization and Machine Learning, Addison-Wesley, Michigan.

[59] Greenhalgh, D., Marshall, S., 2000, Convergence Criteria for Genetic Algorithms, SIAM Journal of Computing, 30(1), pp. 269-282.

[60] Vaclav Dostal, Martin Kulhanek, Research on the Supercritical Carbon Dioxide Cycles in the Czech Republic, Proceedings of Supercritical CO2 Power Cycle Symposium, Troy, NY, 2009.

[61] Vaclav Dostal, Pavel Hejzlar, Michael J. Driscoll, High Performance Supercritical Carbon Dioxide Cycle for Next Generation Nuclear Reactors, Nuclear Technology, 154, June 2006.

[62] Marcin Molga, Czesław Smutnicki, Test functions for optimization needs, Wroclaw University of Technology Publishing House, April 3, 2005.

[63] Solar Electricity Potential - Nathan S. Lewis, Global Energy Perspective, http://nsl.caltech.edu/energy

[64] Romero, M., Buck, R., Pacheco, J.E., 2002, An Update on Solar Central Receiver Systems, Projects, and Technologies, Transaction of ASME, 124, pp.98-108.

[65] Hischier, I., Leumann, P., Steinfeld, A., 2012, Experimental and Numerical Analyses of a Pressurized Air Receiver for Solar-Driven Gas Turbine, ASME J. of Solar Energy Engineering, 134.

[66] Hischier, I., Pozivil, P., Steinfeld, A., 2012, A Modular Ceramic Cavity-Receiver for High-Temperature High-Concentration Solar Applications, ASME J. of Solar Energy Engineering, 134.

[67] Bejan, A., Tsatsaronis, G., Moran, M., 1995, Thermal Design and Optimization, John Wiley and Sons, New Jersey.

[68] Yamamoto T, Furuhata T, Arai N, Mori K. Design and testing of the organic Rankine cycle. Energy 2001;26:239–51.

[69] United States Energy Information Administration (EIA), 2013, International Energy Outlook 2013, source: www.eia.gov.

[70] BCS, Inc. 2008, Waste Heat Recovery – Technology and Opportunities in U.S. Industry, U.S. DOE Industrial Technologies Program.

[71] Naik-Dhungel, Neeharika, 2012, WASTE HEAT TO POWER SYSTEMS, Combined Heat and Power Partnership, U.S. Environmental Protection Agency.

[72] Persichilli, M., Held, T., Hostler, S., Zdankiewicz, E., and Klapp, D., 2011, Transforming Waste Heat to Power through Development of a CO2 - Based Power Cycle, Electric Power Expo, Rosemount, IL U.S.A.

[73] Persichilli, M., Kacludis, A., Zdankiewicz, E., and Held, T., 2012, Supercritical CO2 Power Cycle Developments and Commercialization: Why sCO2 Can Displace Steam, Power-Gen India & Central Asia 2012.

[74] Kacludis, A., Lyons, S., Nadav, D., and Zdankiewicz, E., 2012, Waste Heat to Power (WH2P) Applications Using a Supercritical CO2-Based Power Cycle, Power-Gen International 2012, 11-13 December 2012, Orlando, FL U.S.A.